Influence of cyclic mechanical strain on tissues of the central nervous system

Doctoral thesis

Submitted in partial fulfillment of the requirements for the degree of

Doctor rerum naturalium (Dr. rer. nat.)

to the

Mathematisch-Naturwissenschaftlichen Fakultät der

Rheinischen Friedrich-Wilhelms-Universität Bonn

by

Jella-Andrea Abraham

from Ochsenhausen

Bonn, July 2020

Prepared with the consent of the Faculty of Mathematics and Natural Sciences

1st referee: PD. Dr. Bernd Hoffmann

2nd referee: Prof. Dr. Jörg Höhfeld

Disputation: 17th of November 2020

Year of publication: 2020

Summary

Although the brain is the softest tissue of the human body, cells embedded in the brain are responding to physiological mechanical cues. Tissue homeostasis is, therefore, not only dependent on chemical cues (e.g. growth factors), but also integrates the mechanical input that brain cells can sense from their physical microenvironment. The softness of the brain tissue, as well as the protective role of thick meninges and the hard skeletal skull, are the main reasons why mechanobiology for brain cells remained relatively unattended. Brain cells, in general, were regarded as mechanosensitive elements rather than seeing mechanical cues as an essential part of brain physiology. Recent studies, however, show an imposing involvement of physical cues, such as stiffness alterations and topographical cues.

As brain cells are also subjected to cyclic deformation due to the highly vascularized character of the brain tissue, cyclic mechanical strain is the focus of this thesis. Cyclic mechanical strain might play a relevant role in brain physiology as mechanical strain has shown to influence relevant biological signaling processes and gene expression in other cell types. Further, each cell type found in the brain has its own unique cytoskeletal arrangement. Cytoskeletal systems are involved in mechanotransduction and are the first recipients when cells are exposed to mechanical strain. A different cytoskeletal arrangement in each cell type is further highlighting the question of how mechanoresponses may differ between each individual cell type.

In the context of this dissertation, cells found in the brain were subjected to uniaxial cyclic strain within different developing stages. Therefore, neural stem cells, premature neuronal cells and astrocytes, as well as developed neuronal networks, and astrocytes were exposed to cyclic strain and mechanoresponses were analyzed. All cell types show striking differences in how they handled mechanical forces and revealed individual patterns of cytoskeletal alterations. Two different mechanical stimuli were used to analyze individual responses of the cells. The first part of this work was focused on immediate cell response to the first cycles of substrate deformation. In the second part, all cell types were analyzed according to their long-term adaptation to cyclic mechanical strain.

As an immediate response, neural stem cells revealed a reduced migration velocity and directional extensions of cell processes along the axis of uniaxial strain. Quantitative orientation analysis confirms the parallel alignment of neural stem cell extensions even after long-term stretch experiments. The parallel direction of cell alignment was sustained for neural stem cells that have been committed to an astrocyte phenotype when stretched during the differentiation process, while a neuronal commitment revealed a more random distribution with a slight shift towards a perpendicular direction. When NSCs were subjected to cyclic strain during differentiation, lineage commitment was not altered. However, neural stem cells were more quiescent when subjected to cyclic strain as less proliferative cells were found on stretched chambers.

The neuronal immediate response analysis in live-cell stretch experiments, revealed a drastic response of neuronal cells as they retract their branches within the first cycles of stretch. Such retraction was explicit when neuronal cells have been developed to neuronal networks on the elastomer. With more elongated neuronal branches, such retraction was accompanied by the formation of retraction bulbs filled with destabilized cytoskeletal proteins. A prolonged cyclic stretch triggered an adaptation process and allowed the neuronal cell to regrow their branches even under cyclic mechanical strain. Moreover, live-dead analysis after long-term stretch revealed that neuronal cells can survive long-term mechanical loads and did not show any altered cell vitality. Long-term stretch revealed a clear mechanoresponse and growth of neuronal branches in perpendicular direction. In addition, stretched neuronal cells showed an induced outgrowth with a higher number of branches, an increased sum length, and an enlarged growth cone.

Mature astrocytes isolated from postnatal rat pups did not show any directional mechanoresponse. They thereby behaved contrary to the cells that were differentiating from neural stem cells and committed towards an astrocyte phenotype. In a co-culture of astrocytes and neuronal cells, astrocytes revealed a mechanoprotective role and neuronal cells that grew on top of these astrocytes did show less strain-induced responses compared to cyclically stretched single neuronal cell cultures.

Table of contents

Abbreviations

ADP	adenosine diphosphate
ATP	adenosine triphosphate
APC	adenomatous polyposis coli
BSA	bovine serum albumin
CB	cytoskeletal buffer
CNS	central nervous system
DNA	deoxyribonucleic acid
FBS	fetal bovine serum
FGF	fibroblast growth factor
GFAP	glial fibrillary acidic protein
LSM	laser scanning microscopy
NSC	neural stem cell
NFH	neurofilament heavy
MAP-2	microtubule-associated protein 2
MLCK	myosin light-chain kinase
min	minutes
mRNA	messenger ribonucleic acid
Pa	pascal
PBS	phosphate-buffered saline
PDMS	polydimethylsiloxane
PFA	paraformaldehyde
qPCR	qualitative real-time PCR
RT	room temperature
SOX2	sex determining region Y (SRY)- box 2
TBS	tris-buffered saline
Tuj1	neuron-specific class III beta-tubulin
YAP	Yes-associated protein

1 Introduction

Mechanical cues from the cellular physical microenvironment are integrated as mechanical information and can trigger crucial biological processes. This process, known as mechanosensation, can affect cellular behavior on various levels such as differentiation, proliferation, migration, and even have the ability to induce stem cell differentiation without the need of chemical supplements (Blaschke et al., 2019; Engler, Sen, Sweeney, & Discher, 2006). Most important mechanical stimuli in living systems are topographical cues, mechanical strain, and stiffness. Each of them can have decisive consequences on the function of cells. In the brain, those three categories of mechanical stimuli control the homeostasis of the brain parenchyma and influence cells individually. *In vitro*, topographical cues alone can alter the fate decision of stem cells by mediating focal adhesion formation and geometrical-dependent cytoskeletal reorganization (**Figure 1.1**) (Baek et al., 2018). The stiffness of the culture substrates impacts the cellular morphology remarkably. For instance, changes in environmental stiffness can induce an increased branching of hippocampal neurons (Previtera, Langhammer, & Firestein, 2010). Altered cytoskeletal arrangements influenced by stiffness are even decisive for lineage commitment (Blaschke et al., 2019; Engler et al., 2006) (**Figure 1.1**) and can also determine how fast stem cells differentiate towards their desired fate (Blaschke et al., 2019). Thus, not only chemokines and growth factors, but also the surrounding mechanical environment can induce and change cytoskeletal arrangements (Ambriz, de Lanerolle, & Ambrosio, 2018) that change the behavior of exposed cells. Mechanical strain is mostly present due to pulsative movements around the vasculature, but also during brain development (Essen, 1997; Smith, 2009). In the following sections, tissue deformations due to cyclic physiological movements and their effect on cells embedded in the brain parenchyma are described in detail. Further, as the cytoskeleton of cells

responds to mechanical stimuli and also exerts forces to the surrounding microenvironment, the cytoskeleton is described in detail for each cell type categorically.

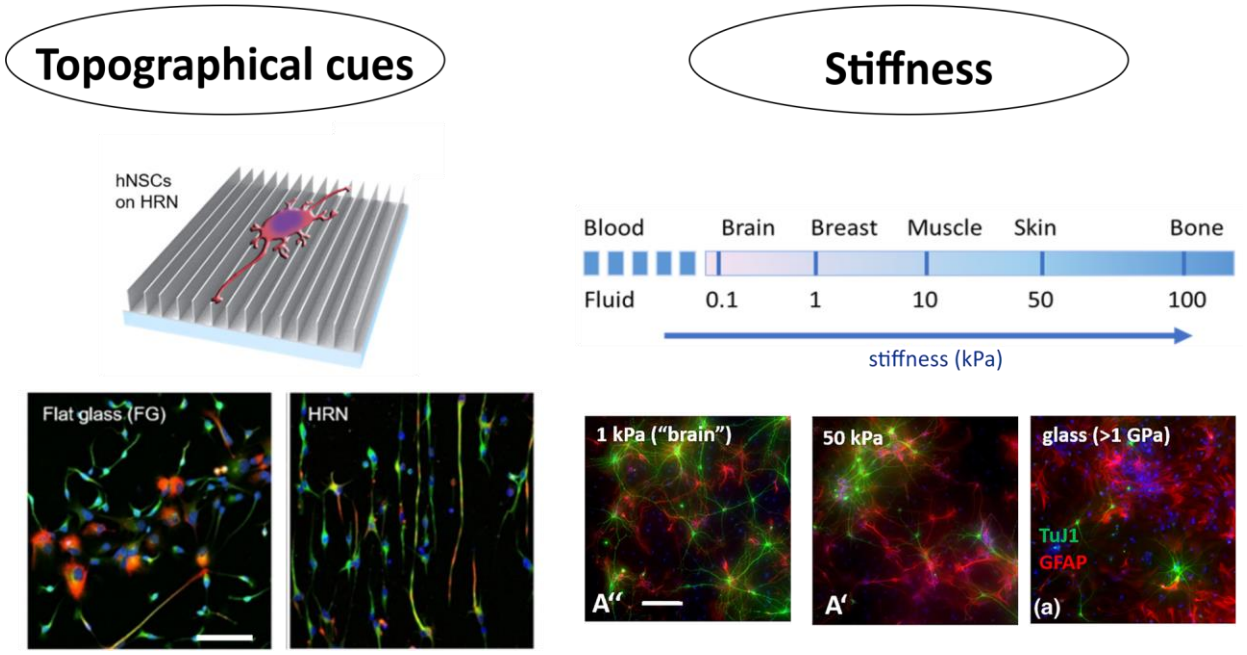

Figure 1.1: Mechanical cues change the fate of stem cells. Topographical cues and substrate elasticities are involved in important processes such as differentiation of stem cells to astrocytes (red) or neuronal cells (green). Stem cells show a different ratio of astrocytes and neurons when grown on nanogroove structure (left) or when changing the substrate stiffness (right). Images are adapted from (Baek et al., 2018; Blaschke et al., 2019; Chien, 2007). Scale bars = 100 µm.

1.1 Mechanics in the development of the brain

Mechanical forces play a fundamental role in the development of the brain. Cortical folding is an essential developmental process, allowing to attain a larger surface area relative to brain volume. Here, tensile forces trigger the formation of brain folds (Essen, 1997), either by differential degrees of expansion or through axons that interconnect cortical areas while the brain is growing (K. Franze, 2013). Mechanical strain is even observed on a cellular level. First postulated by Paul Weiss, nervous tissue growth is accompanied by mechanical forces along axon tracts (Weiss, 1941). Here, the extreme expansion of the nervous tissue results in stretched axon tracts that have already connected to their target cell. The stretch growth of integrated axons triggers the production of cytoskeletal components, axolemma, and other proteins to reduce the mechanical stress (Smith, 2009). Such a phenomenon is referred to as stretch growth and leads to mechanical

tension along the axon. A comparison by Smith illustrates the necessity of neuronal cells to bear mechanical loads during their development: he compares the extreme neuronal volume increase with the intense mass increase in cancer cells and further states that such a volume increase and growth velocity may only be possible when axons were stretched.

Likewise, in the spinal cord and for peripheral growing nervous tissue, neurons grow passively by being stretched due to different growth rates of bone and nervous tissue (Smith, 2009). By using engineered bioreactors (**Figure 1.2**) that apply mechanical tension during growth, axonal growth can be induced and reaches growth rates of up to 10 mm/day (J. R. Loverde, Tolentino, & Pfister, 2011) which is much faster than axonal growth of 1 mm/day without mechanical tension *in vitro*. Axons grown under mechanical tension show normal electrical activity, normal cell morphology, and the same density of organelles placed along the axon (J. Loverde & Pfister, 2015). Thus, neuronal cells may be well equipped to bear mechanical loads.

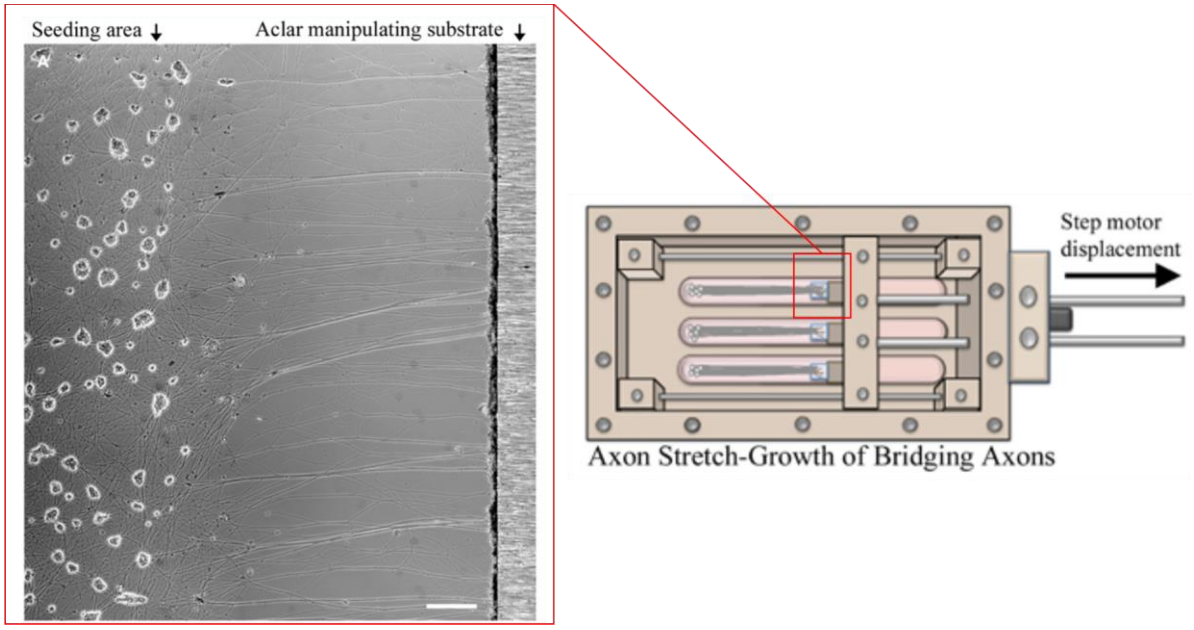

Figure 1.2: Stretch growth of integrated axon tracts. Neurons can form normal axons under tension. The bioreactor subject axons to mechanical tension during growth. Scale bar = 100 µm. Images adapted from (J. Loverde & Pfister, 2015).

1.2 Physiological strain present in the brain tissue

Cells embedded in the brain are daily subjected to mechanical stimuli: rapid movements of the human head can induce mild accelerations that deform the brain matter with strain and compression levels up to 5% (Bayly et al., 2005). Such deformations are based on the motion of the skull, followed by the movement of the brain's central mass while the base of the brain remains constrained. Accelerations resulting in 10-15% strain are experienced during extreme sportive activities such as when heading a soccer ball (Bayly et al., 2005; Bayly et al., 2002). When such head impacts occur more repetitively, there is a higher risk of developing neurodegenerative diseases (Smith & Stewart, 2020). The repetitive cause suggests that the brain tissue develops a 'mechanical memory', leaving a mechanical footprint after each repetition.

The brain has the top priority of blood supply: it gets 20% of the entire blood enriched with oxygen although it represents only 2% of the total body weight in humans (Jain, Langham, & Wehrli, 2010). Thus, despite extreme brain accelerations, physiological tissue strain levels originate also from continuous cyclic movements that result from blood flow through the highly vascularized brain tissue. At the resolution of magnetic resonance imaging, such movements were measured in a 2% range (Wedeen & Ponceleti, 2007) and can increase considerably when brain perfusion is triggered by neural activity. Neural activity causes localized alterations in blood flow and volume, leading to an increased diameter of the blood vessels (Drew, Shih, & Kleinfeld, 2011). To support the brain metabolic activity, such arterial dilatation can induce a tissue deformation amplitude of 30% in mice (Drew et al., 2011). Blood pressure acting on the vascular wall leads to the generation of mechanical stress tangential to the endothelial surface (Chien, 2007) (**Figure 1.3A**). The blood pulsation wave is continually acting on the vascular wall leading to cyclic movements and cyclic mechanical stress on nearby cells (**Figure 1.3B**). The tangential strain on nearby cells can lead further to transduction of mechanical signals and induce subsequent activation of critical biological processes that aim to rebalance the mechanical homeostasis of the cell (Discher, Janmey, & Wang, 2005). Such transduction of mechanical signals can be induced by mechanically activated ion channels (Ranade et al., 2014), or tension derived conformational changes and altered binding affinities of protein domains (Niediek et al., 2012).

A Cylic mechanical stretch

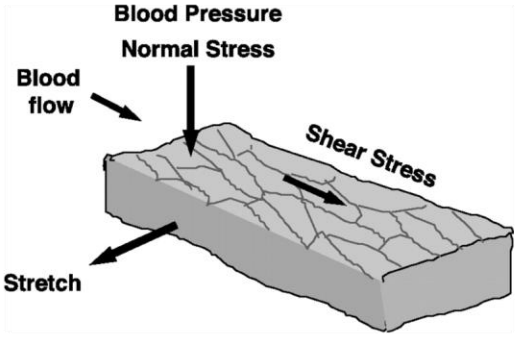

B Close proximity of cells to the vasculature

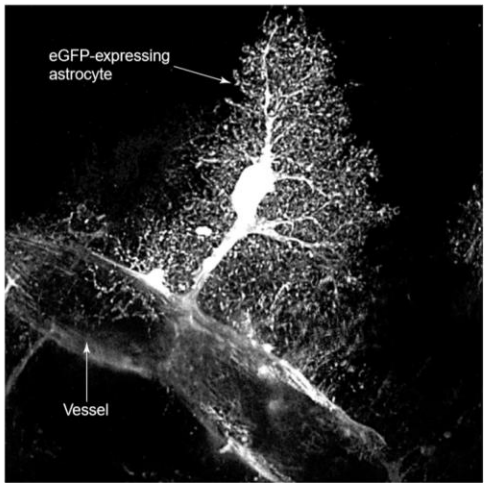

Figure 1.3 Cyclic mechanical tissue movement resulting from blood pulsation leads to mechanical stretch of cells in close proximity of the vasculature (Chien, 2007) (**A**). Cells are in close proximity to the cyclic deformations within the highly vascularized brain. Here an astrocyte wraps around a vessel with its endfeet (**B**) (Nedergaard, Ransom, & Goldman, 2003).

1.3 Cytoskeletal systems and their mechanical properties

Mechanical homeostasis and response to mechanical stimuli are based on the function of the cytoskeleton. Three main cytoskeletal systems are regulating intracellular tension: actin microfilaments, intermediate filaments, and microtubules. They are responsible for mechanical stability and elasticity and form highly complex and very dynamic protein networks. In this way, cells can respond to the changing physical microenvironment, always trying to survive and adapt. Besides, cytoskeletal filaments are involved in intracellular transport mechanisms, cell migration, and cell division. Each of the three cytoskeletal systems has its specific physical property.

1.3.1 Actin filaments

Actin filaments, also termed microfilaments, produce the smallest of the cytoskeletal filaments with a diameter of only 7 nm. Actin monomers (G-actin) are the building units of microfilaments that accumulate to form filamentous actin (F-actin). Filaments show a polarized structure, as its formation can occur on both ends simultaneously but with different polymerization velocities. After G-actin is incorporated in a filament, its bound adenosine triphosphate (ATP) is hydrolyzed to adenosine diphosphate (ADP). As a consequence, most of the filament constitutes F-actin ADP,

while F-actin ATP is found on the ends of the filaments. The F-actin ATP end is called the plus end; here, the polymerization velocity is faster than at the minus end. Actin filaments can form a dense, three-dimensional network located under the plasma membrane, which is termed 'cortical actin'. The function of the cortical actin is control of cell shape, and the organization as well as positioning of transmembrane proteins. Cortical actin is linked to the plasma membrane via membrane anchoring proteins (Bretscher, Edwards, & Fehon, 2002). Actin can form various structures of higher order. Most importantly, densely branched actin networks are mainly found in lamellopodia; parallel aligned actin filaments are present in filopodia as finger-like extensions of the plasma membrane. Furthermore, contractile actin bundles, known as stress fibers, are formed (**Figure 1.4**). Stress fibers are 10-30 bundled actin filaments and have a crucial function in cellular contractility. With the help of myosin motor proteins, the filaments can slide past each other and thereby provide forces necessary for cell adherence, migration, and mechanotransduction that allow the cell to sense the physical environment (Ingber, 2008). ATP hydrolysis induces a conformational change in myosin and thereby a movement of the actin filament relative to the myosin head and generation of displacement by 5-25 nm (Kumar et al., 2006). To generate forces, the stress fibers require to be structurally linked. Therefore, large protein assemblies called focal adhesions, anchor the stress fibers to the cell cortex and the cell exterior. Crosslinking proteins allow the formation of three-dimensional networks.

Actin filaments are described as non-rigid structures. However, due to their ability to be highly crosslinked, they can form highly organized, stiff structures (Fletcher & Mullins, 2010). Therefore, actin filaments are even described to show the greatest resistance to stress (Janmey, Euteneuer, Traub, & Schliwa, 1991).

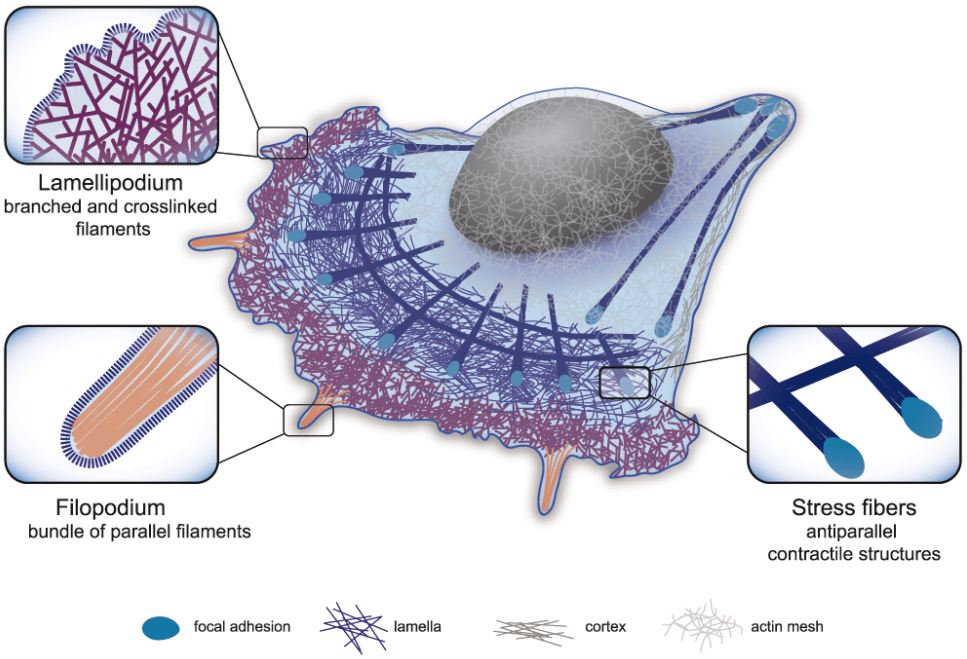

Figure 1.4: Cellular actin organization in lamellopodia, filopodia, and stress fibers (Letort, Ennomani, Gressin, Théry, & Blanchoin, 2015).

1.3.2 Intermediate filaments

The name of intermediate filaments is derived from its diameter of 8-12 nm, which is between the diameter of microfilaments and that of microtubules. Intermediate filaments are cell type-specific and vary greatly in their primary structure, but show common structural and sequence features. They are the least stiff and can resist tensile forces effectively (Fletcher & Mullins, 2010). Intermediate filaments are thought to maintain the basic integrity, contribute to the cell's stability, and ensure a rapid adaptation to intracellular processes (Janmey et al., 1991). The flexible nature of intermediate filaments prevents the cell from being damaged by moderate deformations. In contrast to microtubules and microfilaments, intermediate filaments do not show a polarity as their subunits are organized yet in an antipolar manner. The unique composition of monomers and folding and unfolding of its α-helices are responsible for its elastic properties (Block et al., 2018). Besides its role in achieving flexible properties to the cell, intermediate filaments also have a fundamental role in regulating the polarity in migrating cells (Bernal & Arranz, 2018).

Based on their protein structure and tissue distribution, intermediate filaments are subdivided into six types. Although they are generally very heterogeneous in protein size and tertiary structure, they are characterized by a central α-helical rod domain as a conserved structural motif. This domain is responsible for filament assembly, while head and tail domain, with various length and sequence compositions, are individual and determine specific and diverse functions of the filaments (Loschke, Seltmann, Bouameur, & Magin, 2015). Filament assembly is established first by the formation of dimers, where the central rod domains form a coiled-coil structure (**Figure 1.5**). Then the dimers form tetramers in an anti-parallel fashion. The soluble tetramers are further associated head to tail into protofilaments that pair to form protofibrils. The final intermediate filaments are made of four protofilaments that wind together (Herrmann & Aebi, 2016). To achieve a high resistance towards an ever-changing extracellular environment, the intermediate filament network is dynamic and shows continuous remodeling and filament turnover without failure and disruption of the cytoskeletal network (Windoffer, Beil, Magin, & Leube, 2011).

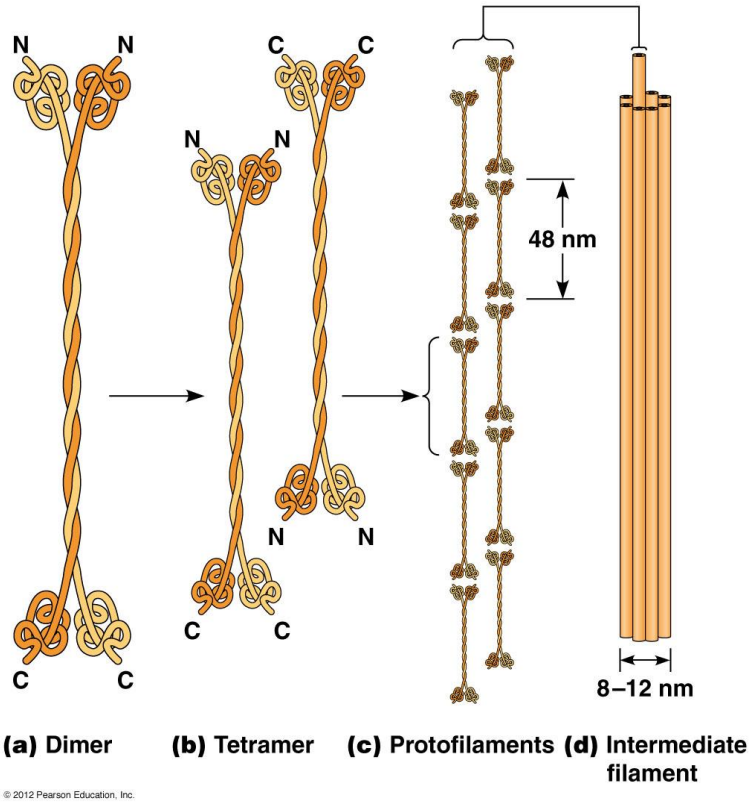

Figure 1.5: Intermediate filament assembly. Image from Becker's World of the Cell, 8th edition (Hardin, Bertoni, & Kleinsmith, 2017).

1.3.3 Microtubules

Microtubules are the stiffest of the three cytoskeletal proteins (Fletcher & Mullins, 2010). Several heterodimer blocks of α- and β-tubulin are forming a hollow microtubule tube of 15-25 nm diameter and a length of 10-100 µm. They exhibit essential roles in the stability and integrity of cells, intracellular trafficking, and cell division. In contrast to intermediate filaments, actin and tubulin can adapt dynamically within seconds after a mechanical signal is present (Ambriz et al., 2018). Although microtubules are regarded as the stiffest cytoskeletal filament, microtubules have very dynamic assembly and disassembly kinetics, also known as 'dynamic instability' (Kapitein & Hoogenraad, 2015). *In vitro*, microtubules are polar with a fast-growing plus-end and a slow-growing minus-end (**Figure 1.6**). *In vivo*, the plus end displays rapid growth and shortening and therefore explores the cellular space, while the minus end is often linked to a microtubule-organizing center and, therefore, non-dynamic (Akhmanova & Hoogenraad, 2015). The plus end assembly or disassembly can be influenced by binding of microtubule adaptor proteins such as motor proteins (Bringmann et al., 2004), post-transcriptional modifications (Magiera & Janke, 2014), microtubule-associated proteins, and plus-end tracking proteins (Kevenaar & Hoogenraad, 2015). The latter are proteins that are recruited to and follow the growing tips of growing microtubules (Jennetta W. Hammond, Cai, & Verhey, 2008). Several post-transcriptional modifications influence function and stability of microtubules (Jennetta W. Hammond et al., 2008). Such modifications are accumulated on stable microtubule structures, as mostly they occur on polymerized tubulin and not on single tubulin units. Tyrosinated microtubules in neurons are involved in neuronal extension and recruitment of plus-end tracking proteins. In contrast, acetylated microtubules are mostly found in stabilized microtubules and are involved in motor-based trafficking (Jennetta W. Hammond et al., 2008). For example, acetylation of tubulin can trigger the localization of motor proteins, such as kinesin-1 to microtubule filaments (J. W. Hammond et al., 2010).

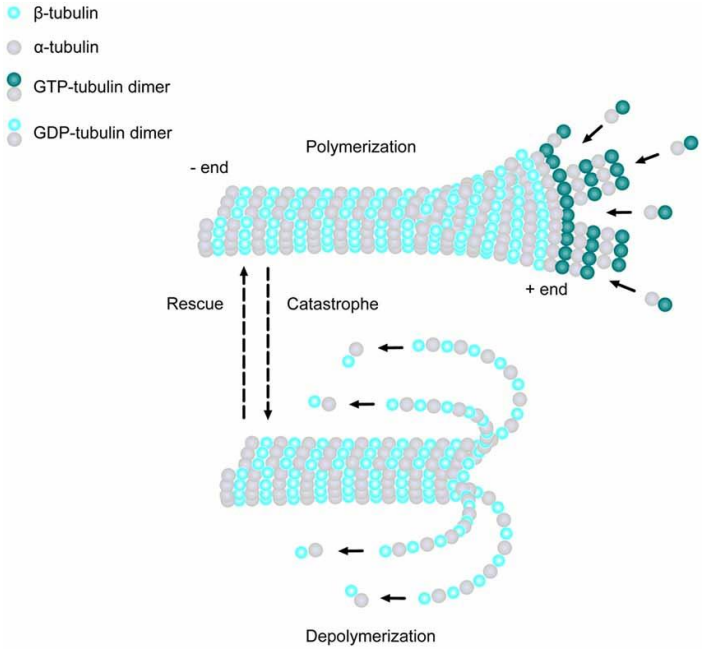

Figure 1.6: Microtubules structure and dynamics (Lasser, Tiber, & Lowery, 2018).

The three major cytoskeletal filament networks are involved in mechanical stability and diverse cellular functions. Although the three cytoskeletal elements are made of distinct proteins, they are in constant communication and interaction with each other. The presence of adaptor proteins enables crosstalk between the three main components of the cytoskeleton. One of them is plectin, exhibiting unique cytoskeletal linker abilities as it can interact with a variety of cytoskeletal structures such as microfilaments, intermediate filaments, and microtubules and is essential for the positioning and organization of the cytoskeleton (Wiche, 1998).

1.4 The influence of cyclic mechanical deformations on mammalian cells

Mechanotransduction can induce cytoskeletal adaptation in mammalian cells. Adaptor proteins such as vinculin and p130Cas can act as mechanotransducer (Niediek et al., 2012). Both proteins undergo a conformational change under mechanical force leading to exposure of relevant protein domains to the protein surface (Geiger, 2006). This change promotes phosphorylation of p130Cas

by Src family kinases and, therefore, integrin-mediated mechanotransduction. Niediek et al. show that a deletion of p130Cas results in a significant reduction of cytoskeletal reorientation. Further, actin filaments itself can sense tension across the filaments and thereby act as a force sensor. Here, tension modulates the affinity of different actin-binding partners, such as a higher affinity to myosin and lower affinity to cofilin (Galkin, Orlova, & Egelman, 2012).

Cyclic deformation induces an adaptation of cell shape and cytoskeletal structures to minimize intracellular strain. The first mechanoresponse is an actin reorganization (**Figure 1.7**) by disruption and rearrangements of actin fibers but also formation of new microfilaments. This reorientation is followed by microtubules and intermediate filaments, which have much slower reorientation dynamics (Zielinski et al., 2018). Further, cytoskeletal reinforcement resulted in an increased number of stress fibers and increased coupling to adhesion structures (Faust et al., 2011).

The pace and degree of reorientation depend on the mechanical parameter: amplitude, frequency, duration, and stretch waveform (Tondon, Hsu, & Kaunas, 2012). Mechanical stimuli of the physical environment can be sensed by the cell through focal adhesions. These multi-protein complexes link the cell interior cytoskeleton to the extracellular microenvironment. Here, as transmembrane proteins, the integrin family plays the fundamental role as they bind to specific proteins of the extracellular matrix and are also linked on the cell interior side with actin filaments through adaptor proteins (Hynes, 2002). Coupling of the cell's interior cytoskeleton to the exterior extracellular matrix allows the cell to exert forces to its microenvironment and, in return, to sense mechanical stimuli of their extracellular physical environment they encounter. In general, cells react to mechanical loads transduced from the environment, by counteracting and exerting forces via the actomyosin cytoskeleton. The reason for such mechanoresponse is the cell's strive to generate mechanical homeostasis (Discher et al., 2005). To avoid further mechanical imbalance due to cyclic mechanical strain, cells restructure their cytoskeleton where minimal mechanical loads are present that is: perpendicular to uniaxial cyclic strain (Faust et al., 2011). The reorientation process is a necessary, vital mechanism that is essential for functional tissue integrity (Discher et al., 2005; Zielinski et al., 2018).

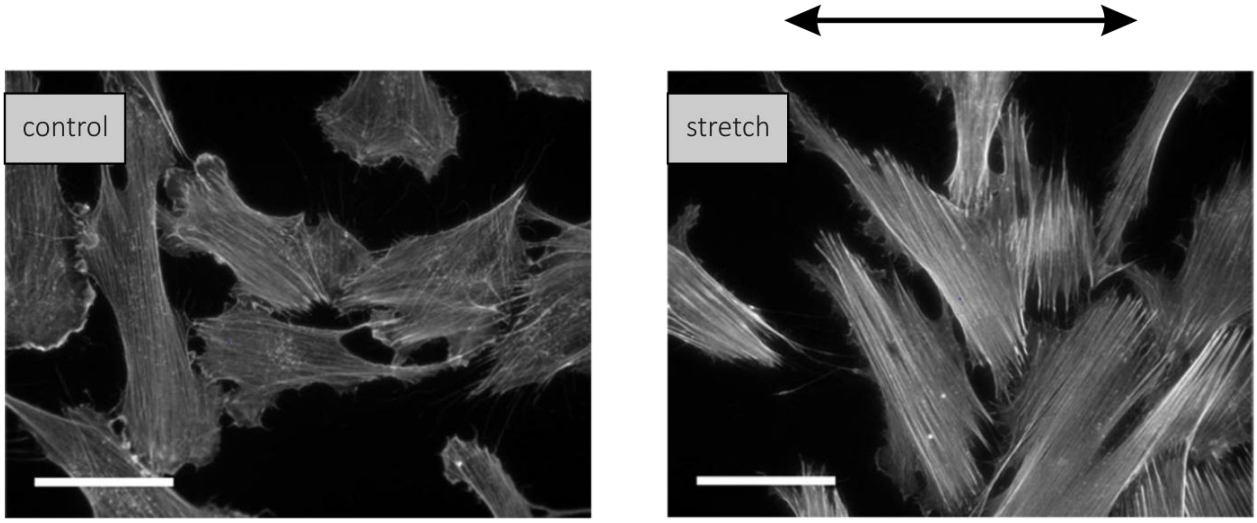

Figure 1.7: Cell orientation upon cyclic stretch. Human umbilical cord fibroblasts were stretched with an amplitude of 14% for 16 hours before fixation and labeling for actin. The black arrow indicates the stretch direction. Scale bar = 50 µm. Images adapted from (Faust et al., 2011).

1.5 The cytoskeleton of neural stem cells and interaction with the microenvironment

Within their stem cell niche, neural stem cells (NSCs) reside and are maintained by their unique extracellular environment in the self-renewal state. Here, essential factors responsible for sustaining the niche environment include the interaction of NSCs with other cell types, interaction with the extracellular matrix, as well as soluble factors. (McMurray, Dalby, & Tsimbouri, 2015). The neural stem cell niche is a highly vascularized microenvironment allowing stem cells to be supplied by relevant biological and chemical cues (e.g. growth and proliferation factors). The close proximity to pulsating movements resulting from the blood flow through the niche vasculature also suggests considering cyclic strain as a mechanical cue that resides in the niche microenvironment. Thus, mechanical strain may maintain the behavior of NSCs as a biological relevant mechanical stimulus.

Two fundamental characteristics of neural stem cells are self-renewal and differentiation. In both processes, the cytoskeleton plays a fundamental role. *In vivo*, stem cell proliferation is responsible for maintaining the neural stem cell pool, while dividing cells results in one stem cell and one differentiating cell when division is asymmetrically (McMurray et al., 2015). *In vitro,* NSCs can be

manipulated to remain in a stem cell stage leading to a homogenous rapid dividing cell population. By the addition of a mitogen factor, such as fibroblast growth factor, symmetrically dividing is induced, which produces identical daughter cells. Cell spreading and intracellular tension are described to directly influence cell proliferation rate (McMurray et al., 2015). Thus, the NSC cytoskeleton has a crucial and central role in stem cell biology.

The cytoskeleton of NSCs comprises actin filaments, microtubules, and intermediate filaments. Actin filaments play a central role in NSC cell migration as they can provide the major driving force for cell motion. Thereby actin polymerizes in cell protrusion and also has a role in formation and maturation of cell-adhesive structures (Etienne-Manneville, 2013). Nevertheless, microtubules also take part in cell migration. Here, microtubules modify cell membranes, interconnect with the other cytoskeletal proteins, control cell polarity, influence adhesive structures, and control their dynamics (Etienne-Manneville, 2013). Despite actin and microtubule, intermediate filaments are also involved in cell migration. Here, they are key players to maintain polarity for cell migration and are also dynamically reorganized during the process (Leduc & Etienne-Manneville, 2015). Cell migration is a crucial process in the development of the nervous tissue, as mostly the position of the premature neuron differs from their terminal destination. NSCs find their target cells through cytoskeletal rearrangement in response to extracellular guidance cues, which can be of chemical but also of mechanical nature (Kristian Franze, 2018).

An NSC-specific cytoskeletal marker is its intermediate filament nestin. The cytoskeletal filament nestin is implicated in survival and the self-renewal process of NSCs (Park et al., 2010). Once cells become differentiated, nestin is downregulated, while other tissue-specific intermediate filaments are upregulated (Park et al., 2010; Wiese et al., 2004). Due to the short N-terminus, which is essential for filament assembly, nestin is unable to polymerize itself and needs the implication of other intermediate filament proteins such as vimentin to form intermediate filaments (Park et al., 2010; Steinert et al., 1999). Besides nestin, vimentin is highly expressed in NSCs, while other intermediate filament members of class III and IV are absent (Park et al., 2010). Although nestin is unable to form filaments, nestin also has important functions to regulate the dynamics of other intermediate filaments. For example, during mitosis, nestin is depolymerized and reincorporated into the intermediate filament network in the G1 phase, while the

disassembly of vimentin is regulated by nestin (Chou, Khuon, Herrmann, & Goldman, 2003). Interestingly, knockout of nestin revealed an induced apoptotic behavior without deficiency in proliferation or differentiation, showing that nestin has relevant functions in NSCs' survival. However, knockout of vimentin does not lead to the same phenotype and therefore indicates that NSC's survival is not dependent on nestin's integration into the cytoskeletal network (Park et al., 2010).

1.5.1 Cell adhesion complexes in the neural stem cell niche

Stem cell renewal is controlled by signals from the niche extracellular environment (S. Chen, Lewallen, & Xie, 2013). Interactions of cell adhesion molecules and the extracellular matrix allow cells to generate tension and to transduce mechanical cues to the cell's nucleus (McMurray et al., 2015). NSCs express high levels of integrin and cadherin and are thereby linked to the surrounding physical microenvironment (Karpowicz et al., 2009). To remain in the stem cell niche and, therefore, supplied by regulating factors, NSCs are anchored via adhesion molecules to other cells of the niche or to the extracellular environment (S. Chen et al., 2013). Such adherence can be integrin or cadherin-mediated (**Figure 1.8**). Cadherins that are abundant in NSCs are E-cadherin and N-cadherin, which can mediate signaling processes via sequestering of α/β catenin complexes. To cluster integrin molecules, integrins interact with the actin cytoskeleton via talin. Integrins consist of α- and β-subunits and form transmembrane proteins responsible for NSC-matrix interaction. On the extracellular side, integrins can interact with extracellular matrix molecules such as laminin, collagens, and fibronectin (Chien, 2007). In addition, other proteins are also suggested to mediate cell adhesion, including gap junctions, Notch receptors, and membrane receptors such as c-Kit and CD44 (**Figure 1.8c**). The communication with the extracellular environment can influence self-renewal, survival, and differentiation of NSCs (Karpowicz et al., 2009).

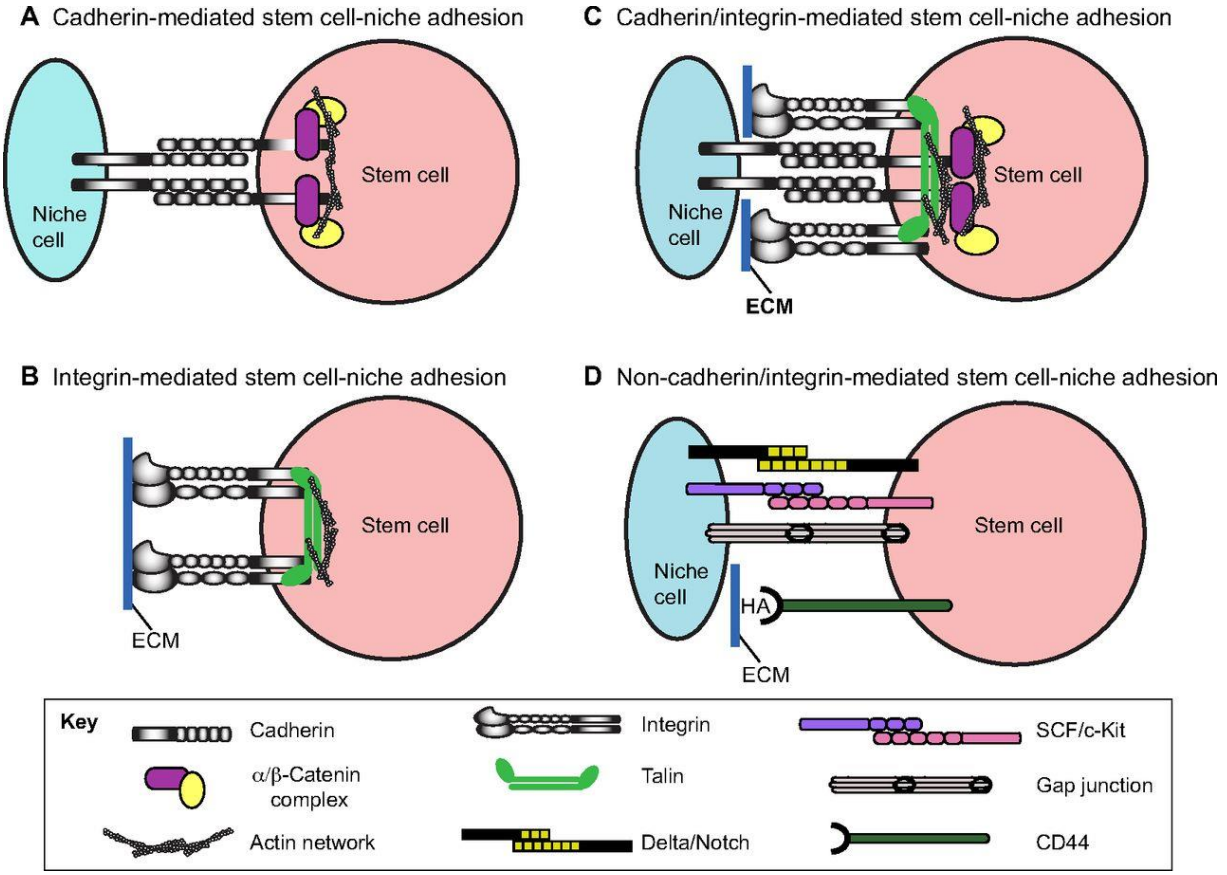

Figure 1.8: NSC cell adherence in the stem cell niche (S. Chen et al., 2013).

1.6 Cytoskeletal changes in the development of neural stem cells to a neuronal phenotype and astrocyte

As previously described, an asymmetric cell division results in one cell that maintains the stem cell pool, while the other is committed to differentiation. For neural stem cells, lineage commitment means they can either develop to a neuronal phenotype, an astrocyte, or an oligodendrocyte. Neurons' primary functions are the transmission, processing, and storage of information. Astrocytes reveal more or less a 'housekeeping' function within the brain as they are involved in ion homeostasis, supply neurons with nutrients, recycle neurotransmitters and remove metabolic byproducts (Potokar et al., 2007).

During differentiation, stem cells adapt their cellular shape but also their cytoskeletal organization. Stem cells become stationary when they differentiate as they reduce cell migration

(Sliogeryte, Thorpe, Lee, Botto, & Knight, 2014). This migration reduction is associated with increased expression of proteins that link the cortical actin to the plasma membrane and slower actin turnover. Further, the actin cytoskeleton is rearranged to form a well-defined actin fiber pattern (Ambriz et al., 2018). In more detail, the cytoskeleton of undifferentiated NSCs contains semistructured, micrometer-sized actin-spectrin-adducin patches in comparison to terminally differentiated neurons, astrocytes, and oligodendrocytes, where the periodicity is long-ranged and show actin-spectrin-adducin periodicity throughout the cytoplasm (Hauser et al., 2018).

Intermediate filaments are constantly remodeled during differentiation, and certain subsets of proteins are expressed in a defined period of time (Bernal & Arranz, 2018). One fundamental change in the cytoskeleton of NSC towards a differentiated cell is the downregulation of nestin (Park et al., 2010), while expression of neurofilaments is upregulated and an expression of glial fibrillary acidic protein (GFAP) replaced nestin in astrocytes (J.-S. Kim et al., 2011).

1.6.1 The organization of the neuronal cytoskeleton

Neurons have a unique cytoskeleton. Their cytoskeletal morphology reveals neuronal processes that contain an actin cortex and are filled with bundled microtubules and neurofilaments (**Figure 1.9**). Such processes termed neurites can either develop to an axon or several dendrites. The axon is the dominating extension sending information from the soma to the target cells, while dendritic branches receive and integrate synaptic signals. Microtubules play a crucial part in the neuronal cytoskeleton. Beside their function in cell integrity and stability, microtubules serve as tracks for long-distance transport and thereby distribute cellular components from the cell soma to synapses (**Figure 1.9A)**. The neuronal cargo transported via microtubule tracks includes cell organelles, synaptic vesicle precursors, receptors, mRNA, and cell adhesion molecules (Kapitein & Hoogenraad, 2015). Furthermore, microtubules also play essential roles in elongation, pathfinding, and neuronal branching (Suter & Miller, 2011). Microtubule-associated proteins (MAP) such as tau or MAP-2 can stabilize the microtubule cytoskeleton.

Neurofilaments are the intermediate filaments specific to neurons. They are particularly abundant in neurons and thereby provide structural support to the long, thin extensions which

can even reach a size over a meter in length. Another functional property of neurofilaments is its control in axonal conductance via defining the axonal diameter. Neurofilaments are subdivided into four types: neurofilament light (NFL), neurofilament medium (NFM), neurofilament heavy (NFH), and α-internexin. Neurofilament proteins belong to class IV intermediate filaments. While α-internexin can assemble to filaments itself, neurofilaments copolymerize to form heteropolymers.

While neurofilaments and microtubules represent the central part of the neuronal processes, actin resembles periodically spaced rings underneath the plasma membrane, which are connected by spectrin (**Figure 1.9B**). The axon initial segment and presynaptic boutons control and fine-tune action potentials that are traveling from the soma to the synaptic endings. Such control is enabled through a distinct organization of membrane channels, adhesion proteins, and cytoskeletal structure.

The leading tip of dendritic and axonal structures, the growth cone, is highly motile and defines the speed and direction of neuronal outgrowth. Growth cone advancement is accompanied by a retrograde actin flow, which results from actin polymerization at the leading tip and a pulling backward of these actin filaments by myosin motors. Such cytoskeletal movements are responsible for force generation during neuronal growth and able to push the leading tip forward. Growth cones express receptors for repulsive or attractive guidance cues. This information is then used to steer the growth cone advance and induce a directional movement towards the target cells (Grzywa, Lee, Lee, & Suter, 2006). The actin filament is the major cytoskeletal element in the growth cone and responsible for proper guidance; microtubules are giving structural support and support in axonal elongation.

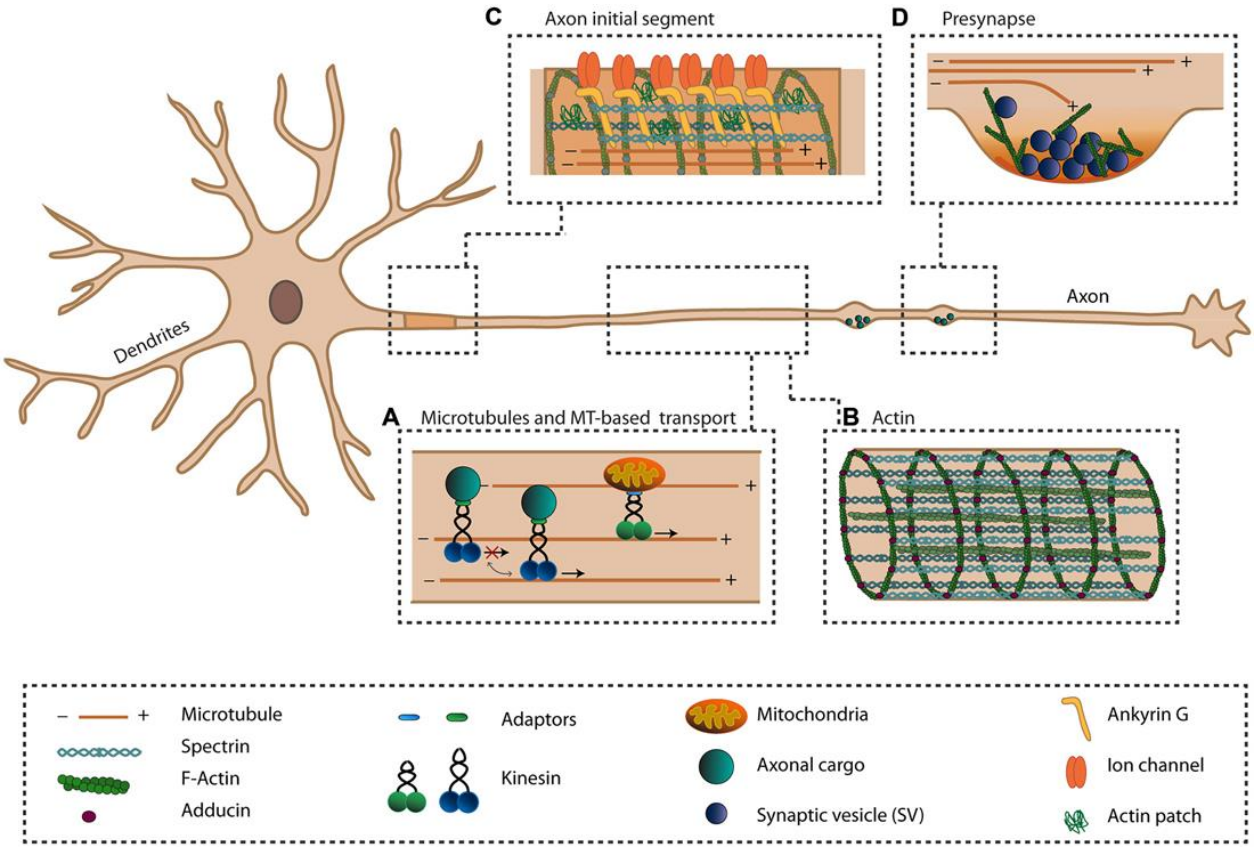

Figure 1.9: The organization of the neuronal cytoskeleton. Microtubules provide support for anterograde and retrograde transport (A). Actin forms a periodically spaced ring-like structure. The axon has several specialized structures: axon initiation segment (C) and presynaptic buttons (D) (Kevenaar & Hoogenraad, 2015).

1.6.2 The cytoskeleton of astrocytes

Astrocytes are actively involved in neuronal functions. They secrete several neurotransmitters, express receptors for neuroactive substances, are involved in ion homeostasis, and can also act as topographical structures to guide migrating neurons (Galou et al., 1997). Furthermore, astrocytes control the number of synapses (Christopherson et al., 2005) and can also regulate the blood flow within the brain (Stobart & Anderson, 2013). *In vivo*, astrocytes have fine cellular extensions and thereby a bristly appearance (**Figure 1.10**). Astrocytes are interconnected via gap junctions that form multicellular networks and allow the distribution of metabolites and ions with long distances (Sofroniew & Vinters, 2010).

For astrocytes, GFAP and vimentin are the most abundant intermediate filaments (Galou et al., 1997). Intermediate filaments in astrocytes contribute to astrocyte motility and activation. In response to many CNS pathologies, astrocytes show an altered activated phenotype. An indication of active astrocytes is an upregulation of intermediate filaments, particularly GFAP, but also reexpression of nestin (Lin, Matesic, Marvin, McKay, & Brüstle, 1995). The activation of astrocytes –also known as reactive astrogliosis- plays an important role in the healing process, yet it is also linked to glial scar formation, a change in the extracellular environment of the brain interfering with its regeneration capacity (Moeendarbary et al., 2017).

Interestingly, astrocytes are closely interacting with blood vessels and thereby regulate the CNS blood flow and vascular diameter (**Figure 1.10**). They are suggested to be the blood flow regulating element in response to neural activity (Iadecola & Nedergaard, 2007; Sofroniew & Vinters, 2010).

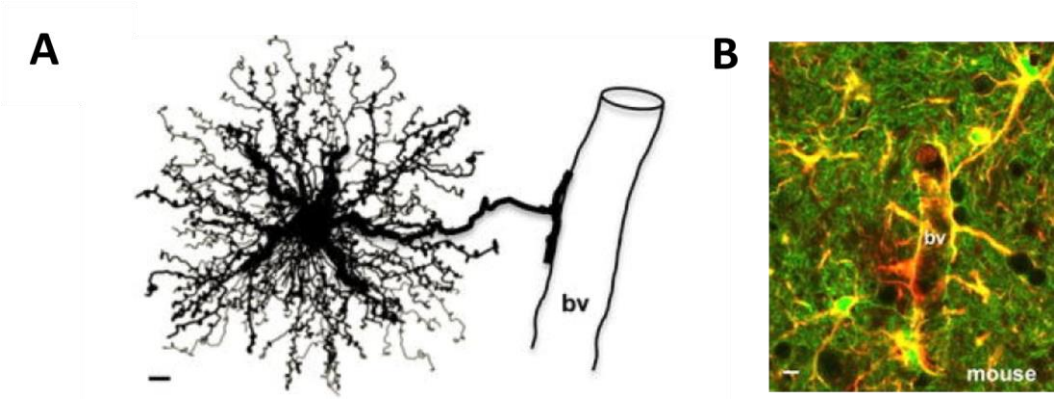

Figure 1.10: Astrocyte morphology. Astrocytes show very finely branched processes and are closely interacting with blood vessels (A). Scale bar = 3 µm. Astrocytes in mouse gray matter stained for GFAP (red) and transgene derived GFP reporter molecule to visualize fine astrocyte extensions which are not stained by the GFAP antibody (B). Scale bar = 7.5 µm. Pictures adapted from (Sofroniew & Vinters, 2010).

1.7 Aim of the thesis

As introduced in the current chapter, cells of the CNS exhibit a unique cytoskeleton. Neuronal cells do not share common features with cells that are constantly exposed to cyclic deformation, such as endothelial cells. Nevertheless, neurons and glial cells reside very close to the brain vasculature and are thereby exposed to physiological strain. The thesis aims to study the responses of brain cells to cyclic mechanical strain and to analyze their responses based on their unique cytoskeleton. Cell responses were assessed according to changes in their morphology and composition of cytoskeletal elements. One hypothesis is that neuronal cells may be more sensitive to strain due to their unique composition of the cytoskeleton.

It is well known that mammalian cells under cyclic mechanical strain reorient their cell shape and cytoskeleton. Cyclic stretch induces a reorientation of the actin cytoskeleton in mammalian cells, followed by reorientation of the two other cytoskeletal filament systems: the microtubule cytoskeleton and intermediate filaments. Considering a different cytoskeletal setup of cells in the CNS, how can they bear mechanical loads and respond to mechanical strain? To answer this question, cells of the CNS should be investigated according to their reorientation behavior in terms of the responses of different cytoskeletal systems.

As cells of the CNS are embedded in soft material *in vivo*, one aim was first to investigate the vitality of stretched cells on elastomer substrates. Furthermore, several amplitudes should be tested to select a suitable stretch parameter that shows a stretch response but does not induce cell apoptosis or cell death.

As the cytoskeletal composition differs between CNS cell types and undergoes several changes along the way from a stem cell to a differentiated cell, distinct developmental stages will be considered in stretch experiments. Cyclic stretch experiments will address immediate responses of distinct cells to cyclic mechanical strain, but also adaptations to long-term mechanical loads will be assessed.

Furthermore, the microtubules have a central role in neuronal cells as they are spanning throughout the neuronal branches providing structural support. The microtubule cytoskeleton is the stiffest cytoskeletal component, however, it can react very dynamically to environmental

changes. Due to the central role of microtubules, this thesis should investigate the microtubule cytoskeleton and its response to cyclic stimuli in neuronal cells. In line with this, microtubules are also involved in neuronal outgrowth, tension generation along the axon (Mutalik, Joseph, Pullarkat, & Ghose, 2018), and are possibly involved in failed regeneration in neuronal cells (Ertürk, Hellal, Enes, & Bradke, 2007). Moreover, it is suggested that stabilization of the microtubule cytoskeleton may be a promising target to interfere with neuronal degeneration progression (Hellal et al., 2011). The mechanoresponse of the microtubule cytoskeleton is therefore relevant to further recognize responses of neuronal cells to extracellular physical stimuli. This will allow to better understand what impact mechanical cues may have on neuronal tissue regeneration. The hypothesis is that the dynamics of microtubules may be changed due to cyclic stretch. Posttranscriptional modifications should be addressed and analyzed after cyclic stretch.

Mechanical strain is a crucial parameter throughout the development of the brain. An involvement of stiffness and topography on neural stem cells was previously characterized (Baek et al., 2018; Blaschke et al., 2019; Hersch et al., 2013). However, the involvement of mechanical strain has not been analyzed previously and will be investigated in this thesis. Further, as mechanical cues are well described to have a tremendous influence on the fate of stem cells in lineage commitment, mechanical strain in developmental processes will be investigated. Stem cell differentiation can be very sensitive to the physical extracellular surrounding. It is even suggested that sensitivity to mechanical cues has a certain temporal window where it can impact neurogenic commitment (Rammensee, Kang, Georgiou, Kumar, & Schaffer, 2017). One hypothesis is that stem cell lineage commitment may also be influenced by mechanical strain as a stimulus. Thus, in this study, cyclic stretch experiments were therefore performed with cells that were still in the stem cell stage and also during the differentiation process from stem cell stage to a neuronal or astrocytic phenotype.

2 Material and Methods

2.1 Material

2.1.1 Hardware

2.1.2 Consumable Materials

Hardware	Company
Cell culture dish 35 x 10 mm	Greiner Bio-one, Frickenhausen, Germany
Cover slip ø 12 mm #1; 25 mm #0	Menzel, Braunschweig, Germany
Immersions oil 518 F	Carl Zeiss, Jena, Germany
Microscope slides, plain	Brand, Werlheim, Germany
Parafilm	VWR, Darmstadt, Germany
PCR plates and seals	VWR, Darmstadt, Germany
Petri dish 3.5 cm with predrilled 2.5 cm holes	Cell E&G , San Diego, USA
Pipette tips (10 µL, 200 µL, 1250 µL)	StarLab, Hamburg, Germany
Reaction tube 1.5 mL, 2 mL	Eppendorf, Wesseling/Berzdorf,Germany
Reaction tube 15 mL, 50 mL	Greiner Bio-one, Frickenhausen,Germany
Whatman, Lens cleaning tissue 100 x 150 cm	GE Healthcare, Freiburg, Germany

2.1.3 Chemicals/ kits

Chemical	Company
Avidin	Thermo Fisher Scientific, Massachusetts, USA
B-27 Supplement	Thermo Fisher Scientific, Massachusetts, USA
β-mercaptoethanol	Merck, Darmstadt, Germany
Bovine serum albumin	Merck, Darmstadt, Germany
Bromodeoxyuridin (BrdU)	Fluka, Munich, Germany
1,4-diazabicyclo[2.2.2]octane (DABCO)	Sigma, Taufkirchen, Germany
DMEM	Thermo Fisher Scientific, Waltham, USA
Ethanol, absolute	Merck, Darmstadt, Germany

Chemical	Company
Ethylenediaminetetraacetic acid (EDTA)	Sigma, Taufkirchen, Germany
Ethylene glycol tetra-acetic acid (EGTA)	Sigma, Taufkirchen, Germany
Fibroblast growth factor	Invitrogen, Karlsruhe, Germany
FIX and PERM Cell Fixation and Cell Permeabilization Kit	Thermo Fisher Scientific, Waltham, USA
Fluoromount Aqueous	Sigma, Taufkirchen, Germany
Formaldehyde 37%	Merck, Darmstadt, Germany
Gentamicin (50 mg/mL)	Sigma, Taufkirchen, Germany
GlutaMAX Supplement (100X)	Thermo Fisher Scientific, Waltham, USA
L-Glutamine	PAN-Biotech, Aidenbach, Germany
Glycine	Sigma, Taufkirchen, Germany
Hank's Balanced Salt Solution (HBSS)	Thermo Fisher Scientific, Waltham, USA
4-(2-hydroxyethyl)-1 piperazineethanesulfonic acid (HEPES)	Sigma, Taufkirchen, Germany
Hibernate-E Medium	Thermo Fisher Scientific, Waltham, USA
Hoechst 33342	Biochemica, Billingham, United Kingdom
Hydrochloric acid	Carl Roth, Karlsruhe, Germany
Isopropanol (2-propanol)	Merck, Darmstadt, Germany
Kapa Sybr Fast	Kapa Biosystems, Wilmington, Waltham, USA
Laemmli loading buffer	Bio-Rad, Hercules, USA
LIVE/DEAD Cell-Mediated Cytotoxicity Kit	Life Technologies, Darmstadt, Germany
Magnesium chloride ($MgCl_2$)	Sigma, Taufkirchen, Germany
MES (2(N-Morpholino)-ethanesulfonic acid)	Sigma, Taufkirchen, Germany
Neurobasal Medium (1X)	Thermo Fisher Scientific, Waltham, USA
Normal Goat Serum	Vector Laboratories, Peterborough, UK
MitoTracker Red CMX Ros	Invitrogen, Eugene, USA
Milkpowder	Roth, Karlsruhe, Germany
N2 supplement	Gibco, Karlsruhe, Germany
Penicillin-Streptomycin	PAN-Biotech, Aidenbach, Germany
Phosphate-Buffered Saline (PBS) pH 7.2	Thermo Fisher Scientific, Waltham, USA

Chemical	Company
Poly-L-lysine solution Mol wt 150,000-300,000; 0.01%	Sigma, Taufkirchen, Germany
Protease inhibitor cocktail	Sigma, Taufkirchen, Germany
Quantitect reverse transcription kit	Qiagen Hilden, Germany
RIPA buffer	Sigma, Taufkirchen, Germany
Skim milk powder	Sigma, Taufkirchen, Germany
Sodium chloride	Sigma, Taufkirchen, Germany
Sodium pyruvate	Gibco, Karlsruhe, Germany
Sylgard® 184 silicone elastomer kit (PDMS)	Dow Corning, Wiesbaden, Germany
Tris(hydroxymethyl)aminomethane	Sigma, Taufkirchen, Germany
Triton-X-100	Sigma, Taufkirchen, Germany
TRIzol™ Reagent	Thermo Fisher Scientific, Waltham, USA
Trypsin-EDTA, 0.05% trypsin 0.2% EDTA	Sigma, Taufkirchen, Germany

2.1.4 Media and buffers

Cytoskeletal buffer (1x CB), pH 6.1

Components	Concentration
EGTA	5 mM
Glucose	5 mM
MES (2(N-Morpholino)-Ethansulfonacid)	1.95 g/L
$MgCl_2$	10 mM
NaCl	150 mM
Streptomycin	1.72 mM

Neural stem cell media

Components	Concentration
DMEM	50 mL
L-Glutamine	0.6 mM
N2 Supplement	1%
Penicillin/strepotomycin	1%
Sodium pyruvate	1%

Neurobasal media

Components	Concentration
Neurobasal medium	48.825 mL
B-27 Supplements	1 X
GlutaMAX Supplement (100 X)	10 X
Gentamicin	50 µg

Astrocyte culture media

Components	Concentration
DMEM	50 mL
L-Glutamine	1%
FBS	10%
Penicillin/strepotomycin	1%

Transfer buffer for western blot

Components	Amount
Methanol	200 mL
Trizma base	3.03 g/L
Glycine	14.4 g/L
H_2O	Ad. 1 L

Tris-buffered saline (TBS) staining buffer for western blot (1x), pH 8.0

Components	Amount
Trizma base	12.1 g
NaCl	87.7 g
H_2O	Ad. 1 L

2.1.5 Instruments

Hardware	**Company**
Centrifuge 5415-D	Eppendorf, Wesseling/Berzdorf,Germany
Centrifuge 3-16K	Sigma, Osterode,Germany
Centrifuge 5415-R	Eppendorf, Wesseling/Berzdorf,Germany

Hardware	Company
CFX Connect™ Real-Time PCR Detection System	BIORAD, Düsseldorf, Germany
Clean bench HeraSafe	Heraeus, Osterode, Germany
CO_2 - Incubator Typ B12	Heraeus, Osterode, Germany
Delta 10 TT spin coater	Suss-Micro Tec, Garching, Germany
Desiccator	Duran Group GmbH, Wertheim/Main, Germany
FLUOstar Omega Microplate Reader	BMG labtech, Ortenberg, Germany
Guava EasyCyte flow cytometer	Merck Millipore, Darmstadt, Germany
Heating block Thermomixer	Eppendorf, Wesseling/Berzdorf, Germany
Heating block	Stuart Equipment, Staffordshire, UK
Heating cabinet E400	Memmert, Schwabach, Germany
Megafuge 1.ORS	Heraeus, Osterode, Germany
Mikro Star 17R centrifuge	VWR international, Darmstadt, Germany
Mini-Protean electrophorese system	Bio-Rad, Hercules, USA
Motor-driven stretch apparatus	IBI-2, research center Jülich, Jülich, Germany
Osmomat 030	Genotec, Gangelt, Germany
Vacuum Pump RC6	Vacuumbrand, Wertheim, Germany
Vortex mixer	VWR, Radnor, USA
Water bath WNB-22	Memmert, Schwabach, Germany
Western blot system Mini Trans-Blot	Bio-Rad, Hercules, USA

2.1.6 Microscopes

Microscope	Company
BZ-9000 Fluorescent microscope	Keyence Osaka, Japan
Laser Scanning Microscope(LSM) 710	Carl Zeiss, Jena, Germany
Laser Scanning Microscope (LSM) 880	Carl Zeiss, Jena, Germany
Microscope Axiovert Imager-M2	Carl Zeiss, Jena, Germany
Microscope Axiovert 40 CFL	Carl Zeiss, Jena, Germany

2.1.7 Objectives

Objective	Company
LDA-Plan Ph1 10x air (NA 0.25)	Carl Zeiss
LDA-Plan Ph1 20x air (NA 0.35)	Carl Zeiss
Plan-Apochromat Ph2 20x air (NA 0.8)	Carl Zeiss
Plan-Apochromat 10x air (NA 0.45)	Nikon
Plan Fluor 40x air (NA 0.6)	Nikon
Plan-Neofluar Ph3 10x air (NA 0.3)	Carl Zeiss
Plan-Neofluar Ph3 40x oil (NA 1.3)	Carl Zeiss
W N-Achroplan 20x (NA 0.5)	Carl Zeiss
W N-Apochromat 40x DIC (NA 1.0)	Carl Zeiss

2.1.8 Software

Software name	Company
Corel draw	Corel, Ottawa, Kanada
Graph Pad Prism	GraphPad Software, San Diego, USA
Image J	Wayne Rasband, U.S. National Institutes of Health, Bethesda, USA
Imaris	Oxford Instruments
Inventor	Autodesk, Inc., San Rafael, USA
Matlab	MathWorks, Massachusetts, USA
Zen black 2012	Carl Zeiss, Jena, Germany
Zen blue 2012	Carl Zeiss, Jena, Germany

2.2 Methods

2.2.1 PDMS based surfaces

Polydimethylsiloxane (PDMS) is a silica-based polymer that can be crosslinked to fabricate soft elastomers. Elastomer systems based on PDMS have great characteristics which make it suitable for cell culture studies: it is biocompatible with no adverse effects to cells, it is transparent allowing it to observe cells that are growing in the chamber via inverse and also upright microscopes, and it can be deformed by applying mechanical forces due to the linear elastic property. The vinyl-terminated polydimethylsiloxane and its cross-linker (methylhydrosiloxane-dimethylsiloxane) forms an elastic polymer network and can be adjusted to reach defined stiffnesses depending on their ratio. For general PDMS chamber fabrication, a mixing ratio of 1:40 (cross-linker: base polymer by weight, Sylgard 184) was mixed for 10 minutes and then degassed in a desiccator to remove air bubbles which may otherwise interfere with the transparency of the culture substrate. The PDMS mix was poured into chamber fabrication molds. The curing mold is composed of an aluminum base plate, a polystyrene mold that forms the chamber shape, four acrylic glass pins forming small holes, and a polystyrene frame (**Figure 2.1**). Curing of the PDMS substrate was performed at 60°C for 16 hours. After curing, the substrates had a Young's modulus of 50 kPa and a Poisson's ratio of 0.5. Fabrication in molds results in elastic chambers with a cell culture area of 4 cm^2 surrounded by 0.5 cm thick wall and a media volume capacity of 550 µL (**Figure 2.1**), which can be used to cultivate cells even for several days under sterile conditions. The thickness of the chamber bottom was 0.4 mm, which must be considered when selecting imaging techniques.

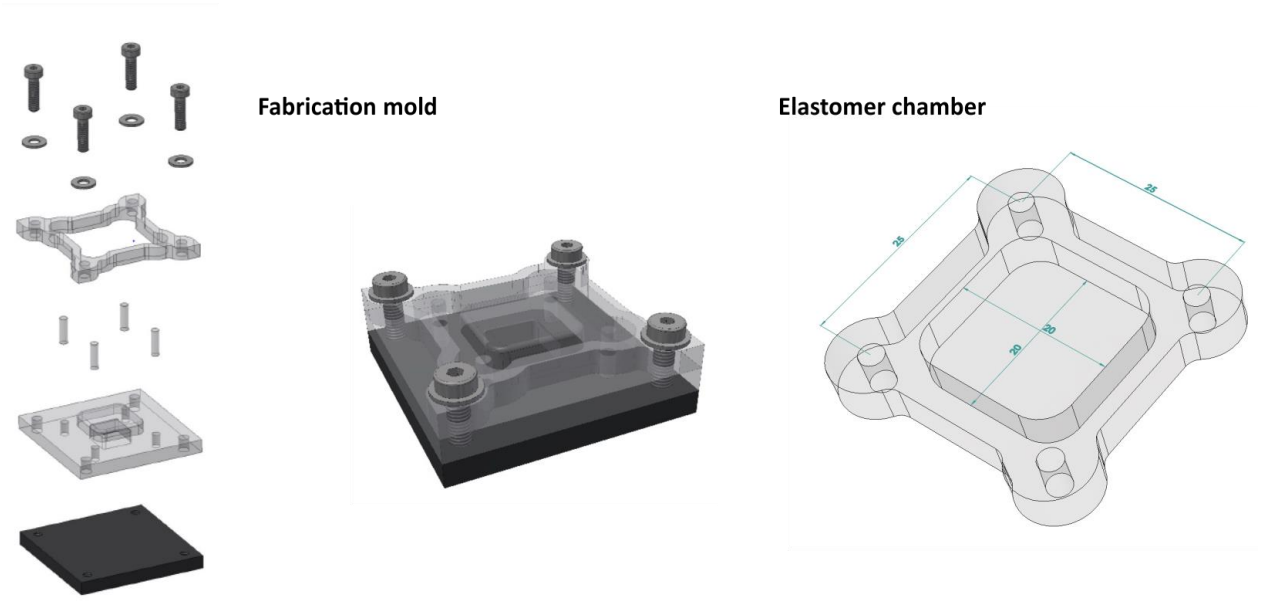

Figure 2.1: Fabrication of PDMS elastomer chambers. Curing in fabrication molds results in a chamber with a cultivation chamber bottom of 2 x 2 cm. Image is not to scale. Pictures were produced with the Inventor software by Jens Konrad.

The system was regularly calibrated in order to guarantee constant material stiffness of the fabricated surfaces. Therefore, 7 mm of PDMS were produced and a force curve was generated by indentation. During indentation measurements, the Young's modulus can be calculated by measuring the indentation length and force. The Young's modulus is a material constant that describes the material's elastic resistance to deformation. Thus, materials with a higher Young's modulus are stiffer and more difficult to deform. As the elastomer chambers are linear elastic, the Young's modulus is constant over a range of strains. The Poisson ratio is the ratio of transverse to axial strain, describing an incompressible material as well as a linear elastic response, which means that mechanical stress is proportional to strain (Faust et al., 2011). The stiffness of the elastomer system used in the study had an adjustable range from 0.6 kPa to several GPa allowing to mimic environmental stiffness that is found within the brain and other microenvironments e.g. cells close to vascular tissues, where cells are subjected to approximate stiffness of 10-40 kPa (Qiu et al., 2010).

Before cell seeding, the chambers were washed in isopropanol and mounted in chamber holders (**Figure 2.2**). The chamber holder stabilized the elastomer system during the cultivation period

and avoided mechanical influences before the actual cell stretching. The chamber holder could also easily screwed in the cell stretched before stretching and thus allowed easy handling of the elastomer culture system. Chamber holders mounted with elastomer chambers were kept at 37°C for at least 6 hours under sterile conditions to ensure the full evaporation of isopropanol, which easily diffuses in the PDMS chamber during the washing step. Remaining isopropanol induced precipitation of the coating solution and thereby hindered efficient surface coating and cell adherence. A cover glass and parafilm were used to seal the chamber edges and thereby avoid evaporation of the media inside the chamber.

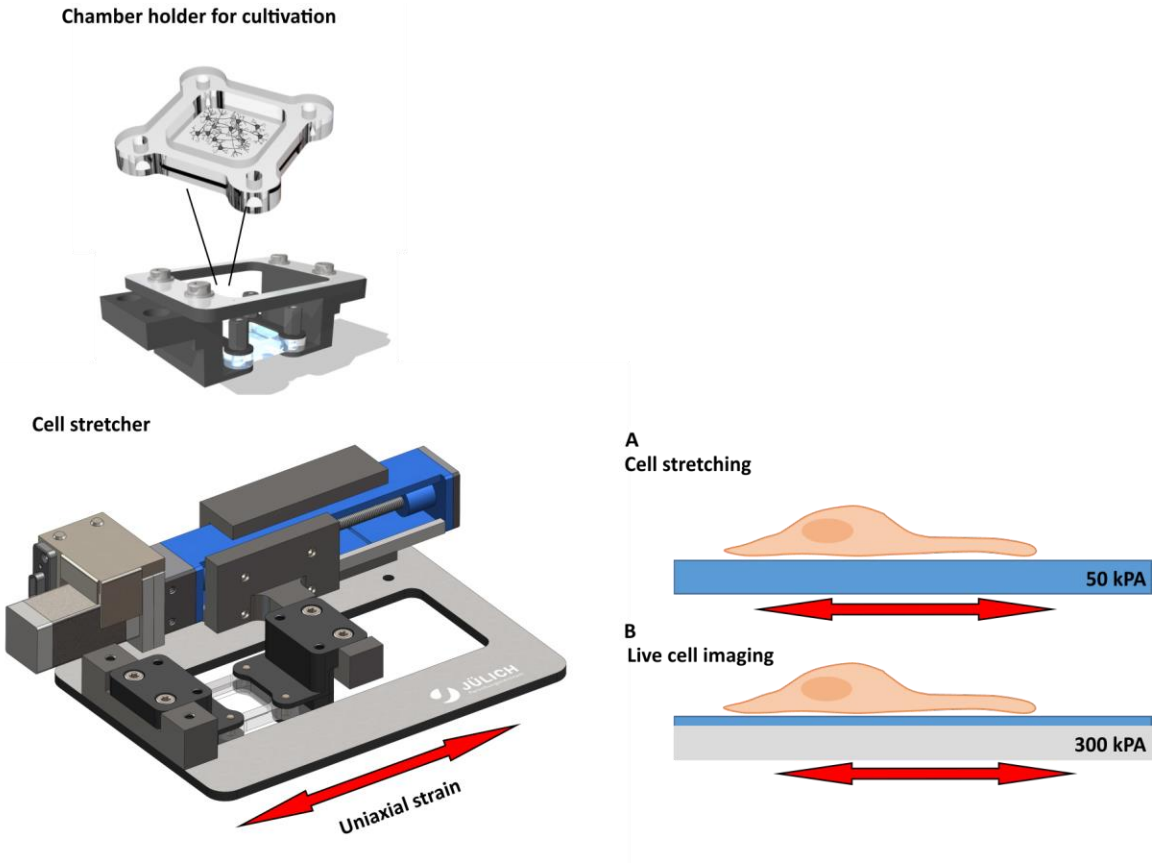

Figure 2.2: In house developed cell stretching system. On the left the chamber holder, which stabilizes the elastomer chamber during cultivation, and the cell stretcher, which can stretch the elastomer chamber uniaxially. Pictures were produced with the Inventor software by Jens Konrad, IBI-2. Two different elastomer systems on the right: stretch experiments were performed with 50 kPa elastomer chambers (**A**). In contrast, live-cell stretch experiments were performed with 300 kPa chambers that were coated with an additional layer of 50 kPa PDMS (**B**).

Chambers used for live cell imaging under the upright microscopy were produced from Sorta Clear by mixing the base and crosslinker in a 1:1 ratio resulting in a stiffness of 300 kPa. The stiffer chamber reduced the z-drift during imaging and was, therefore, easier to handle during live-cell imaging. To ensure comparable settings, the 300 kPa chambers were coated with a 100 µm layer of Sylgard PDMS with a stiffness of 50 kPa (**Figure 2.2B)**. Therefore, the chamber was placed on a Delta 10 TT spin coater, a volume of 150 µL PDMS (1:40) was added in the middle of the chamber, and spin-coating was performed at 900 rpm for 8 seconds followed by curing at 60°C overnight.

To produce surfaces with the same stiffness to study growth patterns on soft substrates 300 µL of the PDMS mixtures was added on a glass surface with a defined thickness of 90 µm to 100 µm (#0, Ø 25 mm, Menzel) and distributed by using a spin-coater with 1800 rpm for 15 seconds. This spin coating technique revealed a thin layer of PDMS on the glass substrate with a thickness of approximately 80 µm. The PDMS coated glass surface was then stuck under a nunc dish with a pre-drilled hole, thus, generating cell culture dishes with defined stiffness and correct working distance for inverse microscopes. This thickness of the PDMS layer was enough to generate a soft cell culture environment of the desired stiffness, while cells were not able to feel the underlying hard glass surface.

2.2.2 Primary neural stem cell culture

2.2.2.1 Neural stem cell isolation

Cell culture dishes were pre-coated with a 15% L-poly-ornithine solution overnight. As soluble poly-ornithine is toxic for cells, the dishes were washed three times with PBS, with the second washing step prolonged for 20 min at 37°C. After the washing steps, bovine fibronectin solution in PBS (2.5 mmol/L) was added to the dishes and incubated for 2 hours. Neural stem cells were isolated from pregnant Wistar rats at 13.5 days of gestation as described in (Blaschke et al., 2019; Rueger et al., 2010). After decapitation, the embryonic chain was removed. Each embryo was isolated from its placenta, and the head was directly cut by a tweezer from the remaining body. The meningeal layer was removed, and hippocampal tissue was detached. The residual cortical tissue was placed in neural stem cell (NSC) media and mechanically dissected by pipetting the

cortex up and down. After dissipation, remaining tissue clumps of the two hemispheres were allowed to settle for one minute, and only the upper part containing dissipated neural stem cells (NSCs) was transferred to a pre-coated cell culture dish. A concentration of 10 ng/mL fibroblast growth factor (FGF) was added to ensure that cells remain their stemness throughout experiments unless stated otherwise. Every day the cell culture dishes were supplied with the mitogen FGF and media change was performed every second day. A continuous supply of FGF was pivotal to repress differentiation and to maintain a homogenous population of rapidly dividing cells. For the stretch experiments, NSCs were used from the second until the fifth passage.

2.2.2.2 Passaging of neural stem cell cultures

When NSC culture dishes reached a confluency of 80-90%, the dish was incubated with 7 mL of PBS for 15 min at a humidified atmosphere of 5% CO2 and 37°C. A 10 mL pipette was used to wash down adherend cells and collect them in a new falcon tube. After centrifugation at 1200 rpm for 5 min, cells were resuspended with pre-warmed NSC media and counted before cell seeding. A number of 100-400 000 cells were seeded on pre-coated cell culture dishes in 7 mL NSC media per dish. When cultivated on elastomer chambers, a density of 23 000 cells/cm^2 was plated for experiments where cells in stem cell stage were analyzed. A number of 40 000 cells/cm^2 were plated for observations during differentiation.

2.2.2.3 Neural stem cell differentiation

To study the effect of cyclic strain on neuronal cell differentiation, the mitogenic factor FGF was withdrawn from the NSCs culture. Without FGF, NSCs lose their stemness and begin to differentiate into astrocytes, neurons, and oligodendrocytes. To distinguish differentiation between astrocytes and neurons, the co-culture was fixed five days after mitogen withdrawal and stained with the NSC staining protocol (see chapter 2.2.5.3). The cell types were differentiated by immunocytochemically stained with primary antibodies against neurons (neuron-specific beta-III tubulin monoclonal antibody (Tuj1) (1:200, R&D Systems) and astrocytes rabbit anti-glial fibrillary acidic protein (GFAP) (1:500, Sigma Aldrich). When using manual counting, the data set was randomized.

2.2.2.4 Proliferation assay

To determine the number of proliferative cells, NSCs were incubated for 6 hours with 10 µM bromodeoxyuridine (BrdU) before cells were fixed with 4% paraformaldehyde (PFA). BrdU is a thymidine analogon that can pass the plasma membrane and intercalates in the DNA of dividing cells. After fixation for 10 min, cells were washed three times with PBS. For epitope retrieval, cells were incubated with 2 N HCl before continuing with the usual staining protocol (see chapter 2.2.5.3) and immunocytochemically labeled by anti-BrdU antibodies (mouse, clone BU-33, dilution 1:200, Sigma Aldrich, St. Louis,USA). To calculate the percentage of proliferative cells, the number of BrdU positive cells was divided by the total cell number stained with Hoechst 33342. When using manual counting, the data set was randomized.

2.2.3 Primary cortical cell culture

2.2.3.1 Cortical cell isolation

Pregnant rats (Wistar, Charles River, Sulzfeld) at 18-19 days of gestation were anesthetized by CO_2 before decapitation. After decapitation, the uterus with the embryo chain was removed from the mother rat, the placenta opened, and the embryo sacrificed via cervical dislocation. Heads were kept in Hanks Balanced Salt Solution (HBSS) on ice until isolation. Cortices were dissected from embryonic heads in 2 mL ice-cold HBSS. Therefore, the meninges and skeletal skull tissue were cut with a micro scissor, and the cortex was removed by using tweezers to separate cortex from the remaining tissue. The cortical tissue was further separated from the hippocampal tissue and striatum and placed in an ice-cold trypsin solution followed by incubation for 15 min at 37°C. The trypsinized tissue was further transferred to pre-warmed neurobasal cell culture medium (NB). Cortices were washed three times to remove residual trypsin. After washing, the tissue was despaired by pipetting up and down. Vital primary cortical neurons were counted by using a Neubauer counting chamber, while dead cells were stained with trypan blue. A number of 60 000 cells per cm^2 was plated on PDMS stretching chambers. Before cell seeding, chambers were coated either with poly-L-lysine or avidin. Poly-L-lysine solution was incubated overnight, followed by three washing steps with H_2O; avidin was diluted to reach a 1 mg/mL concentration and incubated overnight. Media was changed every second day by removing 50% of the old media and replacing it with freshly prepared pre-warmed NB media. Cortical cells were allowed to attach

on the elastomer substrate at least for 4 hours before stretch experiments to guarantee the formation of stable attachment points before inducing cyclic substrate deformation.

2.2.4 Postnatal astrocyte cell culture

Astrocytes were isolated from rat pups (Wistar rats) 0-3 days postnatal. Meniges and skeletal skulls were cut by a scissor and cortical tissue was removed. The cortical tissue was further hackled by tweezers and then trypsinized at 37°C and 5% CO_2. After trypsinization, cells were transferred to pre-warmed astrocyte culture media containing DMEM, supplemented with L-glutamine, penicillin-streptavidin, and FBS. After washing the tissue with culture media, the tissue was further dissociated by pipetting up and down and subsequently centrifuged for 2 min at 1200 rpm. Media change was performed two days after isolation. The cell culture contained astrocytes but also microglia. To generate a homogenous cell culture of astrocytes, 7-10 days after isolation, microglia were gently removed by shaking the cell culture flask for 1 hour at 250 rpm. Astrocytes were trypsinized for 10 min and subsequently centrifuged for 5 min at 1200 rpm. To guarantee cell attachment of astrocytes on the chambers, the plated chambers were allowed to adhere for three days before stretch experiments or adding primary cortical neurons on top of the astrocytes for ratio experiments. For stretch experiments with only postnatal astrocytes, a number of 30 000 cells/cm^2 was plated on the chambers while the ratio experiment contained different numbers of astrocytes while the neuronal cell number was kept constant at 20 000 cells/cm^2.

2.2.5 Mechanical deformation of cells

The above described fabricated surfaces functioned as biocompatible, transparent cultivation chambers. By deforming the cultivation chambers, cells that grow on top of the elastomer were also deformed by the substrate strain. Cells that are attached to the elastomer matrix sense mechanical stress (force per unit area). For stretch experiments, the chamber holder was mounted into an in-house developed stretcher apparatus (developed by Wolfgang Rubner). The stretcher apparatus has a motorized stage and is linked to an in-house developed software

(Werner Hürttlen) design that allows setting different strain parameter. One side of the clamping device is moved by a motor and thereby deforms the chamber uniaxially. For the experiments, central regions of the elastic chamber were examined as here nearly equal strains are applied. To avoid sagging of the chamber bottom, the chambers were pre-stretched by 1.5 mm, and by 2 mm when live-cell stretching was performed. For cell stretching of cortical neurons, an amplitude of 7%, 15%, and 28% was chosen, the frequency was kept at 300 mHz to compare the effect of the strain amplitude itself. The stretcher paused between each stretch and release movement for 0.417 seconds. Stretch and release term parameters were set for each strain amplitude to fit a sinusoidal waveform, which mimics naturally occurring mechanical strain fields. The selected range of 7-28% amplitudes was chosen to mimic physiological strain amplitudes that are present in the brain (Drew et al., 2011). For the stretch experiments with NSC, an amplitude of 15% and a frequency of 300 mHz was chosen as this parameter showed to induce a clear mechanoresponse in previous experiments with cortical neurons. All experiments were performed under sterile conditions, at 37°C and in a humidified atmosphere of 5% CO_2. After each stretch experiment, the chamber holders were stopped in the prestretch position, cells were fixed, and chambers were removed from the stretcher. As controls, cells were cultivated in elastomer chambers but not stretched.

2.2.5.1 Live and dead analysis of cortical cells after cyclic strain

To analyze whether mechanical strain has a toxic effect on primary cortical neurons, cells were stained with 2 µM ethidium homodimer and analyzed by flow cytometry (Guava EasyCyte). After trypsinizing cells from the elastomer chambers, cortical neurons were fixed with 10% of solution A from FIX and PERM Cell Fixation and Cell Permeabilization Kit in PBS for 5 min. The fixed cells were centrifuged and resuspended in PBS to analyze the number of dead cells.

As a positive control for induced cell death, camptothecin was used in a concentration of 5 µM for 24 hours. Camptothecin is an S-phase-specific anticancer agent that inhibits DNA topoisomerase activity and thereby induces neuronal cell apoptosis. (Morris & Geller, 1996).

2.2.5.2 Live and dead analysis of NSCs under cyclic strain

To assess whether cyclic mechanical strain influenced the cell viability of NSCs, cells were stained with propidium iodide that stains DNA of dying cells and can not pass cell membranes of intact cells. NSCs were counterstained with Hoechst 33342 to visualize all cells on the substrates. Images were taken with an Axiovert upright microscope and a 20x objective (Zeiss). Labeled cells were counted manually and the percentage of cell death was obtained by the ratio of propidium iodide positive cell number to the total number of stained cells.

2.2.5.3 Immunocytochemistry

For immunocytochemistry analysis, cortical neurons were fixed with 3.7% of PFA in cytoskeletal buffer (CB buffer) for 15 min at 37°C. Cells were then washed with CB glycine (10mM) and stored in CB glycine until primary and secondary staining was performed. Cells were permeabilized with 0.1% Triton-X in CB for 10 min and washed three times with CB buffer. Subsequently, blocking was performed with 5% milk powder in CB for 1 hour. After blocking, cells were incubated with primary antibody (see table) for 2.5 hours in 1% milk powder followed by washing cells with 1% milk powder in CB. Secondary antibody (see table) was done by incubating cells for 1 hour and washed three times with CB to remove remaining antibodies with unspecific bindings. After washing the chamber with Milli-Q to avoid the formation of salt crystals while drying, the chamber was mounted on a glass dish and 18 µL of fluoromount was added before placing a 15 mm glass coverslip on top. After drying for 24 hours, the chamber was cut with a scalpel and the chamber edges were removed. Cells were observed with an inverted laser scanning confocal microscope LSM 880.

For immunocytochemical analysis of neural stem cells, cells were fixed with 4% PFA in PBS. The sample was blocked and permeabilized with 0.1% Triton-X and 10% serum according to the used secondary antibody (goat/donkey serum) for 10 minutes. The primary antibody incubation was performed overnight at 4°C in PBS supplemented with 3% serum and then subsequently washed three times with PBS. The secondary antibody staining was performed at RT for 1 hour. After the

secondary antibody, chambers were incubated with nuclei staining solution containing Hoechst 33342 in PBS (1:500) for 5 minutes. The chambers were then washed three times with PBS, followed by washing with Milli-Q. For mounting, 18 µL of fluoromount was used. The slides were observed with a BZ-9000 Fluorescent microscope, equipped with a 40x objective (Nikon) and a 10x objective (Nikon) for overview images.

Primary antibody	**Host species**	**Dilution**
Anti-BrdU clone BU-33(B8434), Sigma Aldrich	mouse	1:200
Anti-GFAP (G9269), Sigma Aldrich	rabbit	1:500
Anti-Nestin (MAB353), Sigma Aldrich	mouse	1:500
Anti-Neurofilament heavy (N0142), Sigma Aldrich	mouse	1:500
Anti-MAP-2 (AB5622), Millipore	rabbit	1:200
Anti-SOX2 (AD2018), R&D Systems	goat	1.200
Anit-Tuj1 (MAB1195), R&D Systems	mouse	1:200
Anti-Tubulin YL ½ (MAB1864), Millipore	rat	1:500

Secondary antibody	**Host species**	**Dilution**
Alexa Fluor 488, anti-mouse IgG, ThermoFisher	goat	1:1000
Alexa Fluor 568, anti-rabbit IgG, Thermo Fisher	goat	1:1000
Cyanine Cy^{TM}3 anti-rat IgG, Jackson	goat	1:200
Phalloidin Atto 488		1:500

2.2.5.4 Confocal laser scanning microscopy

Fixed samples were observed upside down with an inverse confocal microscope. Secondary antibodies with an excitation wavelength of 561 were excited with a helium/neon laser at 561 nm. Secondary antibodies with an excitation wavelength of 488 were excited with an argon laser. The mean beam filter 488/543/633 was utilized to detect two fluorophores in one scan. To compare intensities between samples of each individual experiment, laser and gain settings were kept constant. Further, for all experiments, a pinhole of 1 airy unit was used. The dwell time per pixel was kept above 1 µsec.

2.2.5.5 Live-cell imaging

Live-cell microscopy was performed with an upright microscope (an Axiovert M2 imager). Cell analysis by a dip-in objective from above avoids imaging trough the relatively thick chamber bottom. This enables imaging with a much better resolution. The culture media also functions as an immersion media, which avoids optical interference. For live-cell imaging of cells, a communication system between stretcher and microscope was developed. Thereby, cell stretching and live-cell microscopy can be performed in parallel. The system enables defined pausing of the stretcher to enable imaging and back communication to start the stretching cycles once the camera has completed a certain set of images. The communication was enabled by a constant signal of 5 V emitted from a control box. By this 5 V signal, the camera receives the signal to start imaging. After the defined set of images, the camera can transmit a 5 V signal back to the control box, which triggers the motorized stretcher to start with the next stretching cycle.

To understand the immediate response of cortical neurons and NSCs, live-cell imaging during stretch was performed. Therefore, cortical neurons and NSCs were cultivated on Sorta Clear elastomer chambers to allow cell adherence (24 hours for cortical neurons, 12 hours for NSCs). As Sorta clear chambers have higher stiffness, the chambers could be filled with 800 µL of media without sagging of the chamber bottom. Cells were observed 30 min prior to strain in order to detect normal dynamic movements. Cells were further observed for 3-6 hours during stretch. Therefore, every five minutes, the stretcher received the signal to pause the stretching. To ensure that evaporation does not change the osmolarity of the media, media change was performed every hour by removing 425 µL of media and replacing it with 500 µL fresh media. To analyze the migration velocity, the images were analyzed by using the Image J plug-in TrackMate (Tinevez et al., 2017). Here, the cell bodies were manually marked and the migration tracks generated (**Figure 2.3**). The observed tracks were used to calculate the migration velocity and also the migration direction relative to stretch. The latter was performed by the generation of a weighted mean angle, which considers the total cell displacements. Therefore, the angle was multiplied by the displacement at each time point. Subsequently, these values were summed up and divided by the total path length that the cell has traveled.

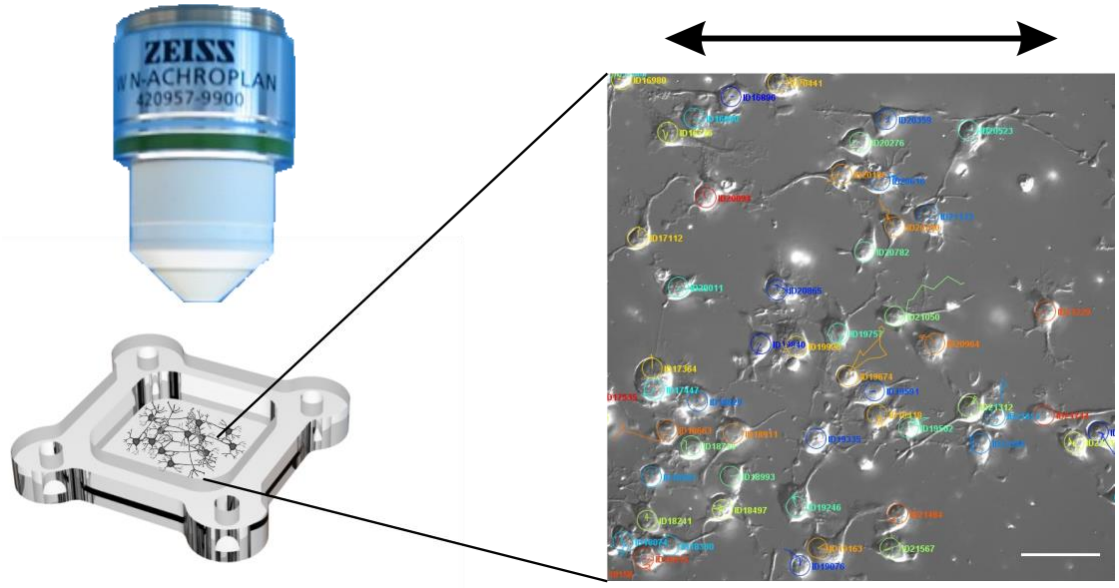

Figure 2.3: Live-cell imaging of NSCs under strain. NSCs cultures on elastomer chambers were observed from above with an upright microscope. Migration tracks were detected by using the ImageJ plug-in TrackMate. Scale bar = 20 µm.

For cortical neurons, the imaging media was phenol red-free neurobasal media supplemented with B27, Glutamax, and gentamicin. Further, 10 µM Hepes was added to avoid pH changes during imaging as the culture chambers were not exposed to CO_2. For NSCs, the media was changed to life cell imaging media, supplemented with FGF to repress differentiation process during imaging. Strain parameters for live-cell imaging were kept at 15% and a frequency of 300 mHz. If a static strain was applied, the stretch and release velocity was 0.05 mm/sec, while the amplitudes were increased stepwise by 4%. Images were taken with differential interference contrast (DIC) that allowed a higher resolution and clear images of neuronal branches with small diameters.

For immunocytochemistry analysis of the neuronal cells observed via live-cell imaging, the position of interest was saved and cells were stained while they were still fixed in the chamber holder. Immunocytochemistry was performed as described above.

2.2.5.6 Quantitative real-time PCR

To compare gene expression profiles of stretched and control samples, quantitative real-time PCR (qPCR) was performed. Therefore, mRNA was extracted by using the TRIzol® Reagent by the protocol of the manufacturer. Immediately after the stretcher was stopped, a volume of 400 µL

reagent was added to the elastomer chamber. The RNA concentration was obtained with photometrical measurements using the BMG Labtach FLUOstar OMEGA microplate reader. To convert total RNA to cDNA by reverse transcription, the Quantitect reverse transcription kit was used. A concentration of 10 ng total RNA was used for the qPCR by following the manufacturer's recommendation and pipetted into a qPCR plate in triplets. Primes for the qPCR were obtained from Biolegio (see table for primer sequences) and used with a final working concentration of 10 pmol/mL. Amplification and quantification were performed by using the CFX Connect™ Real-Time PCR Detection System and the KAPA SYBR DNA Polymerase. Following thermal cycler conditions were used: denaturation at 95°C for 15 sec, annealing 45 sec at 55-60°C depending on the melting temperature (T_m) of the primer (see table), elongation 15 sec at 72°C. The cycle was performed 38 times. For each reaction tube, the mRNA level of a housekeeping gene was measured and mRNA levels of interest were normalized to endogenous RPL expression, which encodes a ribosomal protein. Quantitative analysis was performed with the $2^{-\Delta\Delta Cq}$ relative to the average of controls of the respective experiment.

Primer name	**Sequence**	**T_m in °C**
Actin forward	CTGTGTGGATTGGTGGCTCT	59.96
Actin reverse	CAGCTCAGTAACAGTCCGCC	60.74
GFAP forward	TGCATGTACGGAGTATCGCC	59.96
GFAP reverse	GGGGGAGGAAAGGACAACTG	59.97
Ncad forward	CACCCGGCTTAAGGGTGATT	60.03
Ncad reverse	CGATCCTGTCTACGTCGGTG	59.97
Nestin forward	CTTTGGCTGAAGGCCACAGT	60.83
Nestin reverse	CAGTTCCCAGATTTGCCCCT	59.96
RPL forward	TCTCCGAAAGCGGATGAAC	62.80
RPL reverse	CAACACCTTGAGGCGTTCCA	65.90
Talin forward	CTCTATATGCCACACCCGCC	60.32
Talin reverse	ACACAAGCCACTTCCGAGTT	59.82
Tubulin forward	CGAGAAGAATACCCCGACCG	59.97
Tubulin reverse	CTACCAACTGGTGGACGGAC	60.04
Vimentin forward	GCAGCCTCTATTCCTCGTCC	65.00
Vimentin reverse	TAGTTGGCGAAGCGGTCAT	64.70

2.2.5.7 Western blotting

Western blot analysis was carried out to determine cytoskeletal changes and post-transcriptional protein modification of stretched and control cortical neurons. After cyclic stretch for 24 hours, the chamber holders were removed from the stretch apparatus and placed on an ice-cold plate. After washing twice with ice-cold PBS, RIPA lysis buffer supplemented with 1:100 proteinase inhibitor cocktail was placed on the first chamber and cells were scratched from the elastomer surface with a cell scraper. The lysis buffer was then transferred to the next chamber and the scraping procedure was repeated. For stretched and control cells, proteins were collected from six chambers. The collected solution was then placed into a 1.5 mL pre-cooled Eppendorf tube and cells were pipetted up and down with the help of a syringe and a needle, this step helps to break the cell membrane and to facilitate the release of proteins in the solution. After incubation, the solution was centrifuged at 10,000 g for 10 min at 4°C. The supernatant was transferred to another tube, 4x Laemmli buffer was added and heated at 95°C for 5 min. The protein content of the solution was obtained via BCA assay kit. For the SDS page, 12 µg protein was loaded per well into the gel. SDS gel electrophoresis was performed for 10 min at 80 V followed by 1 hour at 120 V. To subsequently transfer protein to a nitrocellulose membrane, western blotting was performed for 90 min at 4°C in transfer buffer. After protein transfer, the nitrocellulose membrane was placed for 60 min in TBS containing 5% BSA for blocking unspecific bindings of the antibody. Incubation with the primary antibody took place with a 1:1000 dilution in TBS with 5% BSA overnight. The membrane was washed with TBS 3 times for 5 min and then incubated with the second antibody in a 1:10,000 dilution in TBS with 5% BSA for 1 hour. After the secondary antibody was washed down three times with TBS, the membrane was developed by using a BCIP/NBT substrate, which induced a color reaction using the antibody-coupled alkaline phosphatase. The resulting bands were documented with a gel documentation system after drying the membrane.

Primary antibody	Host species	Dilution
Anti-actin β clone D6A8 (8457), Cell Signaling Technology	rabbit	1:1500
Anti-GAPDH clone GAPDH-71.1 (G8795), Sigma Aldrich	mouse	1:1500
Anti-neurofilament heavy (N0142), Sigma Aldrich	mouse	1:1500
Anti-MAP-2 (AB5622), Millipore	rabbit	1:1500
Anti-tubulin α 4a (T6793), Sigma Aldrich	mouse	1:1500
Anti-tubulin β clone Tub 2.1 (T-4026), Sigma Aldrich	mouse	1:1500
Anti-tubulin YL ½ (MAB1864), Millipore	rat	1:500

Secondary antibody	Host species	Dilution
Anti-mouse alkaline phosphatase IgG (A3562), Sigma Aldrich	goat	1:3000
Anti-rabbit alkaline phosphatse IgG (A3812), Sigma Aldrich	goat	1:3000
Anti-rat alkaline phosphatase IgG (A8438), Sigma Aldrich	goat	1:3000

2.2.6 Data analysis

2.2.6.1 Image processing of live-cell imaging data

Live-cell stretch experiments were performed by using a z-stack to avoid out of focus images as the focal plane during imaging changed due to slight evaporation of the media. To generate in focus images, the z-stack was further processes by an algorithm written in Python 3.7 by Georg Dreissen (IBI-2). Here the image stack was smoothed via a Gaussian filter (size 2 sigma) and downscaled by a factor of four. The local standard deviations for each 3x3 pixel array were then calculated for each image. A 2D indices-matrix was created that reflects the z-coordinates of the deviation's maxima. Afterward, a median filter (11x11 pixel) was applied to that matrix and the matrix was subsequently resized to the initial image resolution. To create the final 2D in focus image, the gray values from the initial z-stack were extracted at the z-positions indicated by the indices-matrix.

2.2.6.2 In-house developed program to analyze the number and the sum length of neuronal branches

Immunofluorescence micrographs were analyzed by an in-house developed program (Matlab R2017a, by Georg Dreissen). This program enabled automated measurements of neurite lengths, branch orientations, number of branching (nodal) and endpoints, as well as orientation and intensity of individual branches (**Figure 2.4**). The algorithm was adapted from Li et al. (Li et al., 2015). In detail, images were scaled to a common pixel size of 0.09 µm and smoothed with a narrow Gaussian kernel (0.5 pixel). Masks were created for each neuron and both channels. A first mask contained cell bodies and neurites. This full mask was determined by segmentation with the mean intensity of the image as intensity threshold. In order to reduce artifacts, morphological processes were used. Morphological opening (disk-shaped structure, radius 2 pixels) removed small-scale structures. In addition, objects smaller than 500 pixels were discarded. Subsequently, morphological closing (disk, 10 pixels radius) was performed to fill small holes in the foreground. The result was used as full mask. As cell bodies exhibited higher intensities than neurites, masks containing cell bodies alone could be determined again by intensity thresholding. This time the threshold value was the mean image intensity plus one standard deviation of the latter. Morphological opening (disk, radius 20 pixels) was performed to remove all remaining thin protrusions. Moreover, all objects smaller than 1000 pixels were removed. To finally create the mask for neurites alone, the cell body mask was subtracted from the initial mask. To analyze cells separately, artificial cell borders were created by using the watershed transformation on the cell body mask. The watershed labels were used as cell labels. All further analyses were based on the dendrite mask that followed dendrites visibly closer. This dendrite mask was skeletonized. Using the respective Matlab commands, nodal and endpoints of the branched dendrite network were determined. For statistical analysis, each line connecting two nodal points or one nodal point to an endpoint was considered as branch. The length of branches was simply taken from the length of the skeletonized path. Orientations of branches were calculated as the direction of the longer half axis of ellipses fitted to them. For the construction of angular distributions, branches were weighted by their length. Furthermore, channel 1 and channel 2 gray values within a branch were determined from the dendrite mask.

Finally, distributions of channel 1 and channel 2 intensities depending on the orientation toward the stretch direction were constructed.

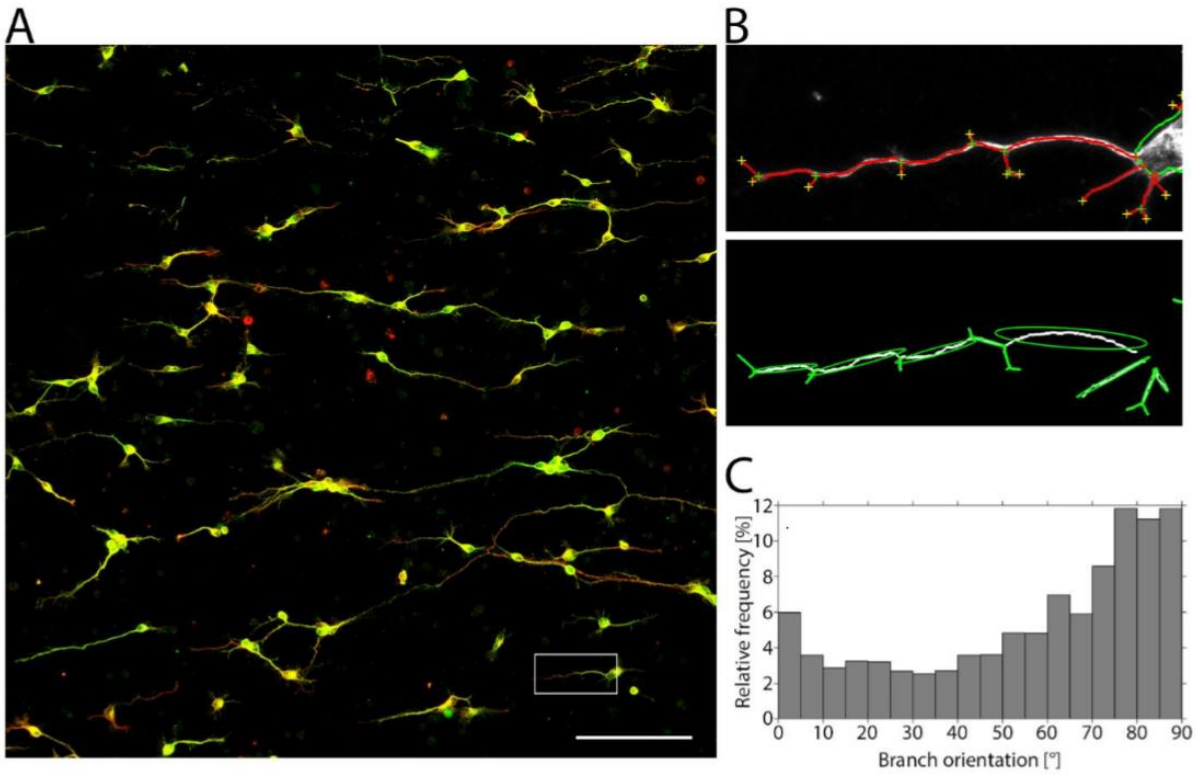

Figure 2.4: Data processing of immunofluorescence images. Quantitative analysis of the immunofluorescence image (A), neurons were identified based on immunofluorescent images. The uniaxial stretch direction in this image is vertical, while cells grew perpendicular in the horizontal direction. Exemplarily, one neuron is indicated (white box) and further analyzed in (B). Here, a mask was generated and skeletonized to detect nodal (green crosses) and endpoints (yellow crosses) of the neurites for each individual neuron. An ellipse was fitted around each detected neurite branch to analyze the branch orientation. The branch orientations of detected ellipses for all cells detected in (A) are depicted in C. Scale bar = 100 µm. Images were taken from (Abraham et al., 2019).

2.2.6.3 Pixel-based analysis of cell extensions

Immunofluorescence images were analyzed using an in-house developed program (Python 3.7, written by G. Dreissen). Cytoskeletal filament orientation was therefore determined at every single pixel (**Figure 2.5**). To analyze the orientation in the red and green channel, first a binary mask for these channels was calculated. Therefore, the image (red and green separately) was binarized using a local mean filter of 55x55 pixel as a threshold. All gray values above this local threshold were defined as signal, all others as background. On this binary image, a morphological

opening was performed using a disk structuring element with a radius of 2 pixels. Additionally, the same procedure was done using a local median filter (again 55x55 pixel). These two binary images were then combined into one mask. To only analyze structures outside of the cell nucleus, all nuclei were detected and removed from the mask. For nuclei detection, the blue channel was used. Therefore the mean gray value of the blue channel was calculated and multiplied by 2. This value was used as a threshold to separate the nuclei from the background. In the next step, the orientation was calculated for the red and green channel separately. First, the image was smoothed using a gaussian filter (filter size: sigma = 3 pixel, pixel size = 0.27 µm). Then the orientation for each pixel was calculated using the structure tensor approach (Faust et al., 2011). Afterward, the orientation and the corresponding gray values were further analyzed at the previously defined mask positions.

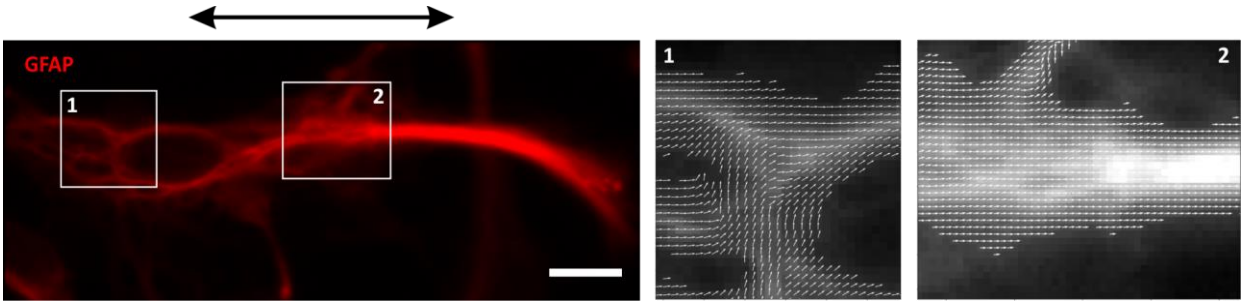

Figure 2.5: Determination of cytoskeletal orientation. Cells were stained for cytoskeletal filaments (here GFAP). Cytoskeletal orientation was determined at every single pixel via image processing. Scale bar = 10 µm.

2.2.6.4 Statistical analysis

To analyze if the data were normally distributed, a one-sided Kolmogorov–Smirnov (KS) was used. For normally distributed data, a student's t-test was used, while the comparison of not normal distributed data sets was performed by a two-sided KS test or Mann–Whitney U test. A one-sample t-test was used to test data sets against a hypothetical value of 1 or 100 when data was normalized for each experiment to the control. P-values are indicated with * for p-values < 0.05, ** for p-values < 0.01, and *** for p-values < 0.001. The number of independent experiments is indicated in the figure legends.

3 Results

Cells of the CNS are subjected to cyclic tissue deformation due to the pulsating nature of the brain perfusion. Within different brain regions, this cyclic movement leads to local mechanical deformations of various cell types and to a general parenchyma movement, which is considered as 'the pulsating brain' (Wagshul, Eide, & Madsen, 2011). Cyclic tissue deformations resulting from brain perfusion are described to reach an amplitude of 2-30% (Drew et al., 2011; Wedeen & Ponceleti, 2007). For the cyclic strains in this thesis, an amplitude of 7-28% and a frequency of 300 mHz was chosen. While the deformation rate was kept constant, the amplitude of the experiment varied to see the effect of the different magnitude of applied mechanical force. If the variation of amplitudes was not the focus of the experiment, a moderate strain of 15% was used for the measurements. The cytoskeletal setup of neuronal cells and astrocytes differs between different developmental stages (Bernal & Arranz, 2018; Hauser et al., 2018; Park et al., 2010). Accordingly, cyclic stretch experiments on four different cell culture systems are described in this chapter: neural stem cells, neural stem cells differentiating to astrocytes and neuronal cells, primary cortical neurons, and postnatal astrocytes.

The results part of this thesis is divided into three subchapters:

3.1 The first part describes the effect of cyclic mechanical strain on neural stem cells. Here the focus is to understand the influence of mechanical strain when cells are not developed, constitute a different, premature cytoskeleton, and are still in the proliferative state.

3.2 The second part of the chapter focuses on cells that are in a differentiating stage- more precise- cells that are in the transition stage between a neural stem cell and a developing neuronal cell or differentiating astrocyte. Here the influence of mechanical strain in the developing process is described, and influences on fate decision and differentiation speed are analyzed.

3.3 The third results chapter highlight influences of mechanical deformation to maturated cell types that are present in the CNS. The impact of mechanical cues on cortical cells, astrocytes, and co-cultures of neuronal cells and astrocytes is described.

3.1 Effect of cyclic mechanical stretch to neural stem cells

The extracellular environment of neural stem cells (NSCs) –the so-called neural stem cell niche- is a highly vascularized tissue (Goldberg & Hirschi, 2009). The close proximity to blood vessels facilitates supplying NSCs with oxygen and nutrients, but also with important stem cell-related factors to sustain a suitable stem cell microenvironment. As a result of this close arrangement, NSCs are subjected to mechanical deformation by pulsating brain parenchyma movements near blood vessels. The consequence of such strains to NSCs is described and analyzed in this chapter.

3.1.1 NSCs remain vital and are deformed by cyclic substrate strain

To examine the immediate response to cyclic strain, NSCs were subjected to mechanical deformation while being observed via live-cell microscopy. The degree of cell deformation was specifically observed when branches are pointing in the direction of stretch prior to the uniaxial substrate deformation **Figure 3.1A**. Despite developing local enlargements of branches when stretched with a higher amplitude of 28%, NSCs did not seem to be negatively affected by cyclic substrate deformation as cells did not retract their cell extensions and did not show any signs of apoptosis. **Figure 3.1A** representatively shows the deformation of NSCs, which are aligned in stretch direction prior to the substrate deformation. The substrate deformation induced morphological transformations of NSCs and dynamically changed their branch size. Here, the length of branches was enlarged with increasing substrate deformation and decreased when stretch was released from the system. In addition, measurements of the soma area prior and when stretched by 28%, showed an enlarged cell body size of 30%. When

the stretch was released from the system, the cell soma was also reduced again to the size prior stretch (p-value = 0.001, 0% strain compared to 28%, n = 59 cells).

Mechanical strain did not cause any cell damage as confirmed via cell viability analysis with a non-significant difference of cell death in the control group or the stretched population when observed after 24 hours of cyclically applied strain (**Figure 3.1B**).

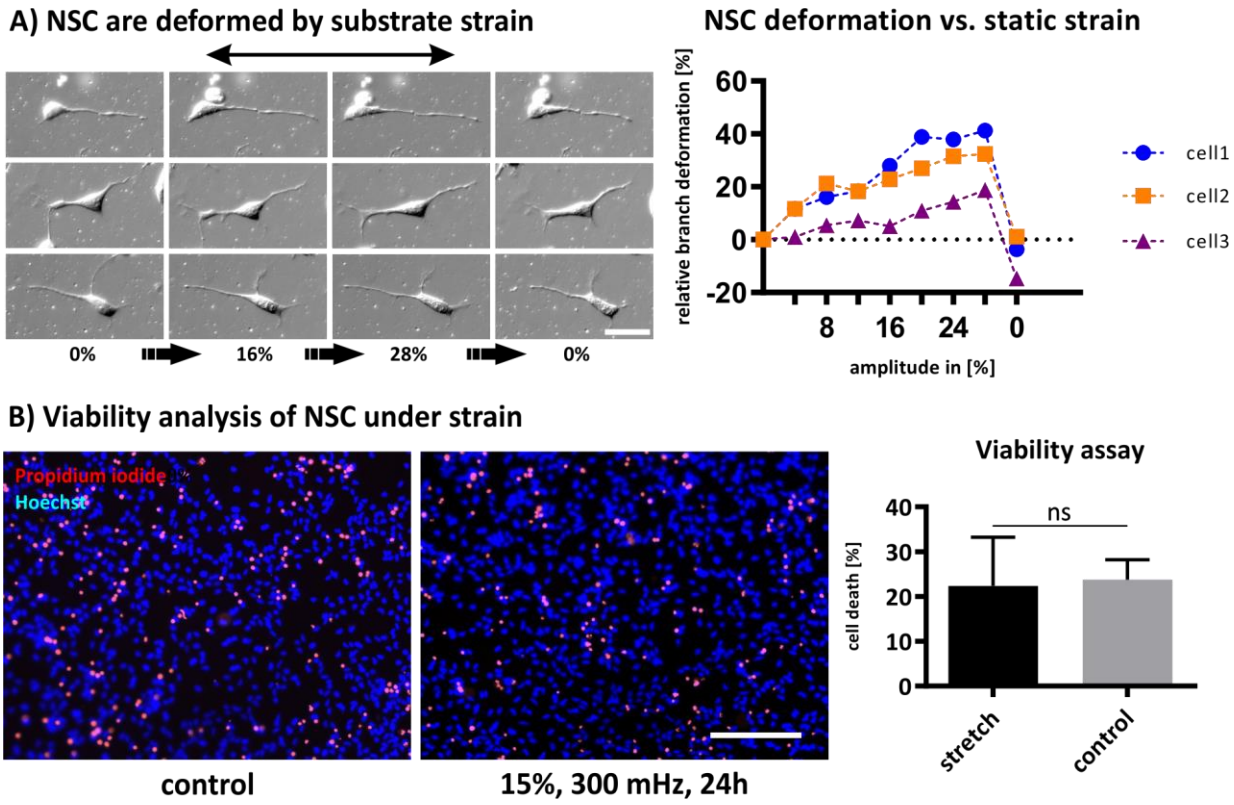

Figure 3.1: NSCs are deformable by substrate deformation and can survive cyclic strain for a long stretching period. NSCs were stretched statically and observed via DIC live-cell microscopy (**A**). Mechanical strain was increased stepwise by an amplitude of 4% and a velocity of 0.5 mm/sec. After reaching 28%, the stretch was released from the system and again observed. Scale bar = 20 µm. The plot represents three exemplary cells and their measured branch deformation. The black arrow indicates the strain direction. Live/Dead staining of NSCs subjected to substrate strain compared to control (**B**). Cells were stained with propidium iodide and counted relative to the number of all cells stained with Hoechst. The values represent the average, and the error bars the standard deviation (p-value = 0.84, n = 4 independent experiments, ns = non significant). Scale bar = 100 µm.

3.1.2 NSCs reduce migration velocity upon initiation of cyclic stretch

As mechanical strain induced a morphological change of NSCs, the effect of such morphological alteration on the dynamic behavior of NSCs was subsequently analyzed. Therefore, the migration pattern of NSCs was investigated via live-cell microscopy while stretched cyclically. Generally, NSCs are highly motile cells. This dynamic nature of neural stem cells was observed before cyclic substrate deformation was induced and also during cyclic stretch. The internal control prior to stretch identifies the difference in the migration velocity of unstretched neural stem cells in comparison to cells that are cyclically strained. **Figure 3.2** depicts the dynamic behavior of NSCs. NSCs migration direction was not altered when cells were stretched cyclically (**Figure 3.2A,** migrating cells are marked with a star). Here, the migration direction was not perturbed by uniaxial strain of the underlying substrate and cells migrate regardless of whether the track direction was pointing in strain direction or perpendicular. Interestingly, the total migration velocity was reduced: while NSCs without strain migrated with a velocity of 0.65 µm/min, cyclically strained NSCs reduced their migration velocity by 29% and showed less dynamic movement compared to control conditions (**Figure 3.2B**). The response was observable after 15 min of cyclic strain but remained comparatively low for longer stretching periods of 80 min. After 15 min, the velocity reduction was significantly reduced. The lower migration speed after 80 min of stretch was not significant as it showed a more disperse mean velocity between the samples.

Although NSCs are less migrative, they still showed a mechanical stretch dependent motion: the branches of neural stem cells aligned in parallel to the stretch direction with time (**Figure 3.2C**). This motion led to a higher number of branches that were aligned towards a smaller angle and shifted the cumulative frequency towards the direction of strain. The cumulative frequency histogram shows the total branch frequencies occurring prior and after stretch and therefore presents the extend of reorientation events in the sample. While a random distribution results in a constant cumulation of events and thereby shows a slope of nearly 1, reorientation towards strain shows a greater slope and a shift towards smaller angles. In comparison, reorientation in perpendicular would result in a smaller slope and a change of

the distribution towards 90°. The change of branch direction was not significant. However, in each of the experiments (n = 3), the orientation shifted towards parallel to the uniaxial strain.

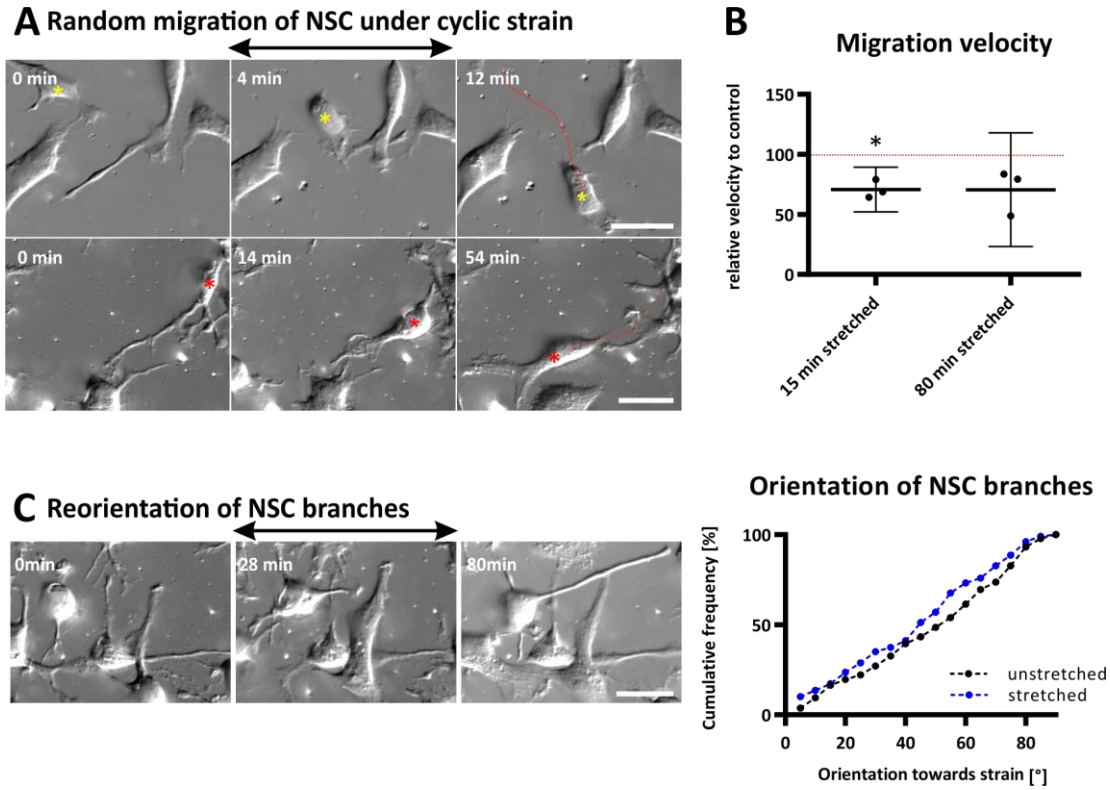

Figure 3.2: Reduced cell migration of NSCs under strain and reorientation of NSCs branches towards strain. NSCs were able to migrate randomly across the elastomer chamber (**A**). Migrating cells are indicated by a red (in stretch direction) and yellow (perpendicular) star. The migration track is indicated by the red line. The black arrow defines the strain direction. The migration velocity was reduced after 15 min (one-sample t-test, n = 3 independent experiments, p-value = 0.021) of cyclic stretch and remained low after 80 min of stretch (p-value = 0.115, n = 3) (**B**). **C** Branches were plotted as cumulative histogram with 0° corresponding to strain direction and 90° perpendicular to it. The cumulative frequency plot depicts n = 3 independent experiments, with a total of 177 cells. All three chambers are observed before and after a stretch period of 80 min. Scale bars = 20 µm.

3.1.3 NSCs proliferate less on cyclically stretched elastomers

Despite the critical role of migration in neocortical development, proliferation is also a crucial endogenous characteristic of self-renewing NSCs. As the proliferative nature of NSCs is associated with migration (Conover et al., 2000), the proliferation frequency of NSCs under

strain was analyzed. Further, the proliferation competence of NSCs has been shown to be mechanically sensitive as the stiffness of the culture substrate influenced their proliferation rate (Blaschke et al., 2019). NSCs were stretched for 24 hours and proliferative cells were labeled by adding BrdU into the media six hours prior to cell fixation. BrdU is incooperated in the DNA of proliferative cells and can be detected by a BrdU specific antibody. After cyclic stretch with an amplitude of 15% for 24 hours, NSCs reduced their number of proliferative cells from 30% to 18% (**Figure 3.3**).

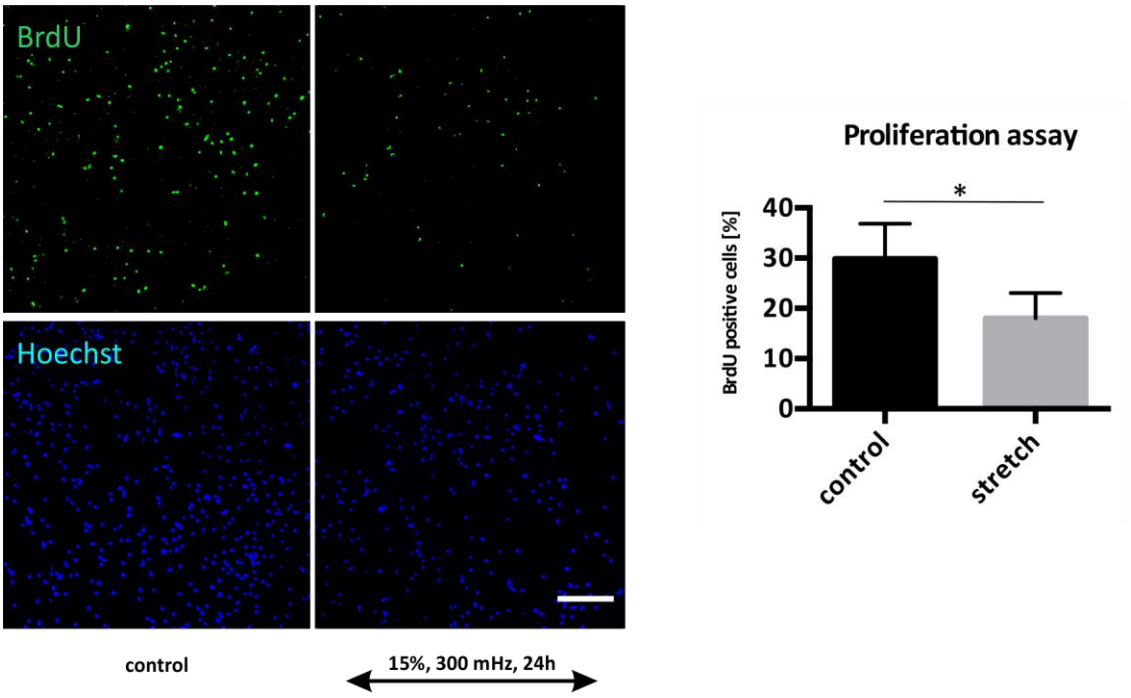

Figure 3.3: Proliferation analysis of NSCs under cyclic strain. NSCs were stretched by 15% and 300 mHz for 24 hours and incubated for 6 hours with BrdU prior fixation. Proliferative cells were stained with an anti-BrdU antibody and all cell nuclei were labeled with Hoechst. The black arrow indicates the strain direction. The values are represented as the average and error bars show the standard deviation (p-value = 0.021 Mann–Whitney U test, n = 7). Scale bar = 100 µm.

3.1.4 Neural stem cells reorient in stretch direction

A common phenomenon of mammalian cells exposed to cyclic strain is the cytoskeletal adaptations to the mechanical stress conditions. Usually, mammalian cells align their cell shape and cytoskeleton towards the perpendicular axis (Faust et al., 2011). In contrast, NSCs clearly showed to point their extensions in the direction of maximal mechanical loads (**Figure 3.4**). The response was observable within a few hours of cyclic strain by live-cell imaging (chapter 3.1.2). However, by stretching for 24 hours, the positioning in stretch direction confirmed the previous findings: branch alignment under cyclic stretch became more prominent and reorientation significant. The alignment in stretch direction could be observed regardless of the cytoskeletal staining (**Figure 3.4A, E**) and was compelling with the intermediate filament staining (42.7° ± 2.0 vs. 45.7° ± 0.6 for vimentin staining; 39.5° ± 3.0 vs. 44.6° ± 0.8 for nestin staining; stretch vs. control, **Figure 3.4E**). Here, NSCs show a fine nestin intermediate cytoskeleton that spans through the NSC extensions, amongst other cytoskeletal proteins. The vimentin intermediate cytoskeleton was colocalized with tubulin (**Figure 3.4D**). Tubulin was more located throughout the NSCs cell shape and revealed a mean orientation of 41.8°± 1.8 in stretched cells (**Figure 3.4E**). The actin cytoskeleton shows a diffuse staining within the cell regardless of whether NSCs were stretched or not. The actin staining was more distributed towards the periphery of the cell and did not show the typical formation of stress fibers and their orientation towards perpendicular to the strain direction (Faust et al., 2011). The cortical actin cytoskeleton, around the cell periphery, defined the major orientation of the cell and thereby indicated the orientation towards strain, although no stress fibers were observed. In addition, protrusions of NSCs showed mainly actin localization. The tubulin cytoskeleton of NSCs showed filamentous structures throughout the cell morphology and thereby indicated the parallel direction of NSCs towards strain. The main intermediate filaments of NSCs are vimentin and nestin (Park et al., 2010). While the nestin cytoskeleton showed a thin filament that spanned centrally through the NSCs and thereby clearly depicted the reorientation of NSCs towards strain, the vimentin cytoskeleton was more located throughout the cell morphology.

Analysis of fluorescence intensity relative to the filaments orientation towards strain revealed a significant increase in perpendicular direction for tubulin (p-value = 0.0193, control vs. stretch, for intensities measured with an angle of 80-90° towards strain) (**Figure 3.4B**). Here, mean intensity values were obtained depending on where the filament was located towards strain and plotted as a normalization relative to mean fluorescence intensity of filaments 0-5° towards strain. This allowed comparing the intensity values over the angles to investigate protein localization relative to the filament orientation. The other cytoskeletal proteins did not show any significant intensity shifts depending on filament orientation. The analysis of protein localization further questioned whether NSCs also undergo cytoskeletal reinforcements under cyclic strain.

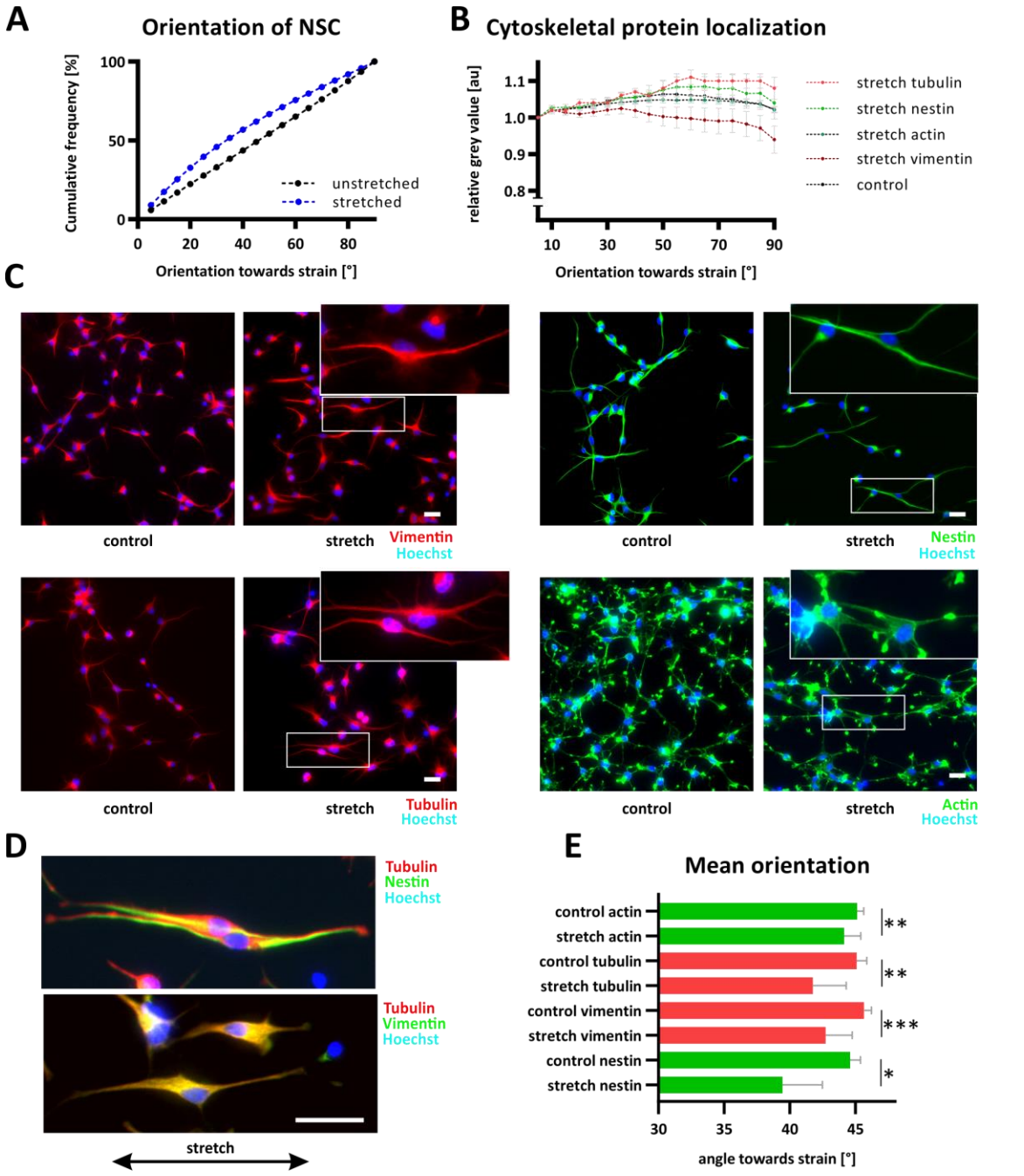

Figure 3.4: Reorientation of NSCs under strain and different cytoskeletal labeling. NSCs were stretched for 24 hours with a frequency of 300 mHz and an amplitude of 15% or grown on elastomer chambers as a control. Cyclic stretch induced a reorientation towards small angles and maximal strain (**A+C**). The cumulative frequency is a representative plot obtained from pixels stained with intermediate filament and their control, the orientation of the pixel is described in the material and methods section (**A**). The intensity of different protein stainings relative to the orientation of the filament indicates different arrangements of the tubulin cytoskeleton (p-value = 0.0193, KS test) (**B**). The plot was generated by normalization of intensity to the intensities measured for branches orientated 0-5° towards strain. The control represents the mean of different protein staining and its

relative intensity. The relative grey value represents variations of protein staining relative to measurements of filaments in maximal strain direction (0°); error bars depict the standard error of the mean. The cytoskeleton of NSCs was differently labeled (**C**). The black arrow indicates the strain direction. Vimentin and nestin filament staining show different colocalization patterns with tubulin (**D**). Different cytoskeletal labeling results in different mean values of branch orientation (**E**), at least n = 3 independent experiments from at least 2 isolations (p-value actin = 0.003; p-value tubulin = 0.002; p-value vimentin =0.0003, p-value nestin = 0.0369, KS test). Scale bars = 20 µm.

3.1.5 Cytoskeletal reinforcement of cytoskeletal proteins in NSCs

The cytoskeletal proteins were further analyzed on their relative intensity by immunofluorescent staining but also by real-time qPCR on mRNA level. The actin immunofluorescence intensity was significantly reduced by 14% when stretched cyclically. Tubulin showed an increase in immunostaining by 50%. While vimentin immunofluorescence intensity was not affected by cyclic strain, nestin showed a substantial increase by around 50% to its control (**Figure 3.5A**). Analysis of respective mRNA levels revealed no change in gene expression of cytoskeletal proteins between the stretched and control group, with the exception of talin. Here, the talin mRNA level was increased by 43% (**Figure 3.5B**). Immunofluorescent labeling against talin shows a higher protein localization at cell protrusions in stretched NSCs (**Figure 3.6**).

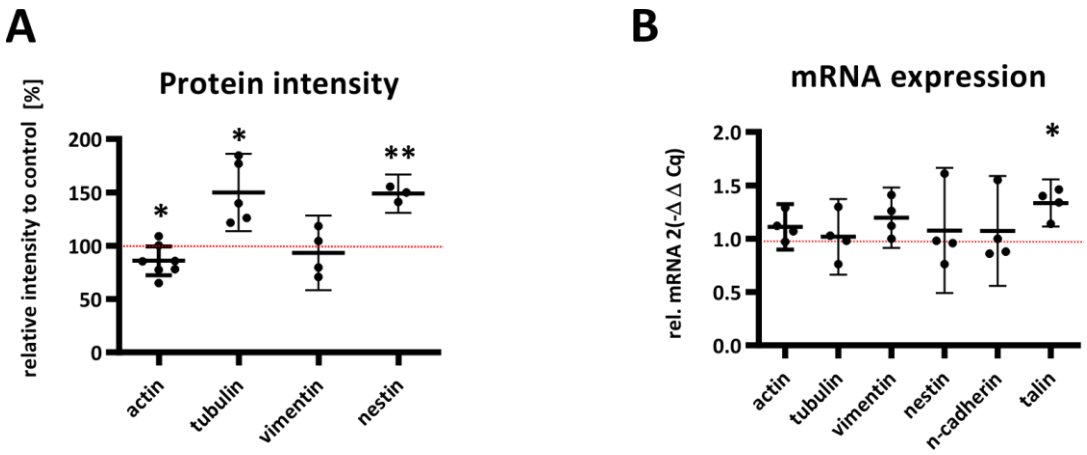

Figure 3.5: Cytoskeletal reinforcement under cyclic strain. (**A**) values express the relative protein intensity of the immunofluorescent staining to its respective controls. Statistics show a one-sample t-test; the hypothetical value of 100% is indicated with a dashed red line (p-

value actin = 0.0443; p-value tubulin = 0.019; p-value nestin = 0.007. The mRNA expression level revealed no significant changes for cytoskeletal proteins, with the exception of talin (p-value = 0.0170) (**B**). Individual mRNA levels were normalized to endogenous RPL expression (ΔCq) and expressed as $2^{-\Delta\Delta Cq}$ relative to the respective controls, n = 4 independent experiments. Plots show the mean + 95% confidence interval. Statistics show a one-sample t-test; the hypothetical value of 1 is indicated with a dashed red line.

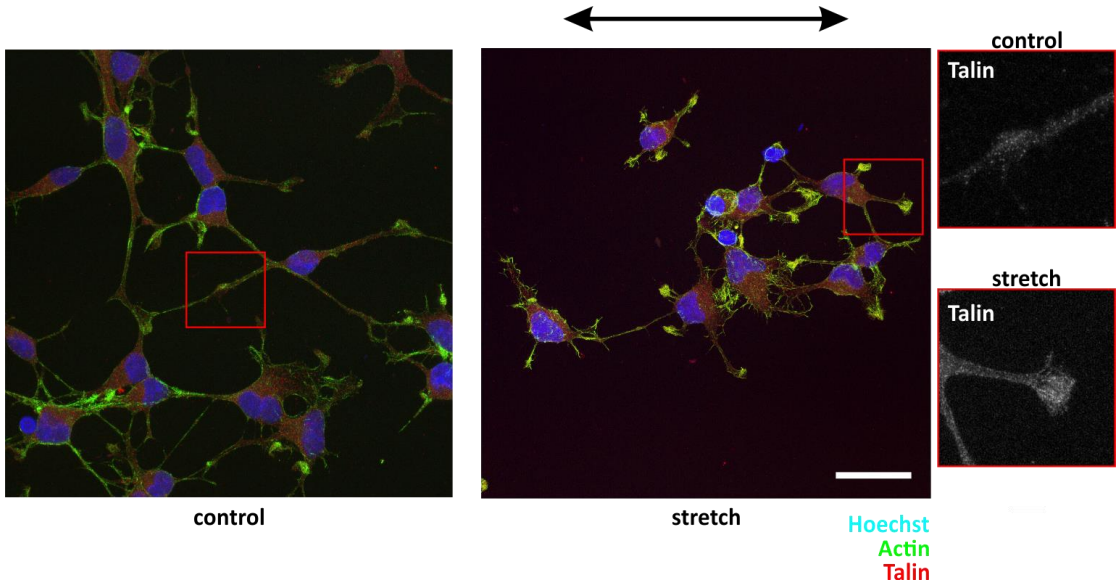

Figure 3.6: Talin localization in stretched and control cells. Cell protrusions show a higher talin localization in stretched cells. NSCs were stretched for 24 hours and 15%. The black arrow indicates the uniaxial stretch direction (n = 2 independent experiments). Scale bar = 20 µm.

In summary, NSCs remained vital and did not show a higher number of dead cells. Further, stretched NSCs under strain were less proliferative compared to unstretched controls. Live-cell imaging confirmed that NSCs were deformed by the underlying substrate deformation and showed a slower migration speed compared to the respective control. While NSCs' cell bodies showed less motion, NSCs point and regrow their branches in stretch direction, which was confirmed after 24 hours stretch by immunofluorescent analysis of different proteins. Interestingly, NSCs reoriented where maximal substrate strain was present and where cells sensed the highest mechanical loads. Actin staining did not show a typical formation of stress fibers and was even reduced in the immunostaining of stretched samples. Staining for tubulin showed a general higher protein localization, as well as an angle-dependent increased

localization in a perpendicular direction. As an intermediate filament, only nestin showed increased immunofluorescent labeling in stretched cells compared to control.

3.2 The response of cell differentiating to astrocytes and neuronal cells under strain

3.2.1 Mechanical strain does not have an influence in fate decision between neuronal cells and astrocytes

Neural stem cells differentiate either to a neuronal, Tuj1 positive phenotype, to an astrocytic GFAP positive phenotype, or to oligodendrocytes. The lineage commitment has been shown to be sensitive to mechanical cues (Baek et al., 2018; Blaschke et al., 2019). Blaschke et al., focused on the influence of substrate stiffness on the differentiation pattern between astrocytes and neurons, while Baek et al. focused on the impact of topographical cues. Both studies proved that the two different categories of mechanical cues have an influence on lineage commitment. In the scope of this study, I investigated the effect of cyclic deformation on the lineage choice between neurons and astrocytes. For this purpose, NSCs were stretched for several days cyclically while withdrawn from the mitogen to study the influence of cyclic strain in the differentiation process. The mitogen keeps NSCs in the stem cell stage and therefore prevents differentiation processes. After five days of differentiation, the ratio of astrocytes to neuronal cells remained similar between the stretched and control group and was not changed when grown on cyclically stretched substrates (**Figure 3.7A**). Further, differentiation speed and the presence of the stemness marker SOX2 were also not affected by cyclic strain (**Figure 3.7B**). The number of SOX2 positive cells did not differ between the stretch and control groups as observed for stretched NSCs that were still in the stem cell stage (data not shown) and also for cells that differentiated for five days. Here, the number of SOX2 positive cells within the differentiating co-culture has not been affected. The similar ratio of neuronal cells to astrocytes and the same count of SOX2 positive cells in stretch and control

conditions reflect that cyclic mechanical strain did not have any effect on fate decision and neither to the differentiation speed.

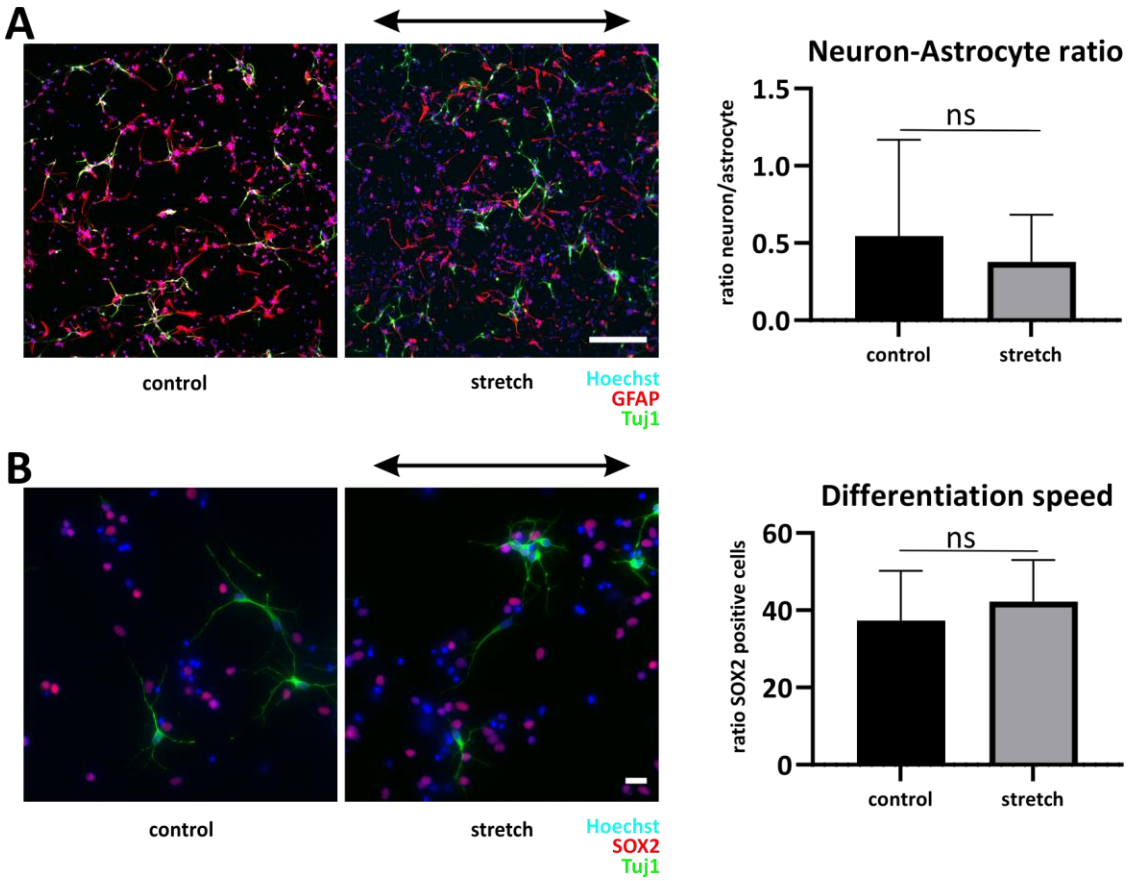

Figure 3.7: Lineage commitment and differentiation speed are not influenced by cyclic strain. Cells were either stretched for five days during mitogen withdrawal or cultivated on elastomer chambers as a control. Neuronal cells labeled with Tuj-1 were counted and compared relative to the number of astrocytes (GFAP labeled) n = 8 independent experiments, with 12 chambers per parameter from 4 isolations (**A**). Stretch and control showed the same ratio of neurons to astrocytes (p-value = 0.93). Scale bar = 100µm. The speed of differentiation was analyzed by counting the number of SOX2 positive cells in the stretched and control cultures (**B**) n = 3 chambers per parameter from 1 isolation. Bar plots depict the average and error bars depict the standard deviation (p-value = 0.2). The black arrow indicates the strain direction. Scale bar = 20 µm.

3.2.2 Developing astrocytes remain in stretch direction

To identify the mechanoresponse of developing astrocytes, the orientation of astrocytic extensions was analyzed. Differentiated astrocytes aligned with their GFAP positive extensions and their cell shape in stretch direction (**Figure 3.8**), similar to the previously described reorientation of stem cells (chapter 3.1.4). The astrocytes pointed with their long extensions (**Figure 3.8A**) in stretch direction and showed a shifted cumulative frequency plot towards small angles (**Figure 3.8B**). The mean orientation of stretched astrocytes also indicated the parallel orientation towards strain with an angle of 34.7 ± 7° for stretched cells compared to 45.4 ± 4° for controls (**Figure 3.8C**).

Thus, as this response was observable in the stem cell stage, but also in differentiating astrocytes, the subsequent question was whether the differentiating cells showed a reorientation behavior or whether alignment in stretch direction was due to parallel alignment when cells were still in stem cell stage.

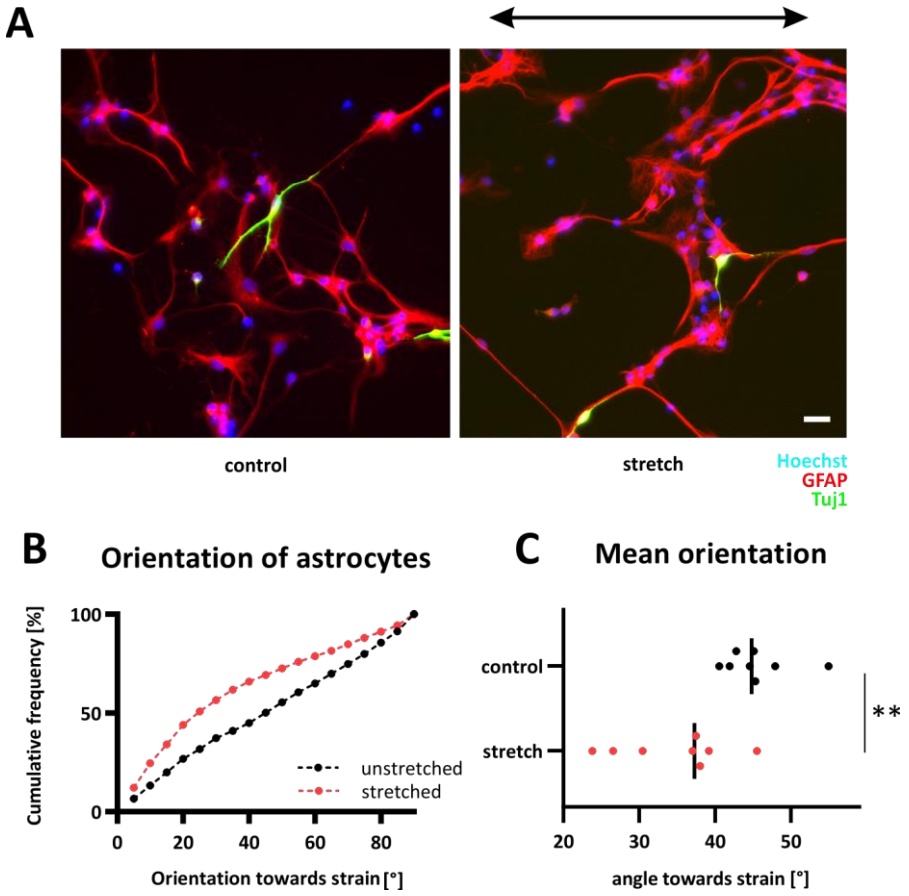

Figure 3.8: Orientation of differentiating NSCs to astrocytes towards strain. NSCs were stretched for five days during mitogen withdrawal and differentiation to astrocytes, which were stained by the astrocyte-specific intermediate filament GFAP (**A**). The black arrow indicates the strain direction. The cumulative frequency is a representative plot obtained from pixels stained with GFAP intermediate filament and their control (**B**). The mean orientation of 8 independent experiments is indicated for unstretched (control) and stretched samples (**C**) (p-value = 0.005). Scale bar = 20 µm.

3.2.3 Changing direction during stretch: differentiating astrocytes reorient towards strain and share a joint response with NSCs

To address the question of whether the reorientation towards strain is a unique response of NSCs or the differentiating astrocytes reorient to maximal mechanical load actively, NSCs were stretched during mitogen withdrawal for three days. After three days of stretch, the chambers were flipped by 90° and further stretched for two additional days. As depicted in **Figure 3.9**, NSCs that have already developed to astrocytes for three days and aligned in stretch direction could change the reorientation when stretch was applied with an angle of

90° towards the initial strain direction. The results indicate that, indeed, the reorientation towards strain is an active mechanoresponse of differentiating astrocytes.

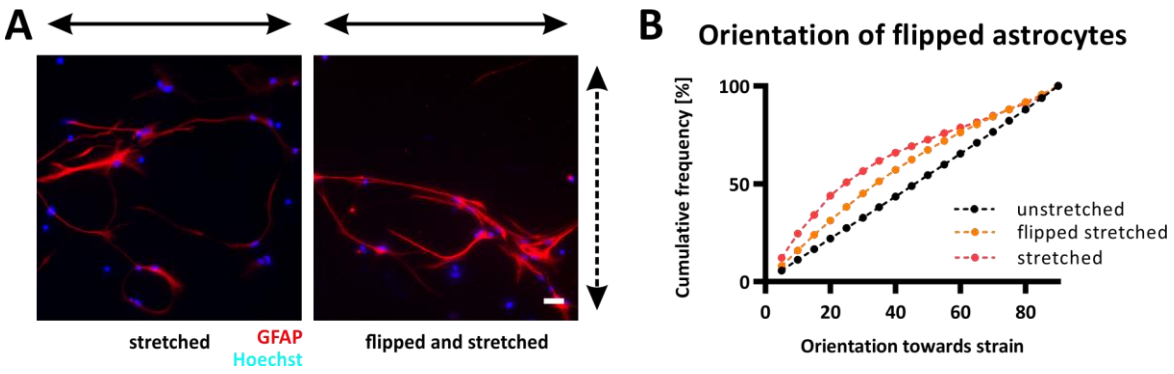

Figure 3.9: Differentiating astrocytes align in stretch direction. NSCs were stretched during mitogen withdrawal for three days with a frequency of 300 mHz and an amplitude of 15%. After three days of stretch, the elastomer chambers were removed from their chamber holder and flipped by 90 degrees (**A**). The stretch was continued for another two days before cells were fixed and stained. The dashed arrow indicates the stretch direction of the first three days; the black arrow indicates the stretch direction of the last two days. As a control, cells were stretched uniaxially in one direction for five days without flipping the chamber, n = 2 chambers per parameter from 1 isolation. The black arrow indicates the stretch direction of the control. Scale bar = 20 µm. The cumulative frequency shows the orientation of the GFAP staining for unstretched, stretched and flipped, and uniaxially stretched samples (**B**).

3.2.4 Cyclic strain induces cytoskeletal reinforcement of the GFAP intermediate filament

When mammalian cells are stretched cyclically, they usually undergo reorientation towards perpendicular to strain and further show to increase the cytoskeletal filament formation. The reinforcement allows cells to further stabilize the cytoskeletal filaments under mechanical loads (Faust et al., 2011). A cytoskeletal reinforcement was present in stretched differentiating astrocytes with more GFAP protein localized in the filamentous structures of astrocytes that were subjected to cyclic strain (**Figure 3.10A,B**). The cytoskeletal reinforcement was further confirmed by real-time qPCR as stretched differentiating cells showed an elevated GFAP mRNA level depicted in **Figure 3.10C**.

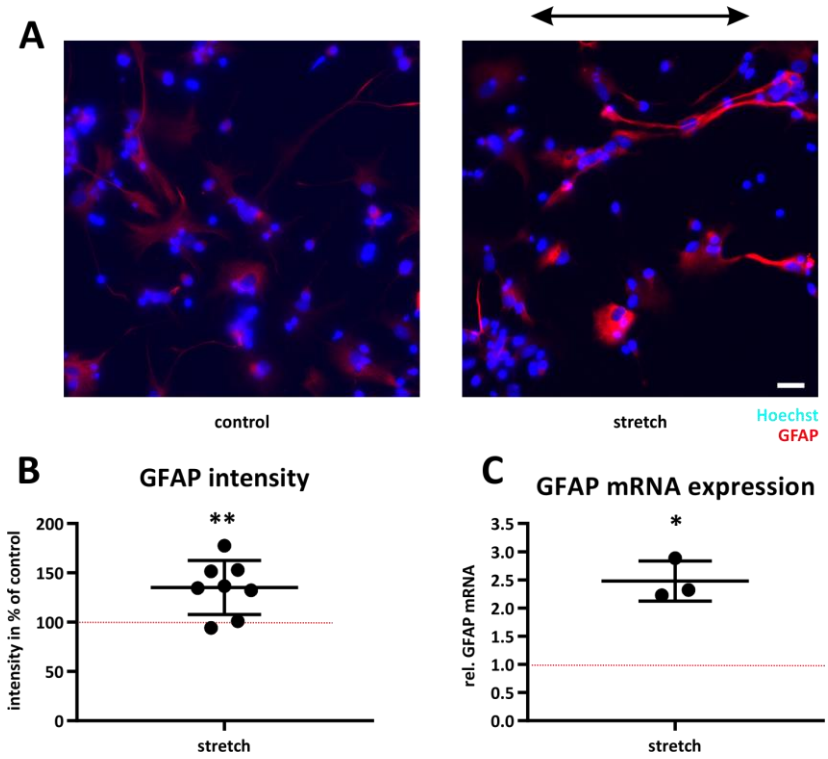

Figure 3.10: Cytoskeletal reinforcement of the GFAP intermediate filament by cyclic strain. NSCs were withdrawn from the mitogen and stretched with an amplitude of 15% and a frequency of 300 mHz during their differentiation to astrocytes. After five days of differentiation, cells were fixed and stained for GFAP (**A**). The black arrow indicates the strain direction. Scale bar = 20 µm. The images of stretch and control were equally contrast-enhanced. Intensity analysis of images shows an elevated GFAP localization (**B**) (n = 8, p-value = 0.008, a one-sample t-test was performed against the hypothetical value of 100% (indicated with a dashed red line)). Quantitative real-time PCR of isolated mRNA of stretch and control also shows an increased expression of GFAP (**C**) (n = 3, p-value = 0.02, a one-sample t-test was performed against the hypothetical value of 1 (indicated with a dashed red line)).

3.2.5 Response of differentiating neurons to cyclic mechanical strain

NSCs primarily develop to astrocytes on soft elastomer substrates but also with denoting number to a neuronal cell type (Blaschke et al., 2019). The resulting co-culture thus mainly consist of cells that have developed to astrocytes but also to a neuronal phenotype. Both phenotypes could possibly have different mechanoresponses as they reveal a different cytoskeletal setup. Interestingly, NSCs that had a lineage commitment towards a neuronal phenotype resided on top of the astrocytes (**Figure 3.11A**), showed a minor mechanoresponse and aligned slightly perpendicular towards mechanical strain (**Figure**

3.11B). The orientation of neurons did not differ between stretch and control (46.6 ± 3°(median ± STD) for stretched cells and 45.4 ± 1° for the control, data not shown). Noteworthy, in general neuronal cells show a clear mechanoresponse to cyclic mechanical when cultivated without astrocytes (chapter 3.3.1), thus indicating that astrocytes influence the behavior of neuronal cells to substrate deformation. Further, no cytoskeletal reinforcement in differentiating neurons was observed for tubulin cytoskeleton, grey values obtained from the Tuj-1 staining did not differ between stretched and control samples (data not shown).

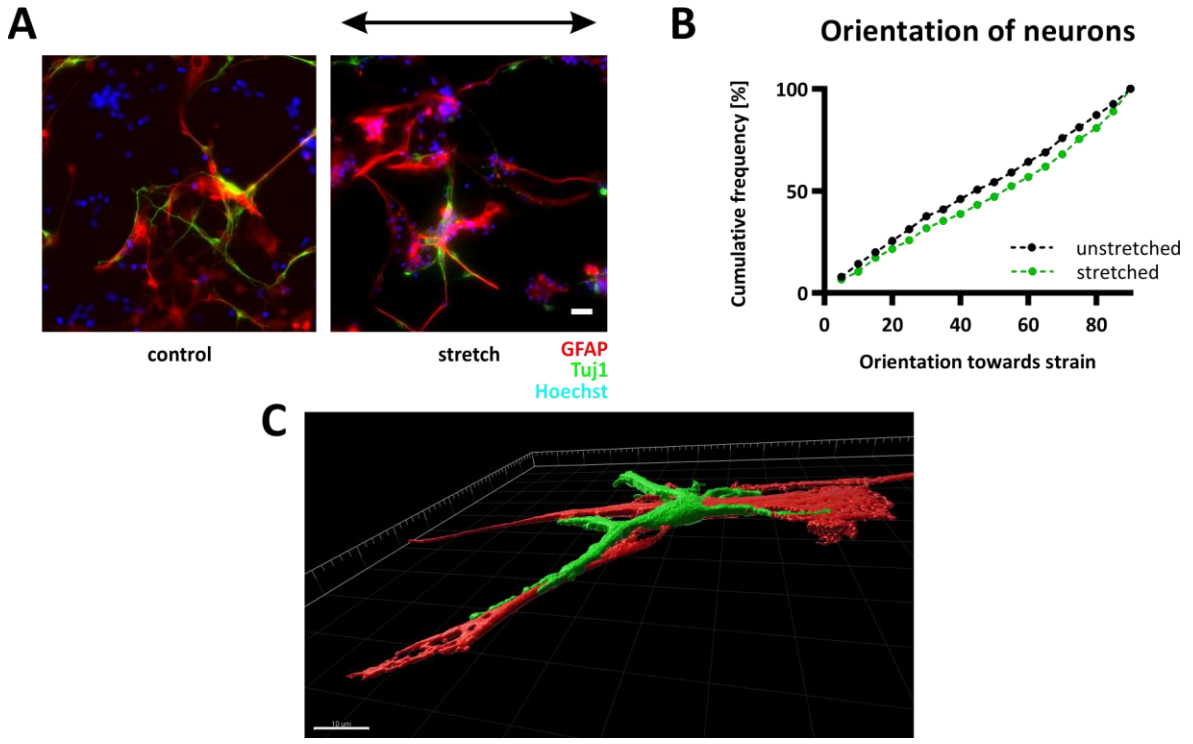

Figure 3.11: Orientation of differentiating NSCs to neuronal cells towards strain. NSCs were withdrawn from the mitogen and stretched with an amplitude of 15% and 300 mHz frequency during their differentiation. After five days of differentiation, cells were fixed and stained for Tuj1, GFAP, and Hoechst (**A**), n = 8 independent experiments, with 12 chambers per parameter from 4 isolation. NSCs differentiated to neuronal cells (Tuj1 positive) grew on top of astrocytes (GFAP positive). The black arrow indicates the strain direction. Scale bar = 20 µm. Cyclic stretch induced a slight reorientation towards perpendicular as represented by the cumulative frequency plot of the orientation of neuronal cells (**B**). Differentiated neurons grew on top of astrocytes (**C**). Images were taken with an LSM 880 and processed with the Imaris software. Scale bar = 10 µm.

3.2.6 Differentiated astrocytes and neurons show differences in the tubulin and actin cytoskeleton independent of stretch

Microtubules are the stiffest of the cytoskeletal components within a cell (Fletcher & Mullins, 2010). Considering that microtubules are described to be less present in astrocytes (Peters & Vaughn, 1967), a further hypothesis was that differentiating astrocytes may also reveal fewer microtubule structures compared to neurons. A different cytoskeletal setup may explain the different mechanoresponse in the differentiating co-culture. Therefore, staining experiments were performed and **Figure 3.12A** illustrates the differences in microtubule staining in developing astrocytes and other cells found in the developing co-culture. Developing astrocytes show distinctly fewer microtubules, regardless of whether they are subjected to cyclic stretch or not. Neurons, however, exhibited a more intensified tubulin staining than astrocytes (an exemplary neuron is marked with a white star). Further, the actin cytoskeleton was also different in astrocytes versus neuronal phenotypes. While astrocytes show a more broadly distributed actin cytoskeleton, neuronal cells show only actin fibers along extensions and within the cell bodies (**Figure 3.12B**). The distribution of actin in differentiating astrocytes was independent of stretch. Differentiated astrocytes showed also no stress fiber formation even when stretched for five days during differentiation. Actin was mainly located as cortical structures.

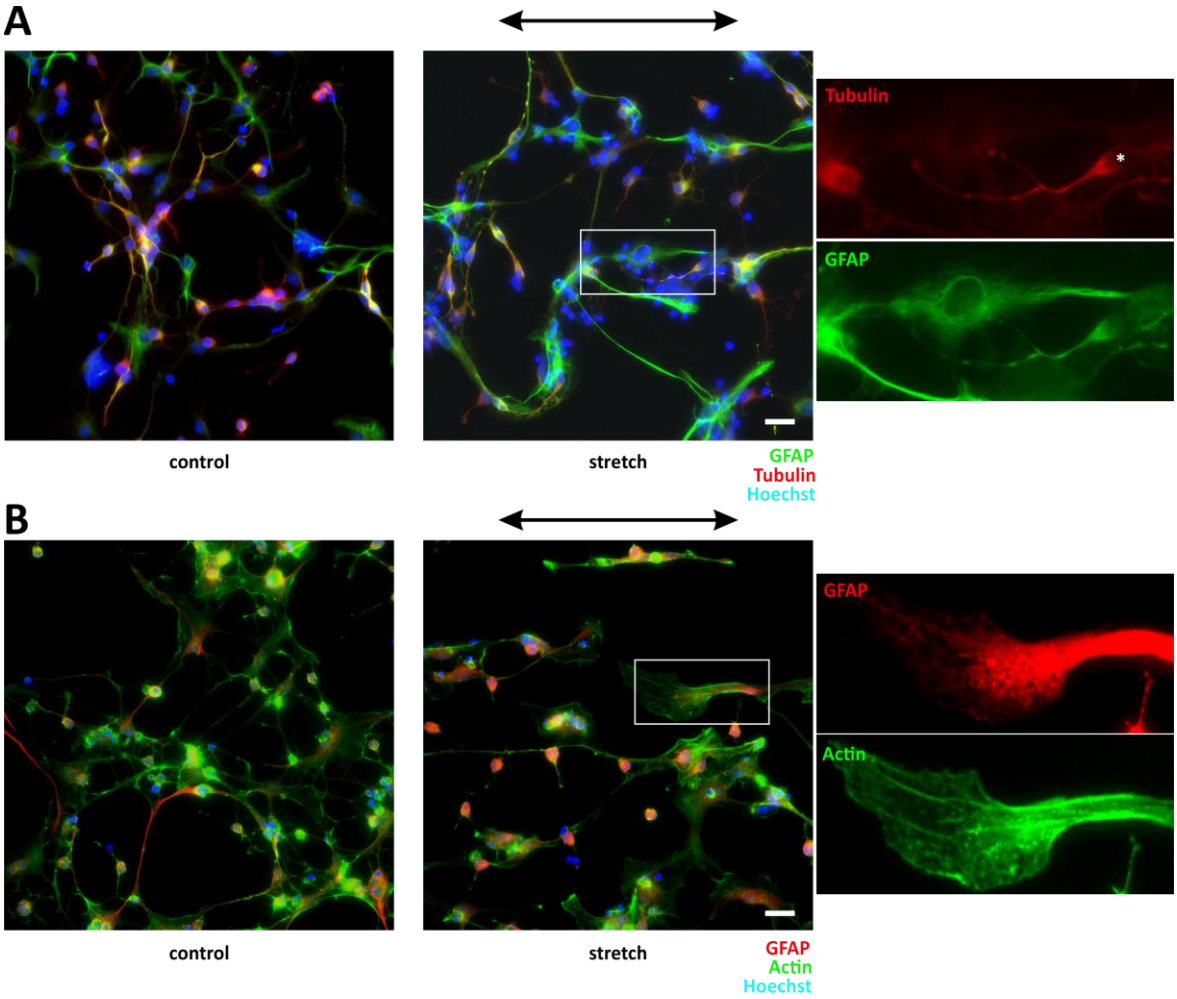

Figure 3.12: Differentiated astrocytes and neurons show differences in the tubulin and actin cytoskeleton independent of stretch. Microtubules are less present in differentiating astrocytes compared to differentiating neurons independent of cyclic strain (**A**). The white start highlights a neuronal cell. Actin localization of neurons and astrocytes also did not differ between stretch and controls (**B**). NSCs were stretched during mitogen withdrawal for five days and then stained for the astrocyte-specific intermediate filament GFAP, tubulin, and phalloidin 488 for actin (n = 3 independent experiments from 2 isolations). Stretch direction is indicated by the black arrow. Scale bars = 20 µm.

To sum up this chapter, cyclic mechanical deformation induced a different mechanoresponse in cells that differentiated from NSCs to an astrocyte compared to NSCs that differentiated to neuronal cells. Neurons did not show any reorientation and no cytoskeletal reinforcement. Cortical neurons grew on top of astrocytes and showed less contact to the deforming

elastomer substrate. Differentiating astrocytes aligned in direction of uniaxial stretch even when the direction of substrate deformation had been changed during the differentiation process. Furthermore, they also showed a reinforcement of their GFAP intermediate filament.

3.3 The response of differentiated cells of the CNS to cyclic strain

3.3.1 The response of primary cortical cells to cyclic substrate strain

Despite cells that develop from a stem cell to a neuronal and astrocyte phenotype - and thus are still in a premature, developing stage- this thesis also comprises the effect of cyclic mechanical signals to more mature cells of the CNS. The development of NSCs to mature neuronal cells and mature astrocyte includes several morphological changes and cytoskeletal adaptations (Hauser et al., 2018). In this work, primary cortical neurons were isolated from E18 rat embryos, while mature astrocytes were isolated from postnatal rat pups. First, the response of primary cortical neurons to cyclic strain is described in this chapter, followed by the effects of cyclic strain on astrocytes, and finally, the co-culture of astrocytes and neuronal cells.

3.3.1.1 Cortical neurons showed retraction under cyclic stretch but redirect their growth cone perpendicular to stretch direction

To study the immediate effect of cyclic strain on neuronal branches, primary cortical neurons were observed via live-cell microscopy. Cortical neurons were plated on elastomer chambers and stretched after adherence of 12 hours. As in this stage, the neuronal cytoskeleton is more dynamic compared to more mature neurons (Kapitein & Hoogenraad, 2015), cortical neurons were also analyzed when grown for six days on PDMS substrates and formed neuronal networks with a more stabilized cytoskeleton. In the following chapter, first, live-cell imaging of newly formed branches under cyclic strain is described, followed by experiments with six days old cortical neurons.

3.3.1.2 Neuronal branches retracted upon initiation of strain

When newly formed branches were cyclically stretched, different reactions were observed depending on the location of the neuronal branch. For neuronal branches that pointed more to the uniaxial strain direction, branches retracted or became thinner (**Figure 3.13A, B**). Neuronal branches that were aligned already perpendicular to the uniaxial strain kept their size and position. After several cycles of mechanical strain, neuronal branches started to regrow perpendicular to the stretch direction, thus, defining the whole cell orientation towards larger angles (**Figure 3.13C, E**). As depicted in **Figure 3.13C**, the leading tip (marked with a white arrowhead), which may represent parts of the growth cone, appeared to be enlarged after 140 min of stretch and remained enlarged during turning towards a perpendicular direction.

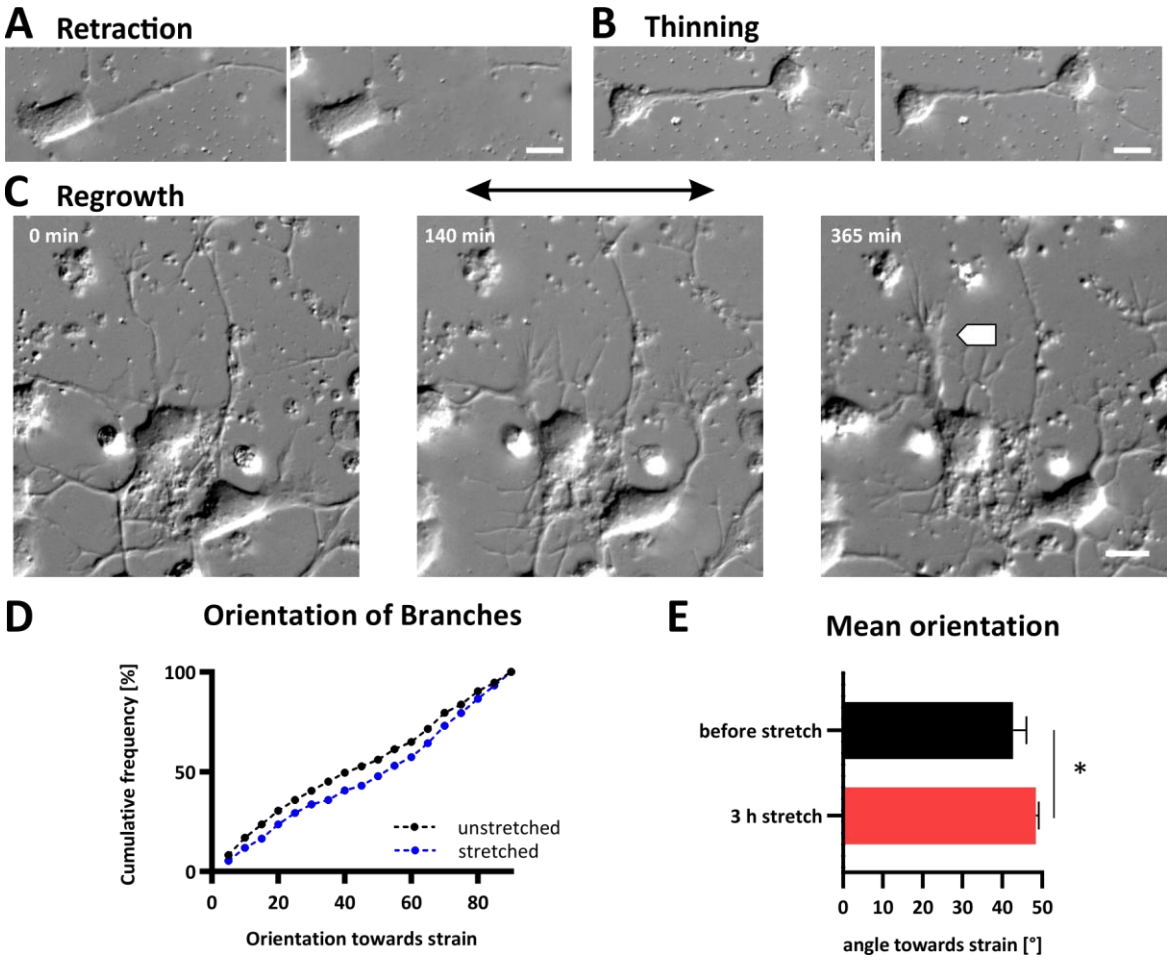

Figure 3.13: Live-cell imaging of primary cortical neurons under cyclic strain. Cells were stretched cyclically after 12 hours in culture to allow cell adherence on the elastomer substrates. Neuronal branches retracted when pointing in stretch direction (**A**) or became thinner (**B**). The cells regrew (white arrow) during stretch in a perpendicular angle towards strain (**C**). The black arrow indicates the strain direction. The events resulted in the orientation of branches towards a perpendicular direction (**D**) and mean orientation that shifted towards larger angles (**E**). Bar plots depict mean plus standard deviation (p-value = 0.03). Scale bar = 10 µm.

Cortical neurons that developed to mature neuronal branches after six days of outgrowth and formed network like structures were also analyzed by live-cell imaging. The immediate reaction was a retraction of neuronal branches regardless of the direction towards uniaxial strain (**Figure 3.14A**). The magnitude of retraction also differed depending on the initial alignment of neuronal branches. Here, neuronal branches in stretch direction retracted with

a higher magnitude of 19-41 µm, while branches aligned in a perpendicular angle retracted 2-11 µm (n = 2 independent experiments, from 2 isolations, 10 branches analyzed).

Further, branches showed to form retraction bulbs near the tip of the branch with sizes between 2-4 µm independent on the initial branch orientation, approximately double the size as the same branch diameter before stretch. Such retraction bulbs were not detected on cortical cells when stretched in an early stage (**Figure 3.13A-C**) when cells had newly formed and smaller branches. To analyze the origin of such retraction bulbs, cortical cells were fixed after the formation of retraction bulbs and stained for the main cytoskeletal systems (**Figure 3.14B**). All cytoskeletal systems curled and showed to roll up in such retraction bulbs, which could explain the enlargements within the branches observed within the DIC contrast images. Although actin was still present at the tip of the branch, it was also localized within the retraction bulb. After several cycles of stretch, between 25-55 min, the branches began to regrow even if pointing in stretch direction (**Figure 3.14A**). Interestingly, releasing the stretch from the system after one hour of cyclic stretch, the neuronal branches regrow by a growth velocity of 0.84 µm/min ± 0.3 (mean ± STD) compared to 0.33 µm/min ± 0.14 µm/min (n = 5 independent experiments, 20 branches analyzed).

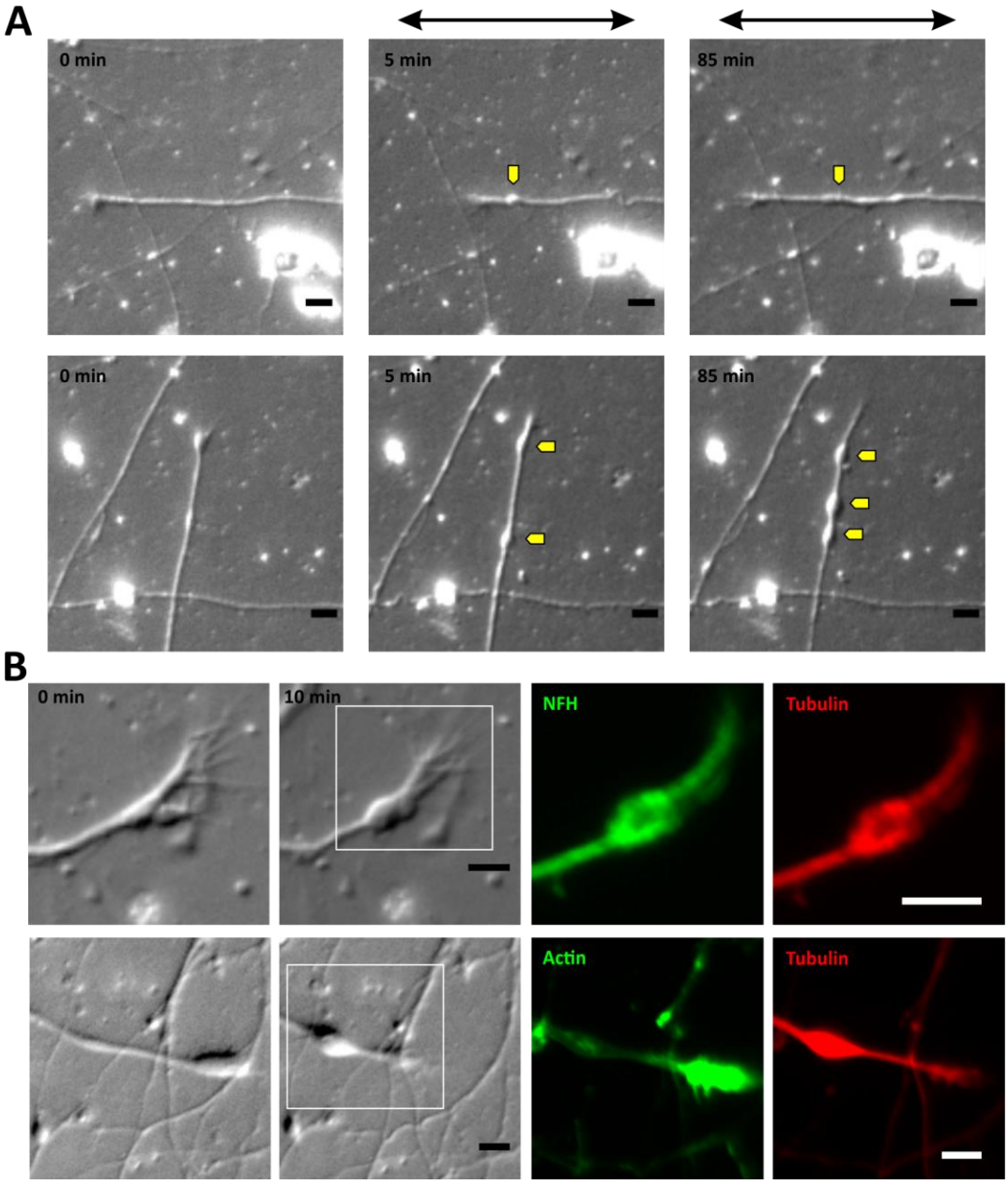

Figure 3.14: Retraction and bulb formation upon initiation of stretch. Cortical cells were cultivated for six days and then stretched cyclically. Cortical branches retracted even in the first few cycles and began to regrow after several cycles of stretch (**A**). The margin of retraction length differed dependent on the initial direction before strain. The black arrow indicates the stretch direction. The yellow arrow indicates the location of retraction bulbs. Scale bar = 10 µm. The retraction bulb formation involved all three cytoskeletal components (**B**). Scale bars = 5 µm. **Figure 3.14A** is adapted from (Abraham et al., 2019).

In summary, live-cell experiments on cortical neurons showed a slightly different response depending on when cyclic stretch was initiated. While newly-formed branches retracted without the formation of remaining retraction bulbs, branches that matured within six days of outgrowth showed retraction bulbs by the initiation of cyclic strain. In addition to the induced outgrowth of branches in a perpendicular direction, retraction of branches previously pointing in stretch direction is responsible for a general reorientation of neuronal branches in the direction perpendicular to strain.

3.3.1.3 Cortical neurons remain vital after stretch and align perpendicular in an amplitude-dependent manner

Although the initial response to cyclic stretch was drastic, cortical neurons survived long stretch periods of 24 hours and developed to neuronal networks even when cyclic stretch was constantly applied for up to six days. Cyclically stretched cortical neurons remained vital and did not show any sign of apoptotic behavior or cell death (**Figure 3.15**). Cortical neurons showed to adapt to the mechanical stress condition by growing their cytoskeleton perpendicular and even grow to perpendicular aligned neuronal networks after six days of constant cyclic mechanical substrate deformation (**Figure 3.15A**). The reorientation behavior was dependent on the mechanical load supplied to the cortical neuron culture (**Figure 3.15B, C**). Here cortical neurons aligned in an amplitude-dependent manner perpendicular to strain. The highest directional outgrowth was observed for an amplitude of 28% with a mean orientation of 70.1 ± 2.7°. As the cell culture of cortical cells looked quite heterogenous, live/dead analysis was performed with flow cytometry by staining cells with ethidium homodimer and compared with positive and negative controls. The latter was obtained by inducing cell death with camptothecin (**Figure 3.15D**).

Thus, cortical cells avoid the mechanical load as they extend their neuronal branches perpendicular to the uniaxial strain. Therefore, they survive high amplitudes of stretch and even grow as neuronal networks under constant mechanical loads.

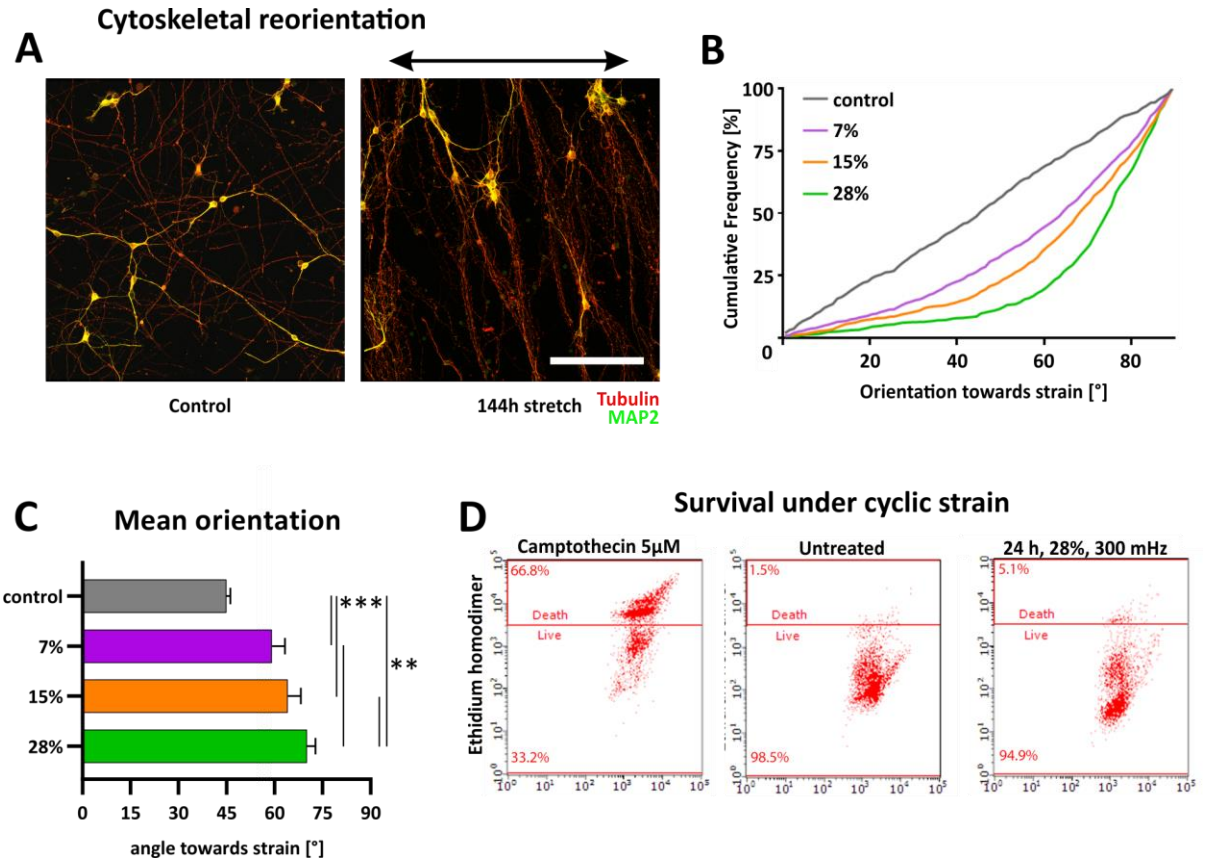

Figure 3.15: Directional outgrowth and survival under cyclic strain towards a perpendicular angle. Cortical cells adapt to cyclic mechanical stretch by growing perpendicular to strain (**A, B**). Cell formed networks under cyclic stretch even when stretched for 144 hours (**A**). The black arrow indicates the strain direction. Scale bar = 100 µm. The reorientation process is amplitude-dependent (**B**) as observed for cells stretched for 24 hours with different amplitudes and a constant frequency of 300 mHz. The plot shows the cumulative frequency of the branch orientations. The mean orientation changed significantly towards higher angles with the degree of different amplitudes (**C**). (p-value = 0.003 control vs.7%; p-value = 0.004 control vs. 15%; p-value = 0.0013 control vs. 28%; p-value = 0.0582 7% vs. 15%; p-value = 0.0003 7% vs. 28%; p-value = 0.0022 15% vs. 28%, n = 6). The survival was analyzed by flow cytometry of ethidium homodimer stained cells (**D**). As a negative control, cell death was initiated by adding 5 µM camptothecin. Control and 28% stretched cells did not show any significant difference according to the percentage of cell death (n = 4, p-value = 0.534). Figure 3.16A,B,D is adapted from (Abraham et al., 2019).

3.3.1.4 Cytoskeletal proteins show different localization towards stretch direction in an amplitude-dependent manner

Cytoskeletal proteins play a fundamental role in cellular mechanoresponse. Cyclic stretch has been shown to induce cytoskeletal reinforcement beside a definite cytoskeletal

reorientation. The protein localization of the three main components of the neuronal cytoskeleton was analyzed according to their strain direction to understand cytoskeletal dynamics of neuronal cells under cyclic strain. **Figure 3.16** depicts the localization of NFH, actin, and tubulin under cyclic strain with increasing amplitudes. For each cytoskeletal protein, the highest immunofluorescent intensity is perpendicular to cyclic strain. This effect was visible already at a low frequency of 7% and is more present with increasing amplitude. As observed previously, there is a clear mechanoresponse and outgrowth in a perpendicular direction. However, some of the branches are still pointing in stretch direction or diagonal and may be exposed to mechanical stress differently. Actin and tubulin showed the highest shift in protein localization towards perpendicular when stretched with a high amplitude of 28% while the response of NFH was slightly less. To analyze the significance of such angle-dependent protein localization shift, the mean intensities of the 80-90° batch were compared between the stretch and control group and reached significant levels in the 15% and 28% stretched group for each protein staining (actin: 15% stretch p-value = 0.018, 28% stretch p-value = 0.008; tubulin: p-value = 0.018, 28% stretch p-value = 0.008; NFH p-value = 0.002, 28% stretch p-value = 0.005).

In addition, stretched cortical neurons showed an amplitude-dependent higher protein intensity detected by immunofluorescence when comparing the relative grey values. Here, there was an amplitude-dependent increase of protein intensity with a significant difference when stretched with 28% for each cytoskeletal protein relative to the smallest stretch amplitude (**Figure 3.17**). To further investigate reinforcement behavior under strain, the proteins isolated from cortical neurons were further analyzed by western blot.

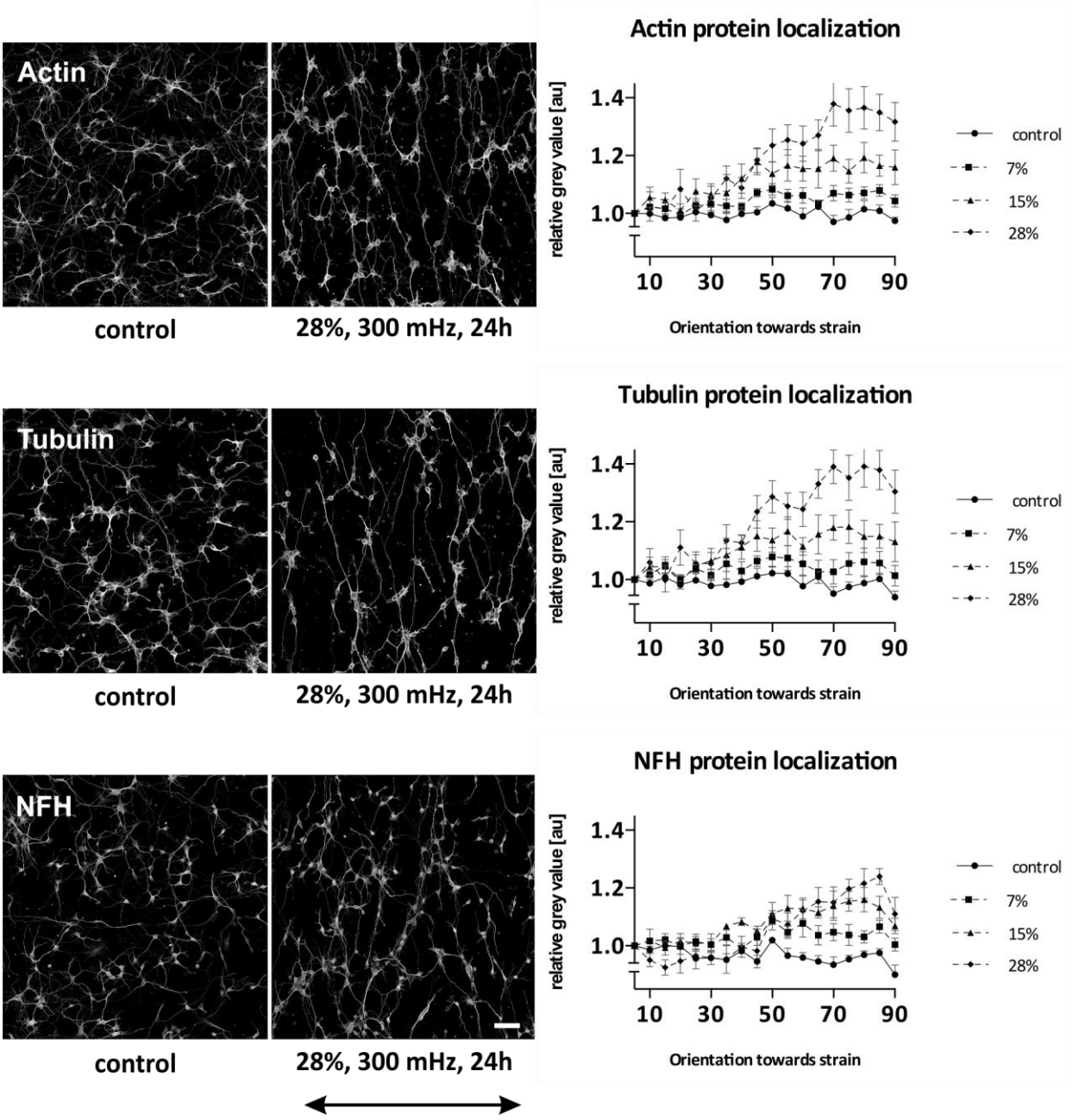

Figure 3.16: Protein localization of stretched cortical neurons. Primary cortical neurons were stretched for 24 hours with a varying amplitude of 7%, 15% and 28% and a constant frequency of 300 mHz. The intensity of the different stainings was higher in branches pointing perpendicular to the uniaxial strain. The black arrow indicates the strain direction. Scale bar = 50 µm. Plots were generated by normalization of intensity to the intensities measured for branches orientated 0-5° towards strain (n = 3 independent isolations).

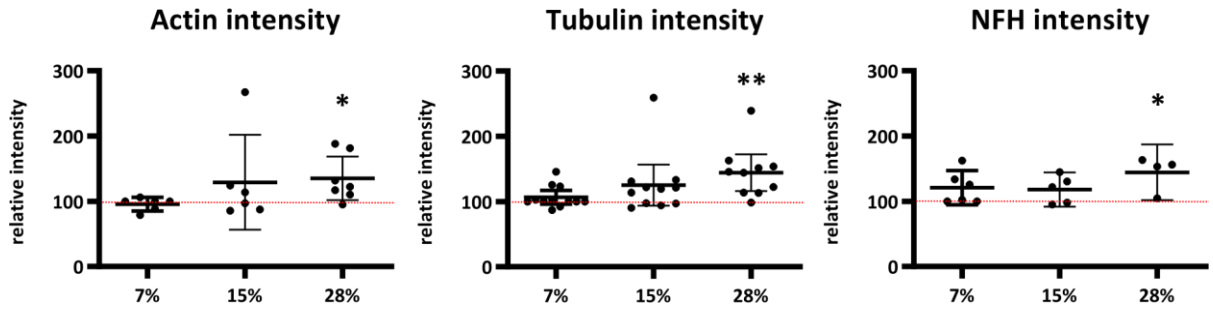

Figure 3.17: Intensity increase of immunostained cytoskeletal proteins under cyclic strain. Cortical neurons were stretched for 24 hours with different amplitudes. Cytoskeletal staining intensity was obtained from the cell mask as described in material and methods. An amplitude of 28% induced a significant higher protein localization in cortical neurons relative to the smallest amplitude (actin: p-value = 0.0409, tubulin: p-value = 0.006, NFH: p-value = 0.0456). Statistics show a one-sample t-test against the hypothetical value of 100%. Plots show the mean of relative intensity + the 95% confidence interval (n = 3 independent isolations).

3.3.1.5 The neuronal microtubule cytoskeleton show a higher intensity of post-transcriptional modifications

To further quantify stretch-induced changes in the cytoskeleton, western blot analyses were performed. Here, proteins were isolated after stretch for 24 hours with an amplitude of 28%. **Figure 3.18** shows the western blot on the left and analysis of three independent experiments on the right. Only NFH showed a significantly higher protein level when normalized to GAPDH as a housekeeping protein and compared between the stretch and control group. Post-transcriptional modified tubulin was normalized to tubulin protein level and showed higher intensity in stretched cells when stained with specific antibodies against acetylated and tyrosinated tubulin. In addition, the microtubule-associated protein MAP-2, showed higher protein expression in stretched cells compared to control cells, suggesting that stretched cells demand more stabilization by its adaptor proteins. The housekeeping protein GAPDH showed a reduced protein content in stretched cells compared to control cells. However, protein concentration was measured with a BCA assay and equal total amounts were loaded on the gel. Such difference may be due to interference of the coating protein with the BCA assay and a reduced number of stretched cells on elastomer chambers, and some of the cells may have detached during stretch.

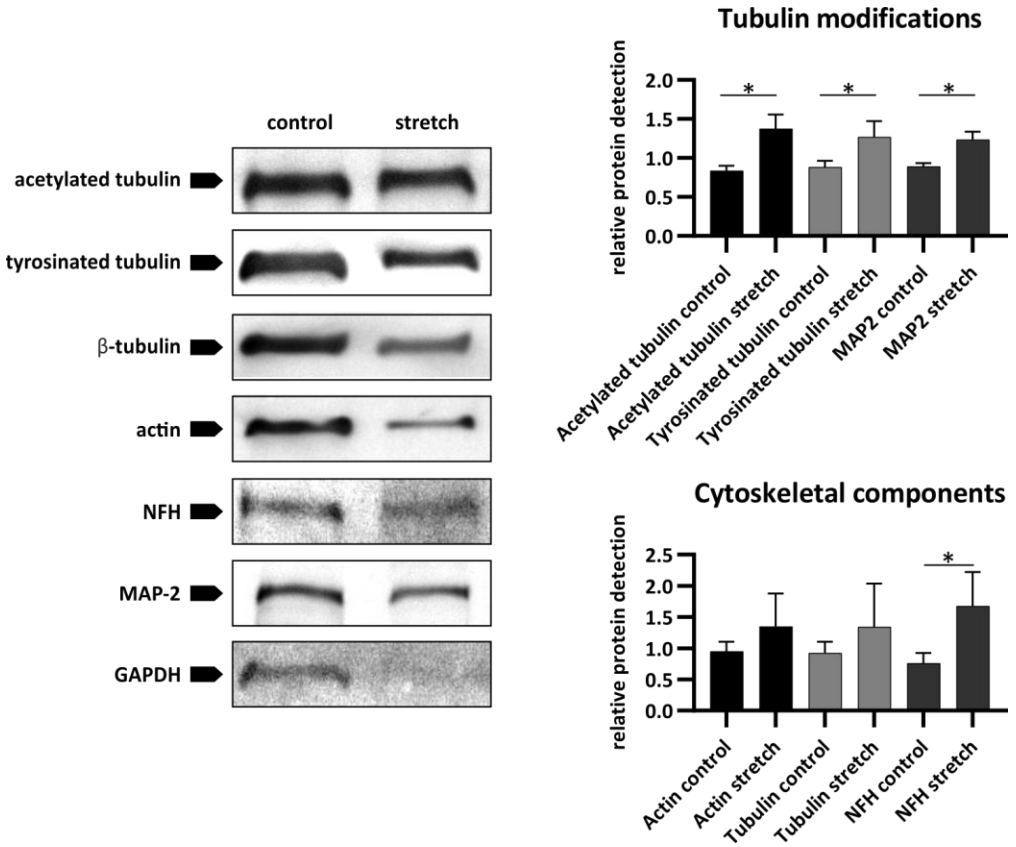

Figure 3.18: Protein levels of stretched and control cortical neurons. Cortical neurons were stretched for 24 hours with a frequency of 300 mHz and an amplitude of 28%. Western blot analysis (n = 3 independent isolations) revealed higher protein intensity of NFH (p-value = 0.033) and of post-transcriptional modified tubulin with a higher level of acetylated (p-value = 0.033) and tyrosinated tubulin (p-value = 0.033). In addition, the tubulin adaptor protein MAP-2 also showed elevated intensities for stretched cells (p-value = 0.033). The plot of cytoskeletal components shows the normalized protein intensity to GAPDH. The plot showing tubulin modifications represents values that were normalized to GAPDH and to tubulin.

3.3.1.6 Stretched neuronal cells showed a higher length growth and induced outgrowth of neuronal branches

To verify if stretched cortical cells showed similar outgrowth during the early steps of neuronal network formation, branch formation and the overall length of neuronal branches were quantified after 24 hours of stretch. The number of branches increased significantly with the highest number of branches when stretched with a smaller amplitude of 7% (**Figure 3.19**). Cells stretched by 15 or 28% showed a slightly less induced outgrowth of branches but

still elevated compared to control. The same growth induced pattern was obtained for the length of neuronal branches, here also the sum length was higher with the smaller amplitude of 7%. Interestingly, although the directional outgrowth of cortical cells occurred perpendicular to stretch, the side branch formation was stably formed away from the main extensions hence in the direction of uniaxial stretch. In summary, stretched cortical cells enhanced the growth and branching when stretched cyclically. Most noteworthy, the most substantial effect was shown for the mild amplitude.

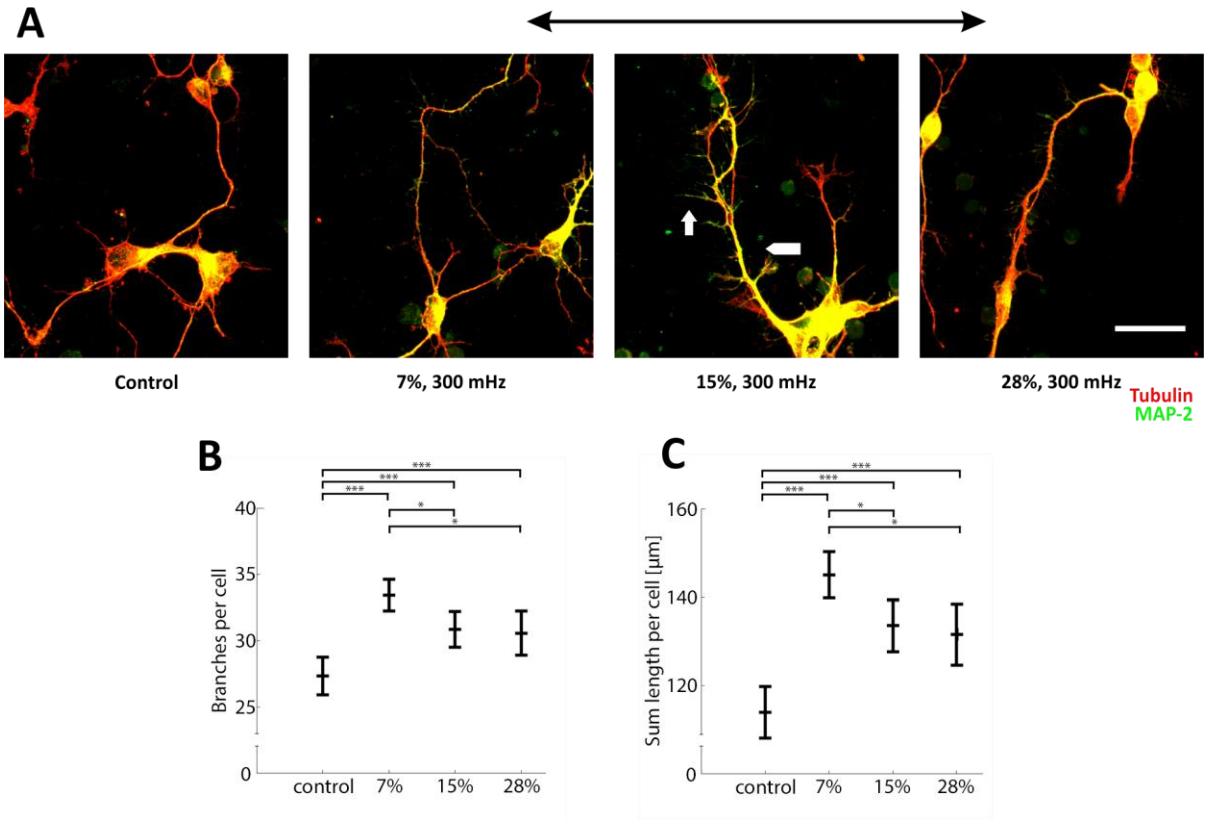

Figure 3.19: Induced length growth and initiation of branch growth under cyclic strain. Cortical cells were stretched for 24 hours with different amplitudes and a constant frequency of 300 mHz. Cells were stained against MAP-2 and tubulin (**A**). Primary extensions are indicated by the white arrowhead, while side branches are indicated by the white arrow. The black arrow indicates the strain direction. Using image processing routines, the overall number of branches (**B**) and the total length of neuronal branches (**C**) were obtained (see material and methods section for further details). The plots show the medians as confidence intervals: control 27.3 ± 1.5; 7% 33.4 ±1.2; 15% 30.9 ± 1.4, 28% 30.6 ± 1.7 branches per cell (**B**). Control 113.9 ± 5.9 µm; 7% 145 ± 5.3 µm; 15% 133.5 ± 5.9 µm; 28% 131.6 ± 6.9 µm (**C**). Scale bar = 20 µm. Figure adapted from (Abraham et al., 2019).

3.3.1.7 Stretched neuronal cells encompass a larger growth cone area in an amplitude-dependent manner

One central cytoskeletal component of the neuronal branches that steers neuronal outgrowth and branch formation is its leading front –the so-called growth cone. The growth cone is an active and motile structure at the end of growing neurites. It is characterized by their F-actin containing filopodia or lamellopodia, forming a 'hand-like' morphology (Fletcher & Mullins, 2010). To verify if the growth cone also undergoes cytoskeletal adaptation to cyclic mechanical strain, immunocytochemical staining of actin and tubulin was used to identify the growth cone cytoskeleton. Stretched cells showed to encompass a larger area of their leading front compared to control cells. While the amplitude of 28% induced the largest area with a mean of 23.9 ± 3.4 µm^2, growth cones of control cells show a mean area of 8.4 ± 20 µm^2 (**Figure 3.20**).

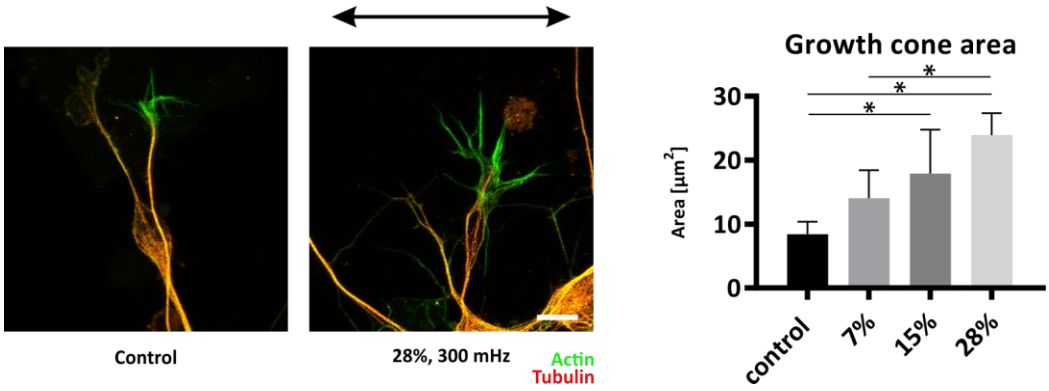

Figure 3.20: Growth cone area is increased under cyclic strain in an amplitude-dependent manner. Cortical cells were stretched for 24 hours with different amplitudes and a constant frequency of 300 mHz. Cells were stained for tubulin and actin to identify the growth cone due to the actin-rich, finger-like extension. The plot depicts the mean growth cone area, analyzed for n = 3 independent experiments, with at least 38 growth cones per parameter (p-value = 0.0326 control vs. 15%; p-value = 0.0326 control vs. 28%; p-value = 0.0326 7% vs. 28%). The black arrow indicates the strain direction. Scale bar = 5 µm.

To summarize chapter 3.3.1, cortical cells behaved differently to cyclic strain depending on the time point of stretch initiation. While newly formed branches retracted without the formation of retraction bulbs, branches that have been developed for six days prior to stretch

retracted dramatically. Although a striking branch pullback was observed after the initiation of stretch, stretching for longer periods induced a regrowth of neuronal branches and even showed a triggered outgrowth with a faster growth velocity. Cortical neurons even adapted to cyclic stretch by growing their branches perpendicular to stretch and demonstrate -besides reorientation in a perpendicular direction- a typical network formation. Cortical cells also experience a cytoskeletal rearrangement and reinforcement when stretched cyclically. Further, stretched cortical cells showed a higher growth of side branches and an induced length growth. Such induced growth could be linked to an enhanced growth cone area in stretched cells.

3.3.1.8 Responses of differentiated astrocytes to cyclic stretch

As previously described, the differentiated culture of NSCs revealed a co-culture with a predominant number of astrocytes when cultivated and stretched on 50 kPa chambers. To investigate in more detail how cyclic stretch influences cells of the CNS, postnatal astrocytes were also subjected to cyclic substrate deformation.

3.3.1.9 Postnatal astrocytes do not show any reorientation behavior to bear mechanical loads

To compare the effect of cyclic stretch to differentiating astrocytes of previous analysis to mature astrocytes, stretch experiments were performed with postnatal astrocytes. Stretched postnatal astrocytes did not align in any specific direction. As depicted in **Figure 3.21**, the orientation of stretched astrocytes remained random when the cytoskeletal intermediate filament GFAP was observed. The cumulative frequency plot (**Figure 3.21B**) shows similar counts compared to the control. Further, the mean orientation between both groups did not differ. Stretched postnatal astrocytes showed a mean orientation of 44.8 ± 1.7° compared to a mean of 45.8 ± 0.9° for control cells (n = 8 independent isolations). In addition, postnatal astrocytes did not show an increased intensity of the GFAP immunostaining. The results suggest that postnatal astrocytes may not be mechanoresponsive and bear the mechanical loads without adjusting their cytoskeleton towards any orientation.

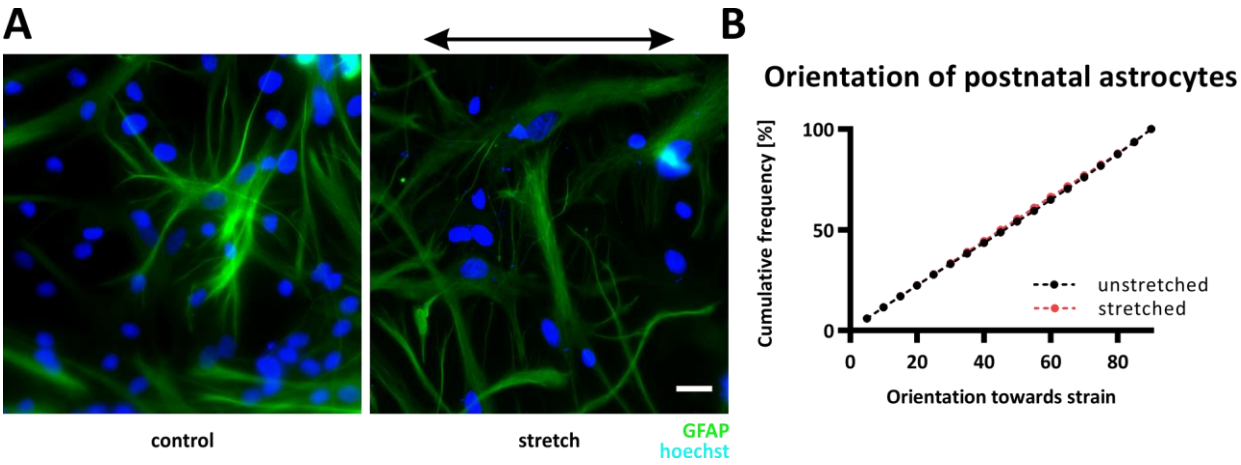

Figure 3.21: Postnatal astrocytes do not reorient when stretched cyclically. Astrocytes were isolated from postnatal cortices of rat pups. After cell adherence, astrocytes were stretched for 24 hours with an amplitude of 15% and a frequency of 300 mHz and stained for GFAP (**A**). The black arrow indicates the direction of stretch. Scale bar = 20 µm. The cumulative frequency plot shows the orientation of astrocytic filaments (n = 8 independent isolations).

3.3.2 Effect of cyclic strain on a co-culture of neurons and astrocytes

3.3.2.1 Postnatal astrocytes and neuronal cells revealed different mechanoresponses to cyclic strain

Since neuronal cells and astrocytes behave completely different to cyclic stretch, the next focus was to analyze how an interacting culture of neuronal cells and astrocytes would behave when subjected to cyclic mechanical loads. Further, this allowed comparing differences between the co-cultures resulted from differentiating NSCs (chapter 3.2) to a co-culture that was produced by cultivating postnatal astrocytes and mature neuronal cells together. In addition, such co-culture also had the possibility to add cell numbers in different ratios of astrocytes and neuronal cells to get a more precise idea of how each cell type contributes to the behavior under cyclic stretch.

Therefore, astrocytes were distributed on the elastomer chambers. After cell adhesion, primary cortical neuronal cells were added with varying cell numbers. Depending on the astrocyte number, neuronal cells aligned more or less towards a perpendicular direction,

indicating a mechanical force scavenging function of astrocytes (**Figure 3.22**). The more astrocytes were present, the less neuronal cells aligned in stretch direction (**Figure 3.22B**).

Stretch experiments with the co-culture of mature neuronal cells and astrocytes revealed that neuronal cells avoid mechanical deformation by growing on top of astrocytes (**Figure 3.22D**). Here, the mean value of neuronal cell orientation was significantly different when fewer astrocytes were present in the co-culture (**Figure 3.22C**). The culture without astrocytes had the highest angle with 53.8 ± 0.8°, while stretched co-cultures showed a mean of 47.2 ± 3.9° when the number of neurons and astrocytes were equal and 52.6 ± 0.6° when fewer astrocytes (4:1, neurons: astrocytes) were cultivated in the co-culture.

This effect could explain previous findings observed in the co-culture of differentiating NSCs (chapter 3.2) and differences of neuronal mechanoresponse with and without the support of astrocytes.

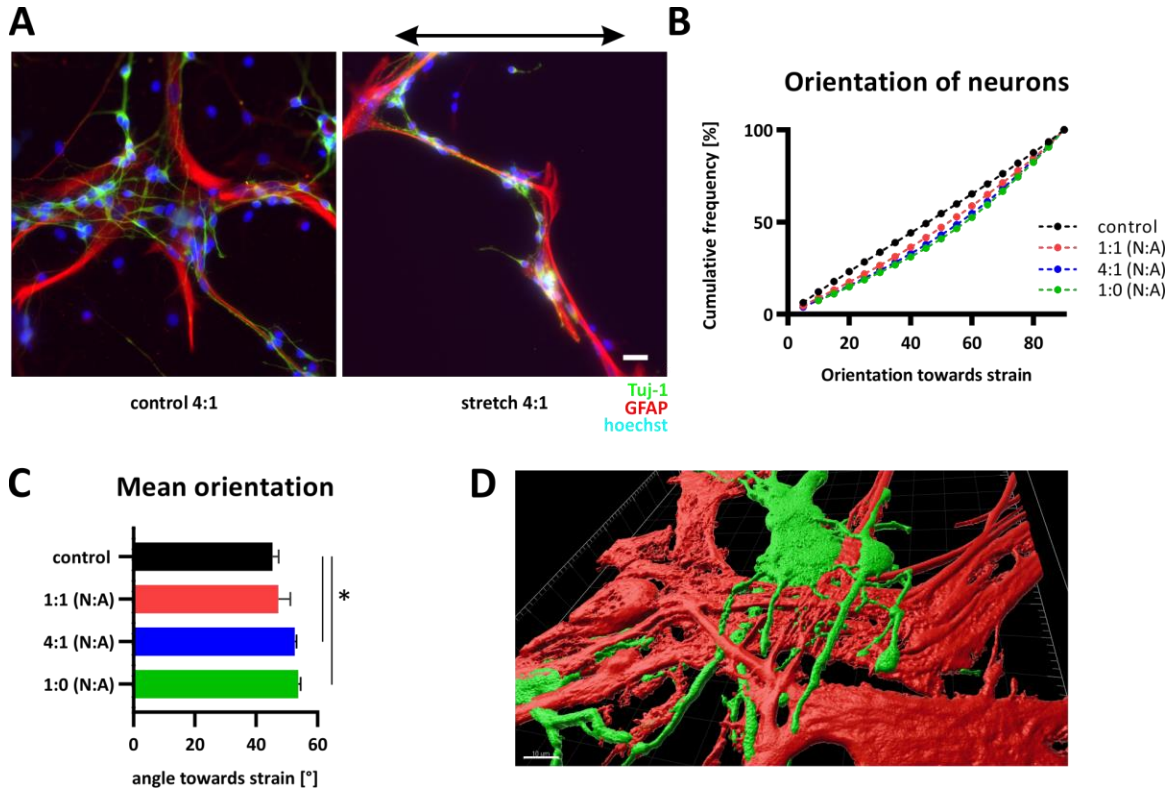

Figure 3.22: Neuronal reorientation depends on different ratios of astrocytes and neuronal cells. Neuronal cells grew on top of astrocytes when observed in a co-culture (**A**). The black arrow indicates the strain direction. Scale bar = 20 µm. The co-culture was stretched for 24 hours with an amplitude of 15% and a frequency of 300 mHz. The cumulative plot (**B**) shows different a degree of reorientation depending on the number of astrocytes. The mean orientation (**C**) was significant different between the control group and when the cocoulture revealed less astrocytes (4:1 neurons (N): astrocytes (A) p-value = 0.0326, 1:0 N:A p-value = 0.0326 , n = 2 independent experiments). Bar plots represent the mean + standard deviation, n = 2 independent experiments. 3D view of neurons on top of astrocytes (**D**). Images were taken with an LSM 880 and processed with the Imaris software. Scale bar = 10 µm.

4 Discussion

Neural activity is directly linked to a localized increase in blood perfusion leading to tissue displacements of 30% around the vasculature in mice (Drew et al., 2011). As most studies focus on stiffness alterations and the effect of topographical cues, responses to cyclic mechanical tissue deformations are unclear. However, several cell types within the brain are subjected to mechanical deformation and, thus, should be equipped to bear cyclic mechanical loads. A detailed look on the cytoskeleton of astrocytes and neuronal cells reveals a completely different setup of cytoskeletal elements compared to cells that have a more obvious association to the vasculature, for example endothelial cells. Those cells exhibit a remarkable formation of stress fibers. In contrast, neuronal cells build their actin cytoskeleton as periodically spaced rings below the plasma membrane of neuronal cell branches (D'Este, Kamin, Göttfert, El-Hady, & Hell, 2015). In this thesis, cellular responses of neuronal cells, astrocytes, stem cells, and differentiating cells were analyzed and are discussed in this section. Different behavior of cyclically stretched cell types was explored.

4.1 Immediate response to mechanical strain differs among cell types and developmental stages

To identify mechanoresponses of the different cell types, live-cell imaging without strain and within the first cycles of strain was performed. Interestingly, different responses were observed depending on the cyclically stretched cell type.

4.1.1 Reduced migration velocity of NSCs

Neural stem cells (NSCs) under strain showed a reduction in migration velocity and pointed their cell protrusions in strain direction (chapter 3.1.2, 3.1.4). The microenvironment in which NSCs reside plays a pivotal role in their migration behavior. Besides chemical stimulators, cell migration can also be influenced by stimuli of mechanical nature. For instance, mechanical strain, shear stress, matrix stiffness, and microgravity have been shown to affect the migration of bone marrow-derived mesenchymal stem cells (BMDSCs) (Fu et al., 2019). Here, mechanical cues can either increase the cell speed or reduce migration across the surface. An

increased migration velocity is associated with elevated activation of focal adhesion kinase among others (Zhang et al., 2015). A reduced migration triggered by mechanical stimuli could result, for example, from F-actin remodeling and change in cellular stiffness (Mao, Chen, Luo, Zhang, & Song, 2016).

Furthermore, cell migration speed can depend on the adhesion strength between the cell and the underlying matrix (D.-H. Kim & Wirtz, 2013). Such adhesion strength is linked to the size of mature focal adhesions, and thus, migration velocity is directly linked to the focal adhesion size. Formation and disassembly of focal adhesion are highly dynamic during cell migration. Stimulation of focal adhesion formation enhances the adhesion strength of cells to the extracellular matrix (Nagano, Hoshino, Koshikawa, Akizawa, & Seiki, 2012). Therefore, the reduced migration speed observed in stretched NSCs may be associated with increased adhesion on the elastomer chamber as a counter-reaction to uniaxial cyclic stretch. This hypothesis was confirmed via staining of talin in NSCs (chapter 3.1.5). Stretched NSCs showed a higher localization of talin in cell protrusions compared to control. Hence, it may be possible that NSCs show an enhanced focal adhesion formation when stretched cyclically to promote cell adhesion to the elastomer substrate. A load-dependent exchange rate of focal adhesion proteins (Lavelin et al., 2013) illustrates that under increased tension focal adhesions recruit new proteins and thus grow (Livne & Geiger, 2016). Talin has a pivotal role in the initial step of focal adhesion formation and mediated crosslinking to filamentous actin as well as actin-binding proteins such as vinculin (Nagano et al., 2012). Further, downregulation of talin is linked to increased migration and proliferation (Wei et al., 2017). This supports the hypothesis that an induced talin expression may trigger focal adhesions formation under strain and subsequently may lead to a slower migration of NSCs across the elastomer surface. In this work, mRNA isolation and talin immunostaining were performed after 24 hours of stretch. Therefore, an increased adhesion strength as a reason for reduced migration (after 15 min and 80 min of stretched) can only be speculated. However, both analyses suggest that cyclic stretch induces changes of talin localization and expression and hence may also explain migration reduction as an immediate response of NSCs to stretch.

Interestingly, the migration direction was independent on the direction of uniaxial stretch. The uniaxial strain did not show to induce a different polarity within the cell to alter the direction of migration. The overall velocity of migrating cells was reduced at 15 min and 80 min stretch. However, comparing the migration speeds between cells that migrated mostly in stretch direction compared to cells that migrated perpendicular showed similar velocities at both time points. This may be based on small sample size (n = 3 independent experiments) analyzed during live-cell imaging and a general high heterogeneity of cell velocities. Furthermore, during migration, cytoskeletal structures have to constantly assemble, stabilize, and disassemble (Fletcher & Mullins, 2010). Therefore, migrative cells exhibit much higher cytoskeletal dynamics compared to sessile cells. A higher dynamics in migration may allow NSCs to be relatively unaffected by cyclic stretch and to crawl across the uniaxial cyclic stretched elastomer chamber without any preferred direction. Besides, the selected time points may not be sufficient to observe a stretch-induced directed cell migration. Controversy, Goldyn et al. observed no migration velocity reduction when they stretched embryonic fibroblasts for 8 hours with an amplitude of 8% and a frequency of 1 Hz. Further, they observed a migration perpendicular to the stretch axis of cyclically stretched cells (Goldyn, Rioja, Spatz, Ballestrem, & Kemkemer, 2009). The discrepancy between the study by Goldyn and colleagues and this thesis could be either due to cell type-specific cytoskeletal differences (further discussed in chapter 4.2) or due to different stretch parameters (e.g., a longer cyclic stretch period of 8 hours). Noteworthy, the cells observed in the study by Goldyn shows a different cytoskeletal architecture due to formation of stress fibers, while NSCs central stress fiber formation was not observed in this thesis. The altered stress fiber formation may be responsible for an opposing response of NSCs to cyclic stretch, as further discussed in the following sections.

4.1.2 Retraction and formation of retraction bulbs in cortical neurons

The immediate response of cortical neurons to cyclic mechanical strain was dependent on how long cortical neurons grew on the elastomer chambers prior to stretch. Newly formed neurites of cortical neurons retracted and regrew perpendicular to strain (chapter 3.3.1.2), while neuronal branches of cortical neurons that have developed for six days retracted drastically with the formation of retraction bulbs. Although neuronal branches retracted extensively, cortical branches showed the ability to adapt to cyclic mechanical loads and even grew out again when the mechanical strain was still present. The formation of abnormal cytoskeletal arrangements and collapsing branches were commonly observed in axonal stretch injury *in vivo* (Ertürk et al., 2007) and *in vitro* (Yap et al., 2017). Such cytoskeletal alterations included smaller axonal growth cones and collapsed structures and were more frequently observed when axonal structures were exposed to repetitive mechanical impacts such as mechanical strain (Yap et al., 2017). Further, retraction bulbs are associated with a swelling of the axonal structure (Ertürk et al., 2007). In live-cell imaging experiments with cortical neurons, stretched neuronal structures also showed a local swelling of axonal branches, collapsed, and retracted neuronal extension (chapter 3.3.1.2). In general, formation of retraction bulbs correlates with an impeded regeneration capacity of neuronal cells (Ertürk et al., 2007). The difference in the behavior of cells with newly formed branches may be based on the cytoskeletal organization. Here microtubules may play a pivotal role, as it has been observed that stabilization of the microtubule cytoskeleton could prevent retraction bulbs (Ertürk et al., 2007). Microtubules near the growth cone are usually dynamic structures that probe the actin-rich growth cone region and generate pushing forces against the plasma membrane. To generate the pushing force, reorganization of the microtubule cytoskeleton is necessary. Thus, a disorganized microtubule structure can impede the outgrowth capacity of neuronal cells. At early stages of neuronal development, the microtubule cytoskeleton is relatively dynamic and mobile (He et al., 2020). At later stages, the microtubule cytoskeleton is largely immobilized (He et al., 2020), which could explain different observations in stretch experiments of freshly adhered cortical neurons compared to longer cultivated neurons. Furthermore, in live-cell imaging experiments, it was observed

that neuronal branches showed more retraction bulbs near the leading tip and retracted only for several micrometers from the distal end, leaving proximal regions unaffected. This could be further explained by the 'sequential stabilization' model (S. Lee & Shea, 2014). In this model, microtubules and neurofilaments in proximal regions of neuronal branches are stabilized while distal regions remain dynamic and continue pathfinding. Therefore, older neuronal cultures may exhibit differences in cytoskeletal stabilization in proximal and distal parts.

In this work, cortical neurons stretched after six days of cultivation showed an accumulation of all cytoskeletal filaments in retraction bulbs. The swollen axonal structure contained delocalized neurofilaments, microtubules, and microfilaments. The latter, however, was also still present at the leading tip (chapter 3.3.1.2).

Interestingly, after several minutes of stretch neuronal branches regrow even with an induced growth velocity after the stretch was relieved from the system, indicating that even besides a delocalized cytoskeleton within the neuronal branches, neurons can reassemble their cytoskeleton in a way that enables regrowth of the neuronal branches even under cyclic stretch. The induced growth after stretch may be due to an increased assembly of cytoskeletal structures in response to mechanical stress. After releasing the stretch, neuronal branches may then have more assembled cytoskeletal structures that do not counteract against any mechanical stimuli anymore and thus thrive and pushes the outgrowth of neuronal branches. A lag between application and removal of a stimulus and its effect is referred to as hysteresis and a common feature of elastic material (Fletcher & Mullins, 2010). In biological systems, such lag is referred to an active process and can be observed, for instance, on growing actin filaments *in vitro* (Parekh, Chaudhuri, Theriot, & Fletcher, 2005). In the study of Parekh et al., actin filaments were subjected to a low level of force during growth. When the force was increased and further reduced to the previous level, the actin network increased its growth velocity. Also, in this study, filament accumulation may have occurred during mechanical loading, allowing neuronal cells to regrow their branches under cyclic strain. Once the mechanical force was relieved from the system, a higher filament assembly may have then promoted an induced outgrowth, resulting in higher growth velocity

of branches in cortical neurons. Initial outgrowth requires local depolymerization of actin filaments and polymerization of microtubules, providing driving forces. Neurofilaments, however, are also required for continued elongation (S. Lee & Shea, 2014) and may therefore also support neuronal outgrowth during cyclic stretch.

4.2 Reorientation of neural stem cells in stretch direction

In general, cells adapt to cyclic mechanical stretch by reorientation of cytoskeletal structures from random orientations to a well-defined angle where cells experience minimal loads (Faust et al., 2011). Cytoskeletal reorientation requires disassembly of cytoskeletal structures in stretch direction and reassembly in perpendicular direction. Cytoskeletal reorientation is followed by cell shape adaptation, also perpendicular to stretch (Zielinski et al., 2018). Experimental findings have also been explained by theoretical models to understand fundamental mechanism of cell reorientation under cyclic stretching. For instance, Safran et al. developed a force dipole model in which the reorientation of the cell is explained by it's strive to maintain minimal stress or static state under cyclic stretching (Safran & De, 2009; Xu, Feng, & Gao, 2018). As reorientation also requires focal adhesion dynamics and can not only be explained by a 1-dimensional dipole model, Livne et al. proposed that their observed reorientation behavior is driven by a process where passively stored elastic energy of a 2-dimensional cell relaxes to a minimum (Livne, Bouchbinder, & Geiger, 2014). Cytoskeletal remodeling is further driven by cytoskeletal fluidization through the direct impact of physical forces that act on weak cytoskeletal cross-links (Schwarz & Safran, 2013). Such fluidization induces cytoskeletal remodeling of the cytoskeleton with a slower reassembly on spatial sites where traction forces were markedly reduced (Schwarz & Safran, 2013). The involvement of focal adhesion dynamics is further highlighted by Kong and colleagues, who showed that binding dynamics of integrins might change under cyclic loading and suggest that focal adhesions lose their stability when cells are stretched with a high frequency (Kong, Ji, & Dai, 2008). Such binding alterations can be explained by catch bonds in focal adhesions that experience an oscillating internal force when subjected to cyclic stretch (B. Chen, Kemkemer, Deibler, Spatz, & Gao, 2012). Cyclic force thereby reduces the life-time of those catch bonds

and induces, thereby, a sliding or relocation of focal adhesion leading to a reorientation of associated stress fiber in a perpendicular direction.

In contrast to the expected behavior and to the reorientation models, NSC showed an opposed reorientation behavior. Indicated with live-cell imaging and statistically confirmed when stretched for 24 hours, NSCs align their cellular protrusions in stretch direction and thus show an overall cell shape orientation parallel to maximal mechanical loads. Such behavior is usually only observed when cells are stretched statically or quasi statically (Collinsworth et al., 2000; de & Safran, 2008; Eastwood, Mudera, McGrouther, & Brown, 1998; Morioka et al., 2011; Xu et al., 2018). Hence, what could be the mechanism and driving force of reorientation parallel to cyclic stretch?

In NSCs, stress fiber formation was less prevalent (chapter 3.1.4) and actin bundles were only observed in the cell periphery. Noteworthy, a reduced formation and a peripheral location of stress fibers are also observed on compliant structures, where human osteosarcoma cells showed a parallel distribution to cyclic stretch (Tondon & Kaunas, 2014). In contrast, when Tondon and colleagues cultivated those cells on stiffer collagen-coated silicone rubber, stress fibers were observed in the central and peripheral parts of the cells and showed a perpendicular alignment to cyclic stretch. The authors hypothesized that the different reorientation behavior on soft gels is due to attenuated contractility by the lack of central stress fibers. Intriguingly, cyclically stretched endothelial cells that were treated with either a RhoA or myosin light chain kinase (MLCK) inhibitor also aligned parallel to stretch (C. F. Lee, Haase, Deguchi, & Kaunas, 2010). In the study by Lee and colleagues, treating cells with the MLCK inhibitor resulted in central fibers alignment in stretch direction, while the RhoA inhibitor induced peripheral stress fibers parallel to uniaxial cyclic stretch; also reflecting the spatial differences in myosin activity regulation by MLCK and RhoA (Totsukawa et al., 2000). Although central and peripheral stress fibers show a different spatial regulation, they are interconnected and distribute forces throughout the cell (Vignaud et al., 2020).

Tondon and colleagues hypothesized that the driving force of parallel alignment is to achieve an optimal level of stress fiber tension (Tondon & Kaunas, 2014). Since stress fiber formation

on the soft gel was relatively low, Tondon and colleagues suggest that stretching of cells on softer gels increased intracellular tension towards an 'optimal level' and thereby to a stress fiber alignment parallel to stretch. They stated that the optimal stress fiber tension may already be high under static conditions when cells are grown on stiffer substrates. When cells were stretched on stiffer substrates, the tension acting on stress fibers probably exceeds the optimal level leading to a reorientation away from maximal mechanical loads (Tondon & Kaunas, 2014). In this work, NSCs exhibit similarities to the cells grown on soft gels or treated with the Rho kinase inhibitor: no central stress fibers were present, actin bundles formation was only observed in the cell periphery and cells aligned parallel to unidirectional cyclic loadings. Hence, according to the model of Tondon and colleagues, the driving force of NSCs alignment may also be to achieve an optimal tension level acting on actin fibers, which are located in the periphery of NSCs. However, the 'optimal tension model' seems conflicting, as the natural environment of NSCs constitutes a very soft brain environment with a stiffness of 0.1-1 kPa. Therefore, the elastomer chambers with a stiffness of 50 kPa already have a higher stiffness than the usual physical microenvironment.

Noteworthy, RhoA, which activates central stress fiber formation is also described to be a key player in reorientation processes to cyclic stretch (Goldyn et al., 2009). RhoA, one of the main Rho GTPases, is described to show elevated activity levels upon cyclic stretching while other GTPases, including Rac and Cdc42, remain constant (Goldyn et al., 2009). In this thesis, the RhoA activity in NSCs has not been investigated, however, due to an absence of central stress fibers (Chrzanowska-Wodnicka & Burridge, 1996) it may be possible that NSCs show a reduced presence of RhoA and thus, besides a lack of central stress fibers, no reorientation perpendicular to cyclic stretch on 50 kPa chambers. In agreement with this hypothesis, an induced RhoA activity has been shown to trigger a different lineage commitment, as seen when NSCs were cultivated on stiffer substrates (Keung, de Juan-Pardo, Schaffer, & Kumar, 2011). However, an altered lineage commitment was not observed when NSCs were subjected to cyclic stretch as discussed in the following section, possibly arguing for no alterations in RhoA activity by cyclic stretch; contrasting to its activation by stiffness as a mechanical stimulus as observed elsewhere (Keung et al., 2011). With a lack of cell

reorientation perpendicular to strain, tension along the stretch axis may still be present and could induce actin bundle formation (Kaunas, Nguyen, Usami, & Chien, 2005). Stretch may supply the necessary tension to induce actin fiber assembly parallel to strain in cells with attenuated myosin II ATPase levels (C. F. Lee et al., 2010) and the inability to reorient perpendicular to strain. Furthermore, it may be possible that due to a relatively limited actin bundle coupling to focal adhesions, based on the absence of stress fibers, catch bonds in assembled focal adhesions may experience a different loading pattern, without an oscillating force. Thereby cyclic stretch may not induce a reduced lifetime of catch bonds. With force, the ECM/integrin binding can further strengthen by catch bond formation and increases the lifetime of the bond (Chighizola et al., 2019). Thus, catch bonds in NSCs may be further stabilized rather than destabilization and sliding of focal adhesion, resulting in a parallel orientation of NSC. Here, lifetime of catch bonds in cytoskeletal filament systems e.g. catch bonds between vinculin and f-actin (Chighizola et al., 2019) may have longer lifetimes when located parallel to the uniaxial strain. However, this and the above discussed possible mechanism for parallel alignment remain only speculations. The parallel alignment of NSCs under cyclic stretched and also observed elsewhere in other cell types (C. F. Lee et al., 2010; Tondon & Kaunas, 2014) are not yet fully understood at the present time.

Interestingly, when NSCs developed to an astrocyte phenotype within five days, cells maintained their parallel alignment to stretch. Reorientation was even an active process of differentiating astrocytes, which was confirmed when the direction of stretch was changed within the five days of stretch (chapter 3.2.3). Here, the differentiating astrocytes were stretched for three days and flipped by 90°, stretched for additional two days and finally showed a reorientation parallel to the final direction of cyclic strain. Thus, parallel alignment is most likely also an active process involving a characteristic cytoskeletal protein setup in differentiating astrocytes that is responsible for parallel reorientation to cyclic stretch. Noteworthy, differentiating astrocytes also did not show central stress fiber formation after five days of differentiation independent of stretch (chapter 3.2.6). Furthermore, differentiating astrocytes were also characterized by a different cytoskeletal arrangement compared to NSCs that have developed to a neuronal phenotype with microtubules less

present in astrocytes compared to neuronal cells. As microtubules are described as the stiffest cytoskeletal system (Fletcher & Mullins, 2010), less abundance in astrocytes may allow the cells to be aligned in stretch direction without rupturing by cyclic stretching. In contrast, neuronal phenotypes showed higher staining of microtubules. This enhanced staining was not only observed in neurons that were differentiated from NSCs, but also in cortical neurons (chapter 3.3.1).

4.3 Influence of cyclic strain to stem cell characteristics

Despite biochemical signals, mechanical cues such as pressure, stretch, stiffness, or topology tune cell behavior during embryogenesis (Keller, Davidson, & Shook, 2003). Mechanical stimuli have been shown to be crucial regulators of stem cell characteristics such as proliferation and fate decisions of NSCs (Baek et al., 2018; Blaschke et al., 2019). While the studies of Blaschke et al. and Baek et al. focus on the effect of mechanical stiffness of the surrounding microenvironment and topographical cues to mimic the extracellular environment of the brain, in this work, the influence of cyclic mechanical strain on stem cell physiology was analyzed. Cyclic mechanical strain reduced the proliferation of NSCs (chapter 3.1.3). A similar reduction was also observed in the study by Blaschke et al. when cells were exposed to stiffnesses that mimic physiological environments of the brain and are plated on 1 kPa PDMS culture substrates (Blaschke et al., 2019). Therefore, NSCs on soft elasticities were more quiescent than NSCs on stiffer, unphysiological substrates. Quiescence is an important characteristic of NSCs as it provides a mechanism to exist for a long period in an unaltered state and thereby preserving its progenitor pool. Yet, NSCs can respond to external stimuli that require higher proliferation rates for example during damage or degeneration (Wang, Plane, Jiang, Zhou, & Deng, 2011). Cyclic mechanical strain also resulted in more quiescent stem cells and may be an additional important regulator to maintain NSCs niche homeostasis and relevant to preserve the stem cell pool.

Another relevant stem cell characteristic is its ability to differentiate into different cell types. Blaschke et al. observed an induced differentiation into a neuronal phenotype when cells were grown on 1 kPa substrates compared to stiffer elasticities and glass substrates, where

most of the cells differentiated to astrocytes. A stiffness induced altered differentiation pattern is based on different Yes-associated protein (YAP) regulations within the stem cell (Rammensee et al., 2017). Rammensee et al. observed that on soft substrates, β-catenin could drive transcription of neurogenesis effectors, while on hard substrates, YAP levels are increased and antagonize available β-catenin. As there was no translocation of YAP protein from a cytoplasmatic and to nuclear localization, the authors argued that YAP dependent neurogenesis is only dependent on the scavenging activity and interaction of β-catenin. However, such nuclear translocation is usually described as the mechanism in YAP dependent mechanotransduction (Cui et al., 2015). Furthermore, Rho GTPases, which activate the cellular contractility machinery, are also described to mediate effects of extracellular matrix-derived mechanical signals, such as stiffness (Keung et al., 2011). Therefore, an increased extracellular stiffness enhanced RhoA and Cdc42 activation and thereby suppressed neurogenesis. In line with this, Baek and colleagues identified YAP also as the mechanosensitive element that guides a different fate decision when human neural stem cells are exposed to different topographic cues (Baek et al., 2018). They found a clearly different cytoskeletal reorganization, with reduced F-actin structures and limited focal adhesion formation of cells grown on top of nanogroove structures. Further, they observed that a reduced RhoA activity is present when these nanostructures restrict cytoskeletal reorganization and identified a cross-talk between RhoA and YAP activity. So far, the influence of mechanical strain has only been described as a promotor in osteogenic lineage commitment (Kearney, Farrell, Prendergast, & Campbell, 2010).

In this thesis, the mechanical stimuli did not influence the lineage commitment and revealed the same ratio of neuronal cells and astrocytes on stretched elastomers and control chambers (chapter 3.2.1). Besides, stretched stem cells and their differentiated co-culture showed the same number of SOX2 positive cells as an indicator of cell number that still express the stemness marker. Thus, contrary to the prior hypothesis that mechanical strain may also influence stem cell characteristics, NSCs lineage commitment possibly shows an independency to mechanical strain. The result may be based on different mechanosensing of strain versus stiffness. Stiffness may affect NSCs to a higher degree and influence the

cytoskeletal arrangement in a YAP- RhoA dependent pathway, while mechanical strain may not induce such cytoskeletal alterations. Noteworthy, NSCs grown on 50 kPa elastomers are subjected to a higher mechanical stiffness as found in their natural physical microenvironment. Experiments on softer elastomers (1 kPa) were performed, however, due to more difficult handling of those chambers and duration of stretch experiments (five days of constant stretch), failed to give relevant insights that could identify the role of cyclic stretch while mimicking the physiological environment rather than using 50 kPa chambers.

In agreement with this, as previously discussed, stretched NSCs did not show any differences in their actin cytoskeleton as the usual stress fiber formation under cyclic strain was not present. In addition, a parallel alignment argued for less central stress fiber formation as observed for cells grown on soft substrates (Tondon & Kaunas, 2014) or NSCs on the elastomer chambers (chapter 3.3.1.4). Thus, despite parallel alignment in stretch direction, cytoskeletal rearrangements were not sufficient to induce a different lineage commitment in stretched NSCs. To what extent central stress fiber formation may be present when NSCs shift their differentiation fate to an astrocyte phenotype when grown on stiffer substrates and glass could further strengthen this hypothesis in following studies. Noteworthy, a different stress fiber formation on soft versus hard elasticities has not been analyzed in the study of Blaschke et al. and other studies.

4.4 Directional outgrowth of cortical neurons and cells grown in an astrocyte-neuronal co-culture

Cyclic stretch induces a reorientation of cytoskeletal proteins perpendicular to strain in fibroblasts (Faust et al., 2011) and other cell types (Morioka et al., 2011). Neuronal cells have a unique cytoskeleton, with their actin filaments forming ring-like structures, while neuronal extensions are filled with several bundles of stiff microtubules and elastic neurofilaments. Thus, it was relatively unclear how neuronal cells would respond to cyclic mechanical stimuli. When cortical neurons were stretched cyclically on elastomer substrates, their branches grew out perpendicular to the uniaxial stretch direction. The growth cone, which is responsible for

growth guidance, may have sensed the mechanical stimuli and thereby lead to a directional outgrowth. Thereby, cyclic mechanical stretch probably triggers local actin bundle reorganization that can steer the growth cone and induce a directional microtubules rearrangement. Such microtubules rearrangement was also observed when actin bundles were eliminated from growth cones (Zhou, Waterman-Storer, & Cohan, 2002), resulting in growth cone turning.

By growing towards perpendicular direction, neurons 'escaped' the cyclic stretch to avoid mechanical stress. Faust et al. showed such reorientation behavior in the direction of zero strain relative to the direction of uniaxial stretch in umbilical cord fibroblasts (Faust et al., 2011). The zero strain angle is defined by the structure of the stretched elastomer substrate. As the experimental setup was similar to the one used in Faust et al., the zero strain direction was assumed to be around 69°. When cortical neurons were cyclically stretched, the outgrowth was also more defined and shifted to larger angles towards zero strain direction in an amplitude-dependent manner (chapter 3.3.1.3). Interestingly, in the differentiating co-culture, which contained a mix of neuronal cells and astrocytes, the orientation of neuronal cells appeared random. Thus, the mechanical impact on cortical neurons seemed to be diminished and scavenged by growing together with astrocytes. Astrocytes support, guide, and enhance neuronal growth (East, de Oliveira, Golding, & Phillips, 2010). In reverse, a close interaction of neuronal cells and astrocytes, as well as neuronal activity, influence astrocytic metabolism and induces specific gene transcription in astrocytes (Hasel et al., 2017). Furthermore, astrocytes can also provide mechanical support, as astrocytes are twice as soft as neurons (Lu et al., 2006), thus embedding neuronal cells in a soft compliant environment and protecting them in case of mechanical trauma. Hence, also in this study, mechanical strain seemed to be scavenged by astrocytes.

Accordingly, neuronal cells also grew on top of the soft astrocytes as observed via fluorescence microscopy and 3D analysis, similar findings were noted for the differentiating NSC co-culture (chapter 3.2.5) and the co-culture by cultivating different ratio of postnatal astrocytes to cortical neurons (chapter 3.3.2.1). In agreement with that, when fewer astrocytes were cultivated with neuronal cells, the growth of neuronal extensions was more

defined perpendicular to uniaxial strain (chapter 3.3.1.3 and 3.3.2.1). Interestingly, postnatal astrocytes did not show any reorientation behavior when exposed to cyclic substrate deformation (chapter 3.3.1.9). A cytoskeletal feature that accommodates astrocytes is its low presence of microtubules (Peters & Vaughn, 1967). Zielinski and colleagues observed a blocked cell shape reorientation in absence of microtubules when cells were treated with nocodazole and cyclically stretched (Zielinski et al., 2018). The authors speculate that microtubules disruption may lead to a cell softening and a resulting attenuated mechanoresponse. In addition, cells lacking microtubules reveal a modified RhoA activity, which is a necessary key regulator for cells to reorient perpendicular to stretch (Goldyn et al., 2009). Thus, a different cytoskeletal protein composition in astrocytes may be responsible for a different mechanoresponse to cyclic mechanical strain.

4.5 Cytoskeletal reinforcement during cyclic stretch

4.5.1 Cytoskeletal reinforcement of stretched NSCs

Cytoskeletal reinforcement under cyclic strain is an adaptation of cells to mechanical stimuli (Faust et al., 2011), which allows the cell to maintain its tensional homeostasis (Discher et al., 2005). Cells under cyclic strain generally show an increased number of stress fibers that allow the cell to achieve its optimal force level (Faust et al., 2011). In NSCs which were subjected for 24 hours to uniaxial strain, there was no increased stress fiber formation (chapter 3.1.4). Analysis of actin staining even showed a slight, yet significant reduction of actin staining intensity compared to control cells. Such change in intensity may be based on stretch-induced disruption of some actin filaments within NSCs, while no reassembly of actin fibers was present.

Microtubule formation in NSCs showed to be induced when subjected to uniaxial cyclic strain. Microtubules contribute to cyclic stretch-induced reorientation perpendicular to stretch and actin remodeling is coupled to that of microtubules (Morioka et al., 2011; Zielinski et al., 2018). But how do microtubules behave during parallel cell alignment? Putnam and colleagues showed that static strain induces tubulin polymerization (Putnam, Cunningham, Dennis, Linderman, & Mooney, 1998). Thus, as actin remodeling in perpendicular direction is

not detectable in NSCs, microtubules may also polymerize in stretch direction and may thereby further stabilize NSCs in direction parallel to strain. In line with this, when local tensile strain is applied, microtubules polymerize towards those focal adhesions that experienced force (Kaverina et al., 2002; Morioka et al., 2011).

While vimentin in NSCs was not changed when subjected to cyclic stretch, nestin and tubulin showed a higher intensity in immunostaining experiments. In control and stretched cells, nestin and tubulin were less colocalized than vimentin and tubulin. This colocalization pattern was thus independent of stretch and was also observed in other studies. In agreement with this, nestin immunoreactivity did not colocalize with tubulin in other studies as well (Sjöberg, Jiang, Ringertz, Lendahl, & Sejersen, 1994). A different staining pattern of vimentin and nestin and different colocalization patterns to tubulin may argue to a different involvement of nestin to stabilize the cell cytoskeleton exposed to uniaxial stretch and its unique role in mechanical stabilization. In line with other intermediate filaments, nestin has been suggested to be relevant in mechanical stabilization and a protein able to withstand mechanical forces (Carlsson, Li, Paulin, & Thornell, 1999; Saito et al., 2009).

Noteworthy, mRNA levels of cytoskeletal proteins were not affected when cells were cyclically stretched for 24 hours. This could point out that after 24 hours, NSCs may again be in the mechanical balanced state where adaptive processes such as an induced temporal formation of cytoskeletal structures are already completed, showing no alterations in mRNA level, except talin, which was elevated after 24 hours. Talin is required to connect the extracellular matrix via integrin to its interior actin cytoskeleton (Nayal, Webb, & Horwitz, 2004). Therefore, induction of talin protein expression could further support NSCs to adhere to cytoskeletal structures on uniaxial cyclic deforming substrates. In this work, other focal adhesion proteins were not investigated, however should also be considered in subsequent studies.

4.5.2 Cytoskeletal reinforcement of stretched cortical neurons and astrocytes

Cortical neurons showed higher protein immunostaining of actin filaments, neurofilaments, and tubulin (chapter 3.3.1.4). The immunofluorescent intensity was higher in branches pointing in perpendicular direction compared to branches pointing in stretch direction. In control cells, actin, tubulin, and neurofilament staining were identical for all extensions segments independent on their orientation. With increasing strain amplitude, the angle-dependent distribution of actin, tubulin, and neurofilaments changed dramatically. Such reorientation implies a remodeling of the neuronal cytoskeleton to allow outgrowth perpendicular to stretch direction. Stretch-induced reinforcement was also confirmed with live-cell experiments, where branches grew with a higher velocity after stretch was released from the system. A stretch-induced reinforcement is in line with the hypothesis of Loverde and colleagues (J. R. Loverde et al., 2011), who suggested that mechanical stretch during stretch growth may lead to rupture of cytoskeletal components withing the neuronal structure followed by incorporation of new cytoskeletal material in neuronal branches.

Interestingly, western blot analysis revealed elevated tubulin posttranscriptional modifications in stretched cortical neurons. Here, tyrosinated as well as acetylated tubulin levels increased as well as the tubulin-binding protein MAP-2. Tyrosination affects the gene-encoded C-terminal tyrosine of α-tubulin (Jennetta W. Hammond et al., 2008). There is a constant detyrosination/tyrosination cycle that regulates the binding of different microtubule end binding proteins. These proteins are known to recognize the plus end growing tips of microtubules. Therefore, a higher abundance of tyrosinated tubulin fits to the result that stretched cortical neurons grew faster than unstretched cells (chapter 3.3.1.6).

Acetylation of α-tubulin takes place at lysine40 and is associated with microtubule stabilization (Jennetta W. Hammond et al., 2008). Besides, acetylated tubulin is described to have a higher binding affinity to motor proteins to induce motor-based trafficking along the microtubule tracks (Reed et al., 2006). Hence, the microtubule cytoskeleton of stretched cells may likely be more stabilized as acetylated tubulin is significantly increased but also shows a

higher affinity to plus-end tracking proteins revealing its ability to grow out during cyclic stretch. Furthermore, microtubules play a relevant role when it comes to axonal injury models. Interestingly, by stabilizing the microtubule cytoskeleton, for instance, with Epothilone D, one can prevent axonal structures from collapsing (Yap et al., 2017). Therefore, the stability of the microtubule cytoskeleton gives great insights into how neuronal cells could adapt to cyclic mechanical stretch.

In the co-culture of stretched NSCs that differentiated to astrocytes or neuronal cells, only astrocytes showed protein reinforcement of the astrocyte-specific intermediate filament GFAP. In contrast, the neuronal cytoskeleton was not affected by cyclic stretch. As the fluorescence images and 3D analysis revealed that neuronal cells grew on top of astrocytes, neuronal phenotypes could thereby avoid mechanical strain. Here, the soft nature of astrocytes may have buffered mechanical impacts and thus presented a soft structure where neurons could grow and extend their branches in any direction. In agreement with this, neuronal phenotypes in the co-culture did not show any reinforcement.

A higher GFAP expression is upregulated by mechanical stress in other studies and is also suggested to be induced by arterial pulsation (Iadecola & Nedergaard, 2007; M. Pekny & Pekna, 2004). However, most studies on elevated GFAP are in the context of neurotrauma. Astrocytes play a significant role in the body's response to neurotrauma. During neurotrauma, ischemia, and neurodegenerative diseases, astrocytes change their intermediate filament expression – a process referred to as reactive gliosis (Milos Pekny & Lane, 2007). Reactive astrocytes reveal increased expression of GFAP, vimentin, as well as a reexpression of nestin. Cullen and colleagues also observed an increased GFAP level within a 3D stretch *in vitro* model. However, they used a much higher strain amplitude of 50% and frequency up to 30 Hz. The upregulation was here also accompanied by astrocyte hypertrophy (Cullen, Simon, & LaPlaca, 2007). Whether the GFAP reinforcement was alongside astrocyte activation has not been investigated within this thesis.

4.6 Branch formation of cortical neurons under cyclic stretch

Stretched cortical neurons revealed enhanced length growth and side branch formation (chapter 3.3.1.6). Most noteworthy, the strongest effect was shown for the mild strain amplitude of 7%, which argues for a potential optimal cyclic strain condition to trigger neuronal growth. Since neuronal cells adapt to cyclic mechanical stretch and align their neuronal extensions perpendicular to stretch, it remains to be elucidated if real mechanical straining or more general mechanical homeostasis perturbation plays a role. In addition to this, also static mechanical strain has been shown to enhance neuronal outgrowth (Pfister, Iwata, Meaney, & Smith, 2004). Further, tension along the axon has been suggested to be an effective inducer of neuronal growth (Pfister et al., 2004). Interestingly, although directed outgrowth occurred perpendicular to strain to avoid minimal mechanical loadings, side branch formation was in the direction perpendicular to the main extensions and thereby parallel to the uniaxial strain. Generally, branch formation is dependent on actin polymerization at the early stages, followed by microtubule infiltration and the formation of stable branches (Dent & Kalil, 2001). Thereby, actin filaments provide the necessary pushing force for the membrane protrusion. The immunofluorescent staining of side branches revealed that microtubules are already present in side branches. However, it may be possible that differences in cytoskeletal structures and binding partners may be responsible for differential mechanosensitive responses of main extensions and side branches. In line with this hypothesis, adapter proteins such as the adenomatous polyposis coli (APC) protein can support microtubule stability (Yokota et al., 2009). However, deletion of the APC protein increases neuronal branch formation. Hence, local differences due to uniaxial cyclic stretch may be responsible for leading to local destabilization of microtubules structures and increased formation of branches. One additional finding gave further insights into the mechanism of elevated outgrowth and triggered length and branch growth: cyclic stretch-induced an enlarged growth cone compared to controls in an amplitude-dependent manner (chapter 3.3.1.7). The growth cone size is described to be enlarged in active growing processes (Ruthel & Hollenbeck, 2000). Therefore, a larger growth cone may provide more force to push the neuronal branch and triggers neuronal outgrowth. In general, growth cone

size and morphology are associated with its underlying F-actin organization (Igarashi, 2019). In addition, branching can also occur due to pausing of the growth cone leaving remnants behind on the axon shaft and filopodia and lamellar protrusion emerge from this active region (Szebenyi, Callaway, Dent, & Kalil, 1998). To what extend the growth cone size played a role in branch formation has not been analyzed in this thesis. However, a different growth cone size and its general involvement in branch behavior argue for a connection of enlarged growth cone size and an elevated number of neuronal branches.

5 Outlook

In the scope of this thesis, the response of cyclic mechanical strain to diverse cell types of the rat brain was analyzed. Neural stem cells, differentiating cells to astrocytes or neuronal cells, primary cortical cells, and mature astrocytes, were accessed according to their mechanoresponse. Each of the different cell types has its unique cytoskeletal composition. Therefore, how cells would react to mechanical deformations was uncertain. Further, the cytoskeletal proteins play an exclusive role in different cell types. The work of this thesis revealed different mechanoresponsive patterns in each cell type, which was discussed based on their unique cytoskeletal arrangements.

Although the brain is among the softest tissues in the human body, cells in the CNS are exposed to mechanical strain due to head movements and also as cells reside near vasculature. The work of this thesis revealed that each cell type of the CNS has a unique mechanoresponse and that the mechanobiology of each cell type needs to be considered individually when exposed to physiological strain or microenvironmental changes during disease. To understand processes in the CNS development, mechanical cues and their effect on brain cells have to be considered in CNS development due to a complex interplay between mechanical and biochemical stimuli. The work of the thesis highlighted differences in the mechanoresponse of neural stem cells, differentiating neurons and differentiating astrocytes, and mature neuronal cells and astrocytes. Further studies should aim to investigate the mechanotransduction pathways in order to completely understand cell-type-specific differences. In this work, cell-type-specific results only allowed to speculate differences based on the cytoskeletal setup. Interestingly, although cyclic mechanical strain had an effect on NSCs, lineage commitment and differentiation were not altered in stretched NSCs. In contrast, it is widely investigated that stiffness and topography have a huge effect on NSC development due to different mechanotransduction pathways and spatial organization of focal adhesions. Therefore, cyclic strain possibly induced a different mechanotransduction pathway compared to stiffness and topography. However, the molecular key mechanotransducers remain unknown.

Further, immediate responses to cyclic stretch revealed drastic responses and neuronal cells retracted. However, neuronal cells showed to adapt to cyclic deformations. Such adaptation processes and changes in cytoskeletal systems is also of pivotal interest to understand responses of brain cells to repetitive mechanical impacts and further to characterize the 'mechanical footprint'. In more detail, even small but repetitive mechanical impacts can lead to neuronal degeneration. Hence, understanding cell responses and characterizing mechanotransductive mechanism could expand the current knowledge of mechanobiology of cells within the CNS and allow to find new strategies to interfere with progressive neurodegeneration as well as to identify physiological relevant mechanical stimuli involved in CNS development and nervous tissue repair.

6 References

Abraham, J.-A., Linnartz, C., Dreissen, G., Springer, R., Blaschke, S., Rueger, M. A., Fink, G. R., Hoffmann, B., & Merkel, R. (2019). Directing Neuronal Outgrowth and Network Formation of Rat Cortical Neurons by Cyclic Substrate Stretch. *Langmuir, 35*(23), 7423-7431.

Akhmanova, A., & Hoogenraad, C. C. (2015). Microtubule minus-end-targeting proteins. *Current Biology, 25*(4), R162-171.

Ambriz, X., de Lanerolle, P., & Ambrosio, J. R. (2018). The Mechanobiology of the Actin Cytoskeleton in Stem Cells during Differentiation and Interaction with Biomaterials. *Stem Cells International, 2018*, 2891957.

Baek, J., Cho, S. Y., Kang, H., Ahn, H., Jung, W. B., Cho, Y., Lee, E., Cho, S. W., Jung, H. T., & Im, S. G. (2018). Distinct Mechanosensing of Human Neural Stem Cells on Extremely Limited Anisotropic Cellular Contact. *ACS Applied Materials and Interfaces, 10*(40), 33891-33900.

Bayly, P. V., Cohen, T. S., Leister, E. P., Ajo, D., Leuthardt, E. C., & Genin, G. M. (2005). Deformation of the human brain induced by mild acceleration. *Journal of neurotrauma, 22*(8), 845-856.

Bayly, P. V., Naunheim, R., Standeven, J., Neubauer, J. S., Lewis, L., & Genin, G. M. (2002, 23-26 Oct. 2002). *Linear and angular accelerations of the human head during heading of a soccer ball.* Paper presented at the Proceedings of the Second Joint 24th Annual Conference and the Annual Fall Meeting of the Biomedical Engineering Society] [Engineering in Medicine and Biology.

Bernal, A., & Arranz, L. (2018). Nestin-expressing progenitor cells: function, identity and therapeutic implications. *Cellular and molecular life sciences : CMLS, 75*(12), 2177-2195.

Blaschke, S., Vay, S. U., Pallast, N., Rabenstein, M., Abraham, J.-A., Linnartz, C., Hoffmann, M., Hersch, N., Merkel, R., Hoffmann, B., Fink, G. R., & Rueger, M. A. (2019). Substrate elasticity induces quiescence and promotes neurogenesis of primary neural stem cells—A biophysical in vitro model of the physiological cerebral milieu. *Journal of Tissue Engineering and Regenerative Medicine, 13*(6), 960-972.

Block, J., Witt, H., Candelli, A., Danes, J. C., Peterman, E. J. G., Wuite, G. J. L., Janshoff, A., & Köster, S. (2018). Viscoelastic properties of vimentin originate from nonequilibrium conformational changes. *Science Advances, 4*(6), eaat1161.

Bretscher, A., Edwards, K., & Fehon, R. G. (2002). ERM proteins and merlin: integrators at the cell cortex. *Nature Reviews Molecular Cell Biology, 3*(8), 586-599.

Bringmann, H., Skiniotis, G., Spilker, A., Kandels-Lewis, S., Vernos, I., & Surrey, T. (2004). A kinesin-like motor inhibits microtubule dynamic instability. *Science, 303*(5663), 1519-1522.

Carlsson, L., Li, Z., Paulin, D., & Thornell, L. E. (1999). Nestin is expressed during development and in myotendinous and neuromuscular junctions in wild type and desmin knock-out mice. *Experimental Cell Research, 251*(1), 213-223.

Chen, B., Kemkemer, R., Deibler, M., Spatz, J., & Gao, H. (2012). Cyclic Stretch Induces Cell Reorientation on Substrates by Destabilizing Catch Bonds in Focal Adhesions. *PloS one, 7*(11), e48346.

Chen, S., Lewallen, M., & Xie, T. (2013). Adhesion in the stem cell niche: biological roles and regulation. *Development, 140*(2), 255.

Chien, S. (2007). Mechanotransduction and endothelial cell homeostasis: the wisdom of the cell. *American Journal of Physiology-Heart and Circulatory Physiology, 292*(3), H1209-H1224.

Chighizola, M., Dini, T., Lenardi, C., Milani, P., Podestà, A., & Schulte, C. (2019). Mechanotransduction in neuronal cell development and functioning. *Biophysical Reviews, 11*(5), 701-720.

Chou, Y.-H., Khuon, S., Herrmann, H., & Goldman, R. D. (2003). Nestin promotes the phosphorylation-dependent disassembly of vimentin intermediate filaments during mitosis. *Molecular Biology of the Cell, 14*(4), 1468-1478.

Christopherson, K. S., Ullian, E. M., Stokes, C. C., Mullowney, C. E., Hell, J. W., Agah, A., Lawler, J., Mosher, D. F., Bornstein, P., & Barres, B. A. (2005). Thrombospondins are astrocyte-secreted proteins that promote CNS synaptogenesis. *Cell, 120*(3), 421-433.

Chrzanowska-Wodnicka, M., & Burridge, K. (1996). Rho-stimulated contractility drives the formation of stress fibers and focal adhesions. *Journal of Cell Biology, 133*(6), 1403-1415.

Collinsworth, A. M., Torgan, C. E., Nagda, S. N., Rajalingam, R. J., Kraus, W. E., & Truskey, G. A. (2000). Orientation and length of mammalian skeletal myocytes in response to a unidirectional stretch. *Cell and Tissue Research, 302*(2), 243-251.

Conover, J. C., Doetsch, F., Garcia-Verdugo, J.-M., Gale, N. W., Yancopoulos, G. D., & Alvarez-Buylla, A. (2000). Disruption of Eph/ephrin signaling affects migration and proliferation in the adult subventricular zone. *Nature Neuroscience, 3*(11), 1091-1097.

Cui, Y., Hameed, F. M., Yang, B., Lee, K., Pan, C. Q., Park, S., & Sheetz, M. (2015). Cyclic stretching of soft substrates induces spreading and growth. *Nature Communications, 6*(1), 6333.

Cullen, D. K., Simon, C. M., & LaPlaca, M. C. (2007). Strain rate-dependent induction of reactive astrogliosis and cell death in three-dimensional neuronal-astrocytic co-cultures. *Brain Research, 1158*, 103-115.

D'Este, E., Kamin, D., Göttfert, F., El-Hady, A., & Hell, S. W. (2015). STED nanoscopy reveals the ubiquity of subcortical cytoskeleton periodicity in living neurons. *Cell reports, 10*(8), 1246-1251.

de, R., & Safran, S. A. (2008). Dynamical theory of active cellular response to external stress. *Physical Review E, 78*, 031923.

Dent, E. W., & Kalil, K. (2001). Axon branching requires interactions between dynamic microtubules and actin filaments. *Journal of Neuroscience, 21*(24), 9757-9769.

Discher, D. E., Janmey, P., & Wang, Y.-l. (2005). Tissue Cells Feel and Respond to the Stiffness of Their Substrate. *Science, 310*(5751), 1139.

Drew, P. J., Shih, A. Y., & Kleinfeld, D. (2011). Fluctuating and sensory-induced vasodynamics in rodent cortex extend arteriole capacity. *Proceedings of the National Academy of Sciences of the United States of America, 108*(20), 8473-8478.

East, E., de Oliveira, D. B., Golding, J. P., & Phillips, J. B. (2010). Alignment of astrocytes increases neuronal growth in three-dimensional collagen gels and is maintained following plastic compression to form a spinal cord repair conduit. *Tissue Engineering. Part A, 16*(10), 3173-3184.

Eastwood, M., Mudera, V., McGrouther, D., & Brown, R. (1998). Effect of precise mechanical loading on fibroblast populated collagen lattices: morphological changes. *Cell motility and the cytoskeleton, 40*(1), 13-21.

Engler, A. J., Sen, S., Sweeney, H. L., & Discher, D. E. (2006). Matrix elasticity directs stem cell lineage specification. *Cell, 126*(4), 677-689.

Ertürk, A., Hellal, F., Enes, J., & Bradke, F. (2007). Disorganized microtubules underlie the formation of retraction bulbs and the failure of axonal regeneration. *Journal of Neuroscience, 27*(34), 9169-9180.

Essen, D. C. V. (1997). A tension-based theory of morphogenesis and compact wiring in the central nervous system. *Nature, 385*(6614), 313-318.

Etienne-Manneville, S. (2013). Microtubules in Cell Migration. *Annual Review of Cell and Developmental Biology, 29*(1), 471-499.

Faust, U., Hampe, N., Rubner, W., Kirchgessner, N., Safran, S., Hoffmann, B., & Merkel, R. (2011). Cyclic stress at mHz frequencies aligns fibroblasts in direction of zero strain. *PloS one, 6*(12), e28963-e28963.

Fletcher, D. A., & Mullins, R. D. (2010). Cell mechanics and the cytoskeleton. *Nature, 463*(7280), 485-492.

Franze, K. (2013). The mechanical control of nervous system development. *Development, 140*(15), 3069-3077.

Franze, K. (2018). The Integration of Mechanical and Chemical Signalling in the Developing Brain. *Biophysical Journal, 114*(3), 19a.

Fu, X., Liu, G., Halim, A., Ju, Y., Luo, Q., Song, & Guanbin. (2019). Mesenchymal Stem Cell Migration and Tissue Repair. *Cells, 8*(8), 784.

Galkin, V. E., Orlova, A., & Egelman, E. H. (2012). Actin filaments as tension sensors. *Current Biology, 22*(3), R96-101.

Galou, M., Gao, J., Humbert, J., Mericskay, M., Li, Z., Paulin, D., & Vicart, P. (1997). The importance of intermediate filaments in the adaptation of tissues to mechanical stress: Evidence from gene knockout studies. *Biology of the Cell, 89*(2), 85-97.

Geiger, B. (2006). A Role for p130Cas in Mechanotransduction. *Cell, 127*(5), 879-881.

Goldberg, J. S., & Hirschi, K. K. (2009). Diverse roles of the vasculature within the neural stem cell niche. *Regenerative Medicine, 4*(6), 879-897.

Goldyn, A. M., Rioja, B. A., Spatz, J. P., Ballestrem, C., & Kemkemer, R. (2009). Force-induced cell polarisation is linked to RhoA-driven microtubule-independent focal-adhesion sliding. *Journal of Cell Science, 122*(Pt 20), 3644-3651.

Grzywa, E. L., Lee, A. C., Lee, G. U., & Suter, D. M. (2006). High-resolution analysis of neuronal growth cone morphology by comparative atomic force and optical microscopy. *Journal of Neurobiology, 66*(14), 1529-1543.

Hammond, J. W., Cai, D., & Verhey, K. J. (2008). Tubulin modifications and their cellular functions. *Current Opinion in Cell Biology, 20*(1), 71-76.

Hammond, J. W., Huang, C. F., Kaech, S., Jacobson, C., Banker, G., & Verhey, K. J. (2010). Posttranslational modifications of tubulin and the polarized transport of kinesin-1 in neurons. *Molecular Biology of the Cell, 21*(4), 572-583.

Hardin, J., Bertoni, G. P., & Kleinsmith, L. J. (2017). *Becker's World of the Cell*: Pearson Higher Ed.

Hasel, P., Dando, O., Jiwaji, Z., Baxter, P., Todd, A. C., Heron, S., Márkus, N. M., McQueen, J., Hampton, D. W., Torvell, M., Tiwari, S. S., McKay, S., Eraso-Pichot, A., Zorzano, A., Masgrau, R., Galea, E., Chandran, S., Wyllie, D. J. A., Simpson, T. I., & Hardingham, G. E. (2017). Neurons and neuronal activity control gene expression in astrocytes to regulate their development and metabolism. *Nature Communications, 8*(1), 15132.

Hauser, M., Yan, R., Li, W., Repina, N. A., Schaffer, D. V., & Xu, K. (2018). The Spectrin-Actin-Based Periodic Cytoskeleton as a Conserved Nanoscale Scaffold and Ruler of the Neural Stem Cell Lineage. *Cell reports, 24*(6), 1512-1522.

He, L., Kooistra, R., Das, R., Oudejans, E., van Leen, E., Ziegler, J., Portegies, S., de Haan, B., van Regteren Altena, A., Stucchi, R., Altelaar, A. M., Wieser, S., Krieg, M., Hoogenraad, C. C., & Harterink, M. (2020). Cortical anchoring of the microtubule cytoskeleton is essential for neuron polarity. *eLife, 9*, e55111.

Hellal, F., Hurtado, A., Ruschel, J., Flynn, K. C., Laskowski, C. J., Umlauf, M., Kapitein, L. C., Strikis, D., Lemmon, V., Bixby, J., Hoogenraad, C. C., & Bradke, F. (2011). Microtubule stabilization reduces scarring and causes axon regeneration after spinal cord injury. *Science, 331*(6019), 928-931.

Herrmann, H., & Aebi, U. (2016). Intermediate Filaments: Structure and Assembly. *Cold Spring Harbor Perspectives in Biology, 8*(11).

Hersch, N., Wolters, B., Dreissen, G., Springer, R., Kirchgeßner, N., Merkel, R., & Hoffmann, B. (2013). The constant beat: cardiomyocytes adapt their forces by equal contraction upon environmental stiffening. *Biology Open, 2*(3), 351-361.

Hynes, R. O. (2002). Integrins: bidirectional, allosteric signaling machines. *Cell, 110*(6), 673-687.

Iadecola, C., & Nedergaard, M. (2007). Glial regulation of the cerebral microvasculature. *Nature Neuroscience, 10*(11), 1369-1376.

Igarashi, M. (2019). Molecular basis of the functions of the mammalian neuronal growth cone revealed using new methods. *Proceedings of the Japan Academy. Series B, Physical and biological sciences, 95*(7), 358-377.

Ingber, D. E. (2008). Tensegrity-based mechanosensing from macro to micro. *Progress in Biophysics and Molecular Biology, 97*(2-3), 163-179.

Jain, V., Langham, M. C., & Wehrli, F. W. (2010). MRI estimation of global brain oxygen consumption rate. *Journal of Cerebral Blood Flow and Metabolism, 30*(9), 1598-1607.

Janmey, P. A., Euteneuer, U., Traub, P., & Schliwa, M. (1991). Viscoelastic properties of vimentin compared with other filamentous biopolymer networks. *J Cell Biol, 113*(1), 155-160.

Kapitein, L. C., & Hoogenraad, C. C. (2015). Building the Neuronal Microtubule Cytoskeleton. *Neuron, 87*(3), 492-506.

Karpowicz, P., Willaime-Morawek, S., Balenci, L., DeVeale, B., Inoue, T., & van der Kooy, D. (2009). E-Cadherin Regulates Neural Stem Cell Self-Renewal. *The Journal of Neuroscience, 29*(12), 3885.

Kaunas, R., Nguyen, P., Usami, S., & Chien, S. (2005). Cooperative effects of Rho and mechanical stretch on stress fiber organization. *Proceedings of the National Academy of Sciences of the United States of America, 102*(44), 15895-15900.

Kaverina, I., Krylyshkina, O., Beningo, K., Anderson, K., Wang, Y. L., & Small, J. V. (2002). Tensile stress stimulates microtubule outgrowth in living cells. *Journal of Cell Science, 115*(Pt 11), 2283-2291.

Kearney, E. M., Farrell, E., Prendergast, P. J., & Campbell, V. A. (2010). Tensile Strain as a Regulator of Mesenchymal Stem Cell Osteogenesis. *Annals of Biomedical Engineering, 38*(5), 1767-1779.

Keller, R., Davidson, L. A., & Shook, D. R. (2003). How we are shaped: the biomechanics of gastrulation. *Differentiation, 71*(3), 171-205.

Keung, A. J., de Juan-Pardo, E. M., Schaffer, D. V., & Kumar, S. (2011). Rho GTPases Mediate the Mechanosensitive Lineage Commitment of Neural Stem Cells. *Stem Cells, 29*(11), 1886-1897.

Kevenaar, J. T., & Hoogenraad, C. C. (2015). The axonal cytoskeleton: from organization to function. *Frontiers in Molecular Neuroscience, 8*(44).

Kim, D.-H., & Wirtz, D. (2013). Focal adhesion size uniquely predicts cell migration. *FASEB Journal, 27*(4), 1351-1361.

Kim, J.-S., Kim, J., Kim, Y., Yang, M., Jang, H., Kang, S., Kim, J.-C., Kim, S.-H., Shin, T., & Moon, C. (2011). Differential patterns of nestin and glial fibrillary acidic protein expression in mouse hippocampus during postnatal development. *Journal of Veterinary Science, 12*(1), 1-6.

Kong, D., Ji, B., & Dai, L. (2008). Stability of adhesion clusters and cell reorientation under lateral cyclic tension. *Biophysical Journal, 95*(8), 4034-4044.

Kumar, S., Maxwell, I. Z., Heisterkamp, A., Polte, T. R., Lele, T. P., Salanga, M., Mazur, E., & Ingber, D. E. (2006). Viscoelastic Retraction of Single Living Stress Fibers and Its Impact on Cell Shape, Cytoskeletal Organization, and Extracellular Matrix Mechanics. *Biophysical Journal, 90*(10), 3762-3773.

Lasser, M., Tiber, J., & Lowery, L. A. (2018). The Role of the Microtubule Cytoskeleton in Neurodevelopmental Disorders. *Frontiers in Cellular Neuroscience, 12*(165).

Lavelin, I., Wolfenson, H., Patla, I., Henis, Y. I., Medalia, O., Volberg, T., Livne, A., Kam, Z., & Geiger, B. (2013). Differential effect of actomyosin relaxation on the dynamic properties of focal adhesion proteins. *PloS one, 8*(9), e73549.

Leduc, C., & Etienne-Manneville, S. (2015). Intermediate filaments in cell migration and invasion: the unusual suspects. *Current opinion in cell biology, 32*, 102-112.

Lee, C. F., Haase, C., Deguchi, S., & Kaunas, R. (2010). Cyclic stretch-induced stress fiber dynamics - dependence on strain rate, Rho-kinase and MLCK. *Biochemical and Biophysical Research Communications, 401*(3), 344-349.

Lee, S., & Shea, T. B. (2014). The high molecular weight neurofilament subunit plays an essential role in axonal outgrowth and stabilization. *Biology Open, 3*(10), 974-981.

Letort, G., Ennomani, H., Gressin, L., Théry, M., & Blanchoin, L. (2015). Dynamic reorganization of the actin cytoskeleton. *F1000Research, 4*, F1000 Faculty Rev-1940.

Li, W., Tang, Q. Y., Jadhav, A. D., Narang, A., Qian, W. X., Shi, P., & Pang, S. W. (2015). Large-scale topographical screen for investigation of physical neural-guidance cues. *Scientific Reports, 5*, 8644-8644.

Lin, R. C., Matesic, D. F., Marvin, M., McKay, R. D., & Brüstle, O. (1995). Re-expression of the intermediate filament nestin in reactive astrocytes. *Neurobiology of Disease, 2*(2), 79-85.

Livne, A., Bouchbinder, E., & Geiger, B. (2014). Cell reorientation under cyclic stretching. *Nature communications, 5*, 3938-3938.

Livne, A., & Geiger, B. (2016). The inner workings of stress fibers−from contractile machinery to focal adhesions and back. *Journal of Cell Science, 129*(7), 1293-1304.

Loschke, F., Seltmann, K., Bouameur, J.-E., & Magin, T. M. (2015). Regulation of keratin network organization. *Current opinion in cell biology, 32*, 56-64.

Loverde, J., & Pfister, B. (2015). Developmental axon stretch stimulates neuron growth while maintaining normal electrical activity, intracellular calcium flux, and somatic morphology. *Frontiers in Cellular Neuroscience, 9*(308).

Loverde, J. R., Tolentino, R. E., & Pfister, B. J. (2011). Axon stretch growth: the mechanotransduction of neuronal growth. *Journal of Visualized Experiments*(54), 2753.

Lu, Y.-B., Franze, K., Seifert, G., Steinhäuser, C., Kirchhoff, F., Wolburg, H., Guck, J., Janmey, P., Wei, E.-Q., Käs, J., & Reichenbach, A. (2006). Viscoelastic properties of individual glial cells and neurons in the CNS. *Proceedings of the National Academy of Sciences of the United States of America, 103*(47), 17759-17764.

Magiera, M. M., & Janke, C. (2014). Post-translational modifications of tubulin. *Current Biology, 24*(9), R351-354.

Mao, X., Chen, Z., Luo, Q., Zhang, B., & Song, G. (2016). Simulated microgravity inhibits the migration of mesenchymal stem cells by remodeling actin cytoskeleton and increasing cell stiffness. *Cytotechnology, 68*(6), 2235-2243.

McMurray, R. J., Dalby, M. J., & Tsimbouri, P. M. (2015). Using biomaterials to study stem cell mechanotransduction, growth and differentiation. *Journal of Tissue Engineering and Regenerative Medicine, 9*(5), 528-539.

Moeendarbary, E., Weber, I. P., Sheridan, G. K., Koser, D. E., Soleman, S., Haenzi, B., Bradbury, E. J., Fawcett, J., & Franze, K. (2017). The soft mechanical signature of glial scars in the central nervous system. *Nature Communications, 8*(1), 14787.

Morioka, M., Parameswaran, H., Naruse, K., Kondo, M., Sokabe, M., Hasegawa, Y., Suki, B., & Ito, S. (2011). Microtubule dynamics regulate cyclic stretch-induced cell alignment in human airway smooth muscle cells. *PloS one, 6*(10), e26384-e26384.

Morris, E. J., & Geller, H. M. (1996). Induction of neuronal apoptosis by camptothecin, an inhibitor of DNA topoisomerase-I: evidence for cell cycle-independent toxicity. *Journal of Cell Biology, 134*(3), 757-770.

Mutalik, S. P., Joseph, J., Pullarkat, P. A., & Ghose, A. (2018). Cytoskeletal Mechanisms of Axonal Contractility. *Biophysical Journal, 115*(4), 713-724.

Nagano, M., Hoshino, D., Koshikawa, N., Akizawa, T., & Seiki, M. (2012). Turnover of focal adhesions and cancer cell migration. *International Journal of Cell Biology, 2012*, 310616-310616.

Nayal, A., Webb, D. J., & Horwitz, A. F. (2004). Talin: an emerging focal point of adhesion dynamics. *Current Opinion in Cell Biology, 16*(1), 94-98.

Nedergaard, M., Ransom, B., & Goldman, S. A. (2003). New roles for astrocytes: Redefining the functional architecture of the brain. *Trends in Neurosciences, 26*(10), 523-530.

Niediek, V., Born, S., Hampe, N., Kirchgessner, N., Merkel, R., & Hoffmann, B. (2012). Cyclic stretch induces reorientation of cells in a Src family kinase- and p130Cas-dependent manner. *European Journal of Cell Biology, 91*(2), 118-128.

Parekh, S. H., Chaudhuri, O., Theriot, J. A., & Fletcher, D. A. (2005). Loading history determines the velocity of actin-network growth. *Nature Cell Biology, 7*(12), 1219-1223.

Park, D., Xiang, A. P., Mao, F. F., Zhang, L., Di, C. G., Liu, X. M., Shao, Y., Ma, B. F., Lee, J. H., Ha, K. S., Walton, N., & Lahn, B. T. (2010). Nestin is required for the proper self-renewal of neural stem cells. *Stem cells (Dayton, Ohio), 28*(12), 2162-2171.

Pekny, M., & Lane, E. B. (2007). Intermediate filaments and stress. *Experimental Cell Research, 313*(10), 2244-2254.

Pekny, M., & Pekna, M. (2004). Astrocyte intermediate filaments in CNS pathologies and regeneration. *The Journal of Pathology, 204*(4), 428-437.

Peters, A., & Vaughn, J. E. (1967). Microtubules and filaments in the axons and astrocytes of early postnatal rat optic nerves. *Journal of Cell Biology, 32*(1), 113-119.

Pfister, B. J., Iwata, A., Meaney, D. F., & Smith, D. H. (2004). Extreme Stretch Growth of Integrated Axons. *The Journal of Neuroscience, 24*(36), 7978.

Potokar, M., Kreft, M., Li, L., Daniel Andersson, J., Pangršič, T., Chowdhury, H. H., Pekny, M., & Zorec, R. (2007). Cytoskeleton and Vesicle Mobility in Astrocytes. *Traffic, 8*(1), 12-20.

Previtera, M. L., Langhammer, C. G., & Firestein, B. L. (2010). Effects of substrate stiffness and cell density on primary hippocampal cultures. *Journal of Bioscience and Bioengineering, 110*(4), 459-470.

Putnam, A. J., Cunningham, J. J., Dennis, R. G., Linderman, J. J., & Mooney, D. J. (1998). Microtubule assembly is regulated by externally applied strain in cultured smooth muscle cells. *Journal of Cell Science, 111 (Pt 22)*, 3379-3387.

Qiu, H., Zhu, Y., Sun, Z., Trzeciakowski, J. P., Gansner, M., Depre, C., Resuello, R. R. G., Natividad, F. F., Hunter, W. C., Genin, G. M., Elson, E. L., Vatner, D. E., Meininger, G. A., & Vatner, S. F. (2010). Short communication: vascular smooth muscle cell stiffness as a mechanism for increased aortic stiffness with aging. *Circulation Research, 107*(5), 615-619.

Rammensee, S., Kang, M. S., Georgiou, K., Kumar, S., & Schaffer, D. V. (2017). Dynamics of Mechanosensitive Neural Stem Cell Differentiation. *Stem cells (Dayton, Ohio), 35*(2), 497-506.

Ranade, S. S., Qiu, Z., Woo, S.-H., Hur, S. S., Murthy, S. E., Cahalan, S. M., Xu, J., Mathur, J., Bandell, M., Coste, B., Li, Y.-S. J., Chien, S., & Patapoutian, A. (2014). Piezo1, a mechanically activated ion channel, is required for vascular development in mice. *Proceedings of the National Academy of Sciences, 111*(28), 10347-10352.

Reed, N. A., Cai, D., Blasius, T. L., Jih, G. T., Meyhofer, E., Gaertig, J., & Verhey, K. J. (2006). Microtubule acetylation promotes kinesin-1 binding and transport. *Current Biology, 16*(21), 2166-2172.

Rueger, M. A., Backes, H., Walberer, M., Neumaier, B., Ullrich, R., Simard, M.-L., Emig, B., Fink, G. R., Hoehn, M., Graf, R., & Schroeter, M. (2010). Noninvasive imaging of endogenous neural stem cell mobilization in vivo using positron emission tomography. *Journal of Neuroscience, 30*(18), 6454-6460.

Ruthel, G., & Hollenbeck, P. J. (2000). Growth cones are not required for initial establishment of polarity or differential axon branch growth in cultured hippocampal neurons. *Journal of Neuroscience, 20*(6), 2266-2274.

Safran, S. A., & De, R. (2009). Nonlinear dynamics of cell orientation. *Physical Review E, 80*(6 Pt 1), 060901.

Saito, S., Suzuki, A., Nozawa-Inoue, K., Kawano, Y., Hoshino, M., Saito, C., & Maeda, T. (2009). Immunohistochemical detection of nestin in the periodontal Ruffini endings of the rat incisor. *Neuroscience Letters, 449*(3), 195-200.

Schwarz, U. S., & Safran, S. A. (2013). Physics of adherent cells. *Reviews of Modern Physics, 85*(3), 1327.

Sjöberg, G., Jiang, W.-Q., Ringertz, N. R., Lendahl, U., & Sejersen, T. (1994). Colocalization of Nestin and Vimentin/Desmin in Skeletal Muscle Cells Demonstrated by Three-Dimensional Fluorescence Digital Imaging Microscopy. *Experimental Cell Research, 214*(2), 447-458.

Sliogeryte, K., Thorpe, S. D., Lee, D. A., Botto, L., & Knight, M. M. (2014). Stem cell differentiation increases membrane-actin adhesion regulating cell blebability, migration and mechanics. *Scientific Reports, 4*(1), 7307.

Smith, D. H. (2009). Stretch growth of integrated axon tracts: Extremes and exploitations. *Progress in Neurobiology, 89*(3), 231-239.

Smith, D. H., & Stewart, W. (2020). Genetic interplay with soccer ball heading. *Nature Reviews Neurology, 16*(4), 189-190.

Sofroniew, M. V., & Vinters, H. V. (2010). Astrocytes: biology and pathology. *Acta Neuropathologica, 119*(1), 7-35.

Steinert, P. M., Chou, Y.-H., Prahlad, V., Parry, D. A., Marekov, L. N., Wu, K. C., Jang, S.-I., & Goldman, R. D. (1999). A high molecular weight intermediate filament-associated protein in BHK-21 cells is nestin, a type VI intermediate filament protein limited co-assembly in vitro to form heteropolymers with type III vimentin and type IV α-internexin. *Journal of Biological Chemistry, 274*(14), 9881-9890.

Stobart, J. L., & Anderson, C. M. (2013). Multifunctional role of astrocytes as gatekeepers of neuronal energy supply. *Frontiers in Cellular Neuroscience, 7*, 38-38.

Suter, D. M., & Miller, K. E. (2011). The emerging role of forces in axonal elongation. *Progress in Neurobiology, 94*(2), 91-101.

Szebenyi, G., Callaway, J. L., Dent, E. W., & Kalil, K. (1998). Interstitial branches develop from active regions of the axon demarcated by the primary growth cone during pausing behaviors. *The Journal of Neuroscience, 18*(19), 7930-7940.

Tinevez, J.-Y., Perry, N., Schindelin, J., Hoopes, G. M., Reynolds, G. D., Laplantine, E., Bednarek, S. Y., Shorte, S. L., & Eliceiri, K. W. (2017). TrackMate: An open and extensible platform for single-particle tracking. *Methods, 115*, 80-90.

Tondon, A., Hsu, H.-J., & Kaunas, R. (2012). *Dependence of Cyclic Stretch-Induced Stress Fiber Reorientation on Stretch Waveform.* Paper presented at the ASME 2012 Summer Bioengineering Conference.

Tondon, A., & Kaunas, R. (2014). The direction of stretch-induced cell and stress fiber orientation depends on collagen matrix stress. *PloS one, 9*(2), e89592-e89592.

Totsukawa, G., Yamakita, Y., Yamashiro, S., Hartshorne, D. J., Sasaki, Y., & Matsumura, F. (2000). Distinct roles of ROCK (Rho-kinase) and MLCK in spatial regulation of MLC phosphorylation for assembly of stress fibers and focal adhesions in 3T3 fibroblasts. *Journal of Cell Biology, 150*(4), 797-806.

Vignaud, T., Copos, C., Leterrier, C., Tseng, Q., Blanchoin, L., Mogilner, A., Théry, M., & Kurzawa, L. (2020). Stress fibers are embedded in a contractile cortical network. *bioRxiv*, 2020.2002.2011.944579.

Wagshul, M. E., Eide, P. K., & Madsen, J. R. (2011). The pulsating brain: A review of experimental and clinical studies of intracranial pulsatility. *Fluids and Barriers of the CNS, 8*(1), 5-5.

Wang, Y.-Z., Plane, J. M., Jiang, P., Zhou, C. J., & Deng, W. (2011). Concise review: Quiescent and active states of endogenous adult neural stem cells: identification and characterization. *Stem cells (Dayton, Ohio), 29*(6), 907-912.

Wedeen, V. J., & Ponceleti, B. (2007). Brain Parenchyma Motion Observed by MRI. *Encyclopedia of Magnetic Resonance*.

Wei, X., Sun, Y., Wu, Y., Zhu, J., Gao, B., Yan, H., Zhao, Z., Zhou, J., & Jing, Z. (2017). Downregulation of Talin-1 expression associates with increased proliferation and migration of vascular smooth muscle cells in aortic dissection. *BMC Cardiovascular Disorders, 17*(1), 162.

Weiss, P. (1941). Nerve patterns: the mechanisms of nerve growth. *Growth, 5*, 163-203.

Wiche, G. (1998). Role of plectin in cytoskeleton organization and dynamics. *Journal of Cell Science, 111*(17), 2477.

Wiese, C., Rolletschek, A., Kania, G., Blyszczuk, P., Tarasov, K. V., Tarasova, Y., Wersto, R. P., Boheler, K. R., & Wobus, A. M. (2004). Nestin expression – a property of multi-lineage progenitor cells? *Cellular and Molecular Life Sciences, 61*(19), 2510-2522.

Windoffer, R., Beil, M., Magin, T. M., & Leube, R. E. (2011). Cytoskeleton in motion: the dynamics of keratin intermediate filaments in epithelia. *Journal of Cell Biology, 194*(5), 669-678.

Xu, G.-K., Feng, X.-Q., & Gao, H. (2018). Orientations of Cells on Compliant Substrates under Biaxial Stretches: A Theoretical Study. *Biophysical Journal, 114*(3), 701-710.

Yap, Y. C., King, A. E., Guijt, R. M., Jiang, T., Blizzard, C. A., Breadmore, M. C., & Dickson, T. C. (2017). Mild and repetitive very mild axonal stretch injury triggers cystoskeletal mislocalization and growth cone collapse. *PloS one, 12*(5), e0176997.

Yokota, Y., Kim, W. Y., Chen, Y., Wang, X., Stanco, A., Komuro, Y., Snider, W., & Anton, E. S. (2009). The adenomatous polyposis coli protein is an essential regulator of radial glial polarity and construction of the cerebral cortex. *Neuron, 61*(1), 42-56.

Zhang, B., Luo, Q., Chen, Z., Sun, J., Xu, B., Ju, Y., & Song, G. (2015). Cyclic mechanical stretching promotes migration but inhibits invasion of rat bone marrow stromal cells. *Stem Cell Research, 14*(2), 155-164.

Zhou, F. Q., Waterman-Storer, C. M., & Cohan, C. S. (2002). Focal loss of actin bundles causes microtubule redistribution and growth cone turning. *Journal of Cell Biology, 157*(5), 839-849.

Zielinski, A., Linnartz, C., Pleschka, C., Dreissen, G., Springer, R., Merkel, R., & Hoffmann, B. (2018). Reorientation dynamics and structural interdependencies of actin, microtubules and intermediate filaments upon cyclic stretch application. *Cytoskeleton, 75*(9), 385-394.

7 Figures

8 Acknowledgment

I am extremely grateful to my supervisor Dr. Bernd Hoffmann for his vital encouragement and guidance throughout my Ph.D. research. I am very happy I could work on such a fascinating topic. I am thankful for his support and patience throughout my work at the IBI-2, and every scientific discussion and motivation. I would further like to thank Prof. Rudolf Merkel enable my research at IBI-2 and to support my extracurricular activities. I am also lucky that I was supported by two experts in two different fields –physics and biology- that allowed to discuss several different aspects and interdisciplinary questions regarding my project.

I would like to thank the rest of my committee members Prof. Höhfeld, Prof. Wachten, and Prof. Kubitscheck.

I am further very thankful that I had the opportunity to work in two different laboratories, exploring the science of neural stem cells at the University Hospital in cologne at AG stem cells and Prof. Rügers laboratory. Here I would like to thank Prof. Maria Adele Rüger, Prof. Gereon Fink, and Prof. Michael Schröter for this unique opportunity and several scientific discussions. I would also like to thank Dr. Stefan Blaschke and Dr. Sabine Vay for helping me throughout the work with stem cells and for their scientific input and inspiration.

Further, I would like to thank Dr. Guillermo Beltramo for his support to finalize the thesis, for scientific discussions, and his constructive feedback.

I am further extremely thankful that I could join the BioSoft graduation school and would like to thank Dr. Thorsten Auth for the organization of several inspiring courses.

I also thank my fellow lab members for the support. They also inspired me in research through our interactions and discussions in the lab. Especially Tabea Wiedenhöft and Dr. Rejhana Kolasinac for daily discussions, for support throughout the years, and for proofreading of the thesis. I also thank Georg Dreissen and Dr. Ronald Springer for their support in analyzing the data and writing algorithms for image processing. A special thanks also to Jens Konrad, who helped with hardware settings, innovated, and improved the handling of stretching chambers.

For me, it was important to discuss the research with people who are not in the same field. Therefore, I would also like to thank Prof. Ivica Pelivan and Cornelia Braun for their support.

Last but not least, my deepest gratitude goes to my family for their love and support.

9 Publications

Parts of the dissertation have been published:

- Abraham, J.-A., Linnartz, C., Dreissen, G., Springer, R., Blaschke, S., Rueger, M. A., Fink, G. R., Hoffmann, B., & Merkel, R. (2018). Directing Neuronal Outgrowth and Network Formation of Rat Cortical Neurons by Cyclic Substrate Stretch. *Langmuir, 35*(23), 7423-7431.

- Blaschke, S., Vay, S. U., Pallast, N., Rabenstein, M., Abraham, J.-A., Linnartz, C., Hoffmann, M., Hersch, N., Merkel, R., Hoffmann, B., Fink, G. R., & Rueger, M. A. (2019). Substrate elasticity induces quiescence and promotes neurogenesis of primary neural stem cells—A biophysical in vitro model of the physiological cerebral milieu. *Journal of Tissue Engineering and Regenerative Medicine, 13*(6), 960-972.

- Blaschke, S., Demir, S., Koenig,A, Abraham, J.-A, Vay, S. U., Rabenstein, Olschewski, D. N, Hoffmann, C., Hoffmann, M. Hersch, N., Merkel, R., Hoffmann, B., Schroeter, M, Fink, G. R., & Rueger, M. A (2020). Substrate elasticity exerts functional effects on primary microglia in vitro via stretch-activated chloride channels. *Frontiers in Cellular Neuroscience, 14*(367), 1662-5102.

Publications in progress:

- Ahrens, D., Abraham, J.-A, Puellen, R, Seedorf, A., Huerttlen, W., Konrad, J., Dreissen, G., Hoffmann, B., & Merkel, R. Live-cell system for automized imaging of fast cellular responses to mechanical stretch.

- Abraham, J.-A, Blaschke, S., Dreissen, G., Vay, S.U., Rueger, M. A., Fink, G. R., Hoffmann, B., & Merkel, R. Mechanoprotective role of differentiating astrocytes in a cyclically stretched co-culture with differentiating neurons.

- Tarazi, S., Dreissen, G., Abraham, J.-A, Hoffmann, M., Gerlach, S., Loevenich, L., Springer, R., Scharr, H., Merkel, R. & Hoffmann, B. Functional resistance of neuronal networks against strain.